Design, Modelling, and Optimisation of an Upper Stage Propulsion System for the Barracuda Sounding Rocket

Thesis Report

Wim Jodehl

TU Delft

Design, Modelling, and Optimisation of an Upper Stage Propulsion System for the Barracuda Sounding Rocket

Thesis Report

by

Wim Jodehl

to obtain the degree of Master of Science

at the Delft University of Technology,

to be defended publicly on Tuesday, 16th of July, 2024 at 13:00.

Student number: 4676874

Project duration: 4th of December, 2023 – 16th of July, 2024

Thesis committee:

Dr. A. Cervone,	TU Delft, Chair
Ir. M.C. Naeije,	TU Delft, Examiner
Dr. B.V.S. Jyoti,	TU Delft, Supervisor
Ir. H. Olthof,	T-Minus Engineering, Supervisor

Cover: Barracuda Rocket launching

An electronic version of this thesis is available at `http://repository.tudelft.nl/`.

TU Delft

Preface

The following report provides a complete record of my Master Thesis project which entailed designing the propulsion system for the Barracuda upper stage, implementing the preliminary design into a numerical model, and then subsequently using this model to optimise the design of the propulsion system for the optimal. After the literature study, I was convinced that a steerable and controlled upper stage for the Barracuda rocket is the best next step to enhance the capabilities of the rocket. At the very core of this sits the propulsion system, and I believe that the design, that has ultimately resulted out of this work, while being novel in this application can very much support the goals set for the upper stage of the Barracuda rocket.

I would like to thank T-Minus Engineering for providing me with the opportunity to my Master's Thesis on this topic about which I am so passionate and also for enabling me to bring novel technology into this field. After my internship and part-time work at this company, I was glad to continue working with T-Minus Engineering. I look forward to working together in the future. In particular, I would like to thank Hein Olthof for supervising this research from the side of T-Minus Engineering and for providing guidance and support. I would also like to thank Sven Balfoort and Wesley Toussaint for the insights they gave into the HyProp project.

I would also like to thank Dr Botchu Vara Siva Jyoti and Dr. Iklim Akay for their support and guidance throughout this whole project, and for supervising it from the side of the Delft University of Technology.

Finally, I would like to thank Dr Angelo Cervone and Marc Naeije for being part of the assessment committee for this Master's Thesis

Wim Jodehl
Delft, July 2024

Executive Summary

The goal of this thesis project was to design, model and optimise an upper-stage propulsion system for the T-Minus Engineering Barracuda sounding rocket and this goal was captured in the following research question:

> *"Design, model, and mass-optimise a propulsion system for the steerable upper stage for the T-Minus Barracuda using hydrogen peroxide that falls within the operational and technological envelope of T-Minus Engineering"*

Based on this objective, four main research question questions with three sub-questions each were defined covering the use of hydrogen peroxide as a propellant in this system, the optimisation process, the integration with the remainder of the Barracuda rocket, and the special considerations on the design imposed by the unique nature of T-Minus Engineering respectively. Based on these questions, the approach and scope of the project were defined. The goal was specifically not to develop a design to such a level that it can enter production right after this project, but rather explore the design space available for this novel and unique application, and determine where the optimum design point for the system lies.

After this, and due to its closely related nature, the currently ongoing HyProp project within T-Minus Engineering was analysed closely to determine which technologies should be carried over into the propulsion system for the Barracuda upper stage. It was concluded that the technology surrounding the catalytic decomposition of high-test peroxide (HTP) can provide key benefits to the Barracuda upper-stage propulsion system. By using the process to auto-ignite the fuel with the decomposed products of the HTP, the construction of the propulsion system can be vastly simplified when compared to more conventional liquid bi-propellant propulsion systems. Next to this, it also became apparent that the HyProp project can provide an excellent test bed for many technologies which need to be developed for the propulsion system developed in this work.

Based on these insights, a preliminary design was defined for the propulsion system. First, the system-level requirements were defined, constraints were identified, and a system-level conceptual design was derived. Here, it was decided to utilise the previously described decomposition-based auto-ignition of the thruster. In order to enable, this the fuel had to be carefully selected. Since the final selection of the fuel was going to be made during the optimisation process, a list of six fuel candidates was selected based on factors such as auto-ignition temperature, handleability and the existence of combustion models for these fuels. Finally, the system architecture was defined and the subsystems of the propulsion system were designed to the extent required for the propulsion system to be represented in a numerical model.

After this phase, a numerical model was developed that was used to optimise the design. For this, 11 modules were created with tasks ranging from sizing propellant tanks to computing the heat transfer into the combustion chamber wall. In some cases, multiple design options were modelled such that the optimisation algorithm can select the most ideal design based on considering as many aspects as possible. The model was then subsequently verified.

The previously developed numerical model was then optimised by implementing a genetic algorithm. This type of optimisation algorithm was determined to be the ideal method given the characteristics of the model. The outcome was a thruster using HTP as its oxidiser and gasoline as its fuel, while notably using the HTP to regeneratively cool the combustion chamber and nozzle. The entire system remains below a total mass of 15 [kg] including propellants. After this, the optimisation outcomes were validated against the requirements defined at the beginning of this project.

Finally, the conclusions from all chapters were drawn and compiled, and based on these, the previously defined research questions were revisited and answered to the extent possible based on the work performed. Finally, based on the answers to the research questions, recommendations for future work on the numerical model, optimisation algorithm and the surrounding testing and development activities were made.

Contents

List of Figures

List of Tables

List Of Symbols

Roman

Table 1: Roman Symbols

Parameter	Symbol	Default Unit
Ablator Area	A_{abl}	$[m^2]$
Catalyst Cross-sectional Area	A_{cat}	$[m^2]$
Cooling Channel Area	A_c	$[m^2]$
Nozzle Exit Area	A_e	$[m^2]$
Chamber/Nozzle Segment Area	A_{seg}	$[m^2]$
Nozzle Throat Area	A_t	$[m^2]$
Quadratic Nozzle Shape Parameter	a	$\left[\frac{1}{mm}\right]$
Speed of Sound	a	$\left[\frac{m}{s}\right]$
Linear Nozzle Shape Parameter	b	$[-]$
Catalyst Bed Loading	CBL	$\left[\frac{kg}{m^2 \cdot s}\right]$
Injector Discharge Coefficient	C_d	$[-]$
Characteristic Velocity	C^*	$\left[\frac{m}{s}\right]$
Constant Nozzle Shape Parameter	c	$[mm]$
Bulk Coolant Specific Heat	c_{b_c}	$\left[\frac{J}{kg \cdot K}\right]$
Chamber Wall Specific Heat	c_w	$\left[\frac{J}{kg \cdot K}\right]$
Catalyst Diameter	D_{cat}	$[m]$
Combustion Chamber Diameter	D_c	$[m]$
Feed Line Hydraulic Diameter	D_H	$[m]$
Tank Inner Diameter	D_i	$[m]$
Tank Outer Diameter	D_o	$[m]$
Chamber/Nozzle Segment Diameter	D_{seg}	$[m]$
Chamber/Nozzle Segment Outer Diameter	$D_{o_{seg}}$	$[m]$
Throat Diameter	D_t	$[m]$
Hydraulic Diameter	d_h	$[m]$
Injector Orifice Diameter	d_i	$[m]$
Coolant Channel Hydraulic Diameter	d_{h_c}	$[m]$

Continued on next page

Roman Symbols – continued from previous page

Parameter	Symbol	Default Unit
Chamber/Nozzle Segment Length	dx	$[m]$
Darcy Friction Factor	f_D	$[-]$
Heat of Ablation	H_{abl}	$\left[\frac{J}{kg}\right]$
Chamber Coolant Side Heat Transfer Coefficient	h_{α_c}	$\left[\frac{W}{m^2 \cdot K}\right]$
Chamber Hot-gas Side Heat Transfer Coefficient	h_{α_g}	$\left[\frac{W}{m^2 \cdot K}\right]$
Specific Impulse	I_{sp}	$[s]$
Volume Flow Pressure Loss Factor	Kv	$\left[\frac{m^3}{h \cdot \sqrt{bar}}\right]$
Chamber Wall Thermal Conductivity	k	$\left[\frac{W}{m \cdot K}\right]$
Feed Line Bend Loss Coefficient	k_b	$[-]$
Coolant Thermal Conductivity	k_c	$\left[\frac{W}{m \cdot K}\right]$
Length	L	$[m]$
Combustion Chamber Length	L_c	$[m]$
Cylindrical Tank Section Length	L_{cyl}	$[m]$
Nozzle Divergent Length	L_d	$[m]$
Catalyst Length	L_{cat}	$[m]$
Characteristic Length	L^*	$[m]$
Catalyst Length-over-Diameter	L/D_{cat}	$[-]$
Nozzle Length fraction	Lf	$[-]$
Tank Length	L_t	$[m]$
Injector Orifice Length	l_i	$[m]$
Injector Spray Cone Length	l_{sc}	$[m]$
Mach Number	M	$[-]$
Ablator (Segment) Mass	m_{abl}	$[kg]$
Chamber Mass	m_c	$[kg]$
Tank Endcap Mass	m_{ec}	$[kg]$
Tank Fluid Mass	m_{fl}	$[kg]$
Pressurant Gas Mass	m_g	$[kg]$
Chamber/Nozzle Segment Mass	m_{seg}	$[kg]$
Tank Wall Mass	m_w	$[kg]$
Propellant Mass Flow	$\dot{m}$	$\left[\frac{kg}{s}\right]$
Tank Fluid Mass	$\dot{m}_{fl}$	$\left[\frac{kg}{s}\right]$

Continued on next page

Roman Symbols – continued from previous page

Parameter	Symbol	Default Unit
Coolant Mass Flow	$\dot{m}_c$	$\left[\frac{kg}{s}\right]$
Fuel Mass Flow	$\dot{m}_F$	$\left[\frac{kg}{s}\right]$
Oxidiser Mass Flow	$\dot{m}_O$	$\left[\frac{kg}{s}\right]$
Coolant Nusselt Number	Nu	$[-]$
Chamber Mean Molar Mass	n_c	$\left[\frac{kg}{mol}\right]$
O/F Ratio	OF	$[-]$
Ohnesorge Number	Oh	$[-]$
Cooling Channel Perimeter	P_c	$[m]$
Prandtl Number	Pr	$[-]$
Cooling Channel Prandtl Number	Pr_c	$[-]$
Pressure (generic)	p	$[Pa]$
Chamber Pressure	p_c	$[Pa]$
Maximum Decomposition Chamber Pressure	$p_{d_{max}}$	$[Pa]$
Nozzle Exit Pressure	p_e	$[Pa]$
Final Pressurant Pressure	p_{p_f}	$[Pa]$
Initial Pressurant Pressure	p_{p_i}	$[Pa]$
Catalyst Pores-per-inch	ppi	$[-]$
Nozzle Throat Pressure	p_t	$[Pa]$
Tank Pressure	p_t	$[Pa]$
Injector Pressure Drop	Δp_i	$[Pa]$
Feed Line Volumetric Flow	Q	$\left[\frac{m^3}{h}\right]$
Chamber/Nozzle Segment Heat Flow	Q_{seg}	$[W]$
Conducted Heat Flux	q_{cond}	$\left[\frac{W}{m^2}\right]$
Coolant Heat Flux	q_{cool}	$\left[\frac{W}{m^2}\right]$
Radiated Heat Flux	q_{rad}	$\left[\frac{W}{m^2}\right]$
Chamber Hot-gas Side Heat Flux	q_{w_i}	$\left[\frac{W}{m^2}\right]$
Gas Constant	R	$\left[\frac{J}{mol \cdot K}\right]$
Feed Line Bend Radius	R_b	$[m]$
Reynolds Number	Re	$[-]$
Coolant Channel Reynolds Number	Re_c	$[-]$
Pressurant Gas Constant	R_g	$\left[\frac{J}{mol \cdot K}\right]$
Throat Radius	R_t	$[m]$

Continued on next page

Roman Symbols – continued from previous page

Parameter	Symbol	Default Unit
Nozzle Divergent Round-off Radius	R_{l_d}	$[m]$
Chamber Convergent Round-off Radius	R_{l_c}	$[m]$
Inner Radius (generic)	r_i	$[m]$
Outer Radius (generic)	r_o	$[m]$
Injector Spray Cone Radius	r_{sc}	$[m]$
Safety Factor	SF	$[-]$
Coolant Bulk Temperature	T_{b_c}	$[K]$
Chamber Temperature	T_c	$[K]$
Chamber Wall Hot Gas Temperature	T_g	$[K]$
Nominal Thrust	T_{nom}	$[N]$
Nozzle Throat Temperature	T_t	$[K]$
Tank Temperature	T_t	$[K]$
Chamber Coolant-Side Wall Temperature	T_{w_c}	$[K]$
Chamber Hot-gas-Side Wall Temperature	T_{w_i}	$[K]$
Chamber Radiation-Side Wall Temperature	T_{w_o}	$[K]$
Ablator Thickness	t_{abl}	$[m]$
Tank Endcap Thickness	t_{ec}	$[m]$
Chamber Thermal Wall Thickness	t_w	$[m]$
Flow Velocity in Catalyst	u	$\left[\frac{m}{s}\right]$
Axial Flow Velocity in Chamber	u	$\left[\frac{m}{s}\right]$
Coolant Channel Flow Velocity	u_c	$\left[\frac{m}{s}\right]$
Chamber Volume	V_C	$[m^3]$
Cylindrical Tank Section Volume	V_{cyl}	$[m^3]$
Tank Spherical End Cap Volume	V_{ec}	$[m^3]$
Tank Fluid Volume	$V_f l$	$[m^3]$
Injection Velocity	V_{inj}, V_i	$\left[\frac{m}{s}\right]$
Tank Volume	V_t	$[m^3]$
Pressurant Tank Volume	V_{t_p}	$[m^3]$
Tank Ullage Volume	V_u	$[m^3]$
Throat-Divergent Transition Point x-coordinate	x_P	$[mm]$
Throat-Divergent Transition Point y-coordinate	y_P	$[mm]$

Greek

Table 2: Greek Symbols

Parameter	Symbol	Default Unit
Conical Nozzle Divergence Angle	α	$[^\circ]$
Specific Heat Ratio	γ	$[-]$
Chamber Specific Heat Ratio	γ_c	$[-]$
Nozzle Area Expansion Ratio	ϵ	$[-]$
Chamber Area Contraction Ratio	ϵ_c	$[-]$
Nozzle Flow Divergence Loss	ϵ_{div}	$[-]$
Coolant Channel Wall Roughness	ϵ_{w_c}	$[mm]$
Chamber Wall Emissivity	ε	$[-]$
HTP Concentration	η	$[-]$
Injector Spray Cone Angle	θ	$[^\circ]$
Feed Line Bend Angle	θ_b	$[^\circ]$
Initial Nozzle Parabola Angle	θ_P	$[^\circ]$
Final Nozzle Parabola Angle	θ_E	$[^\circ]$
Injector Friction Drag Coefficient	λ	$[-]$
Injector Flow Parameter	μ	$[-]$
Coolant Viscosity	μ_c	$[Pa \cdot s]$
Injector Viscosity	ν	$[Pa \cdot s]$
Oxygen Mass Fraction	ξ	$[-]$
Injector Inlet Coefficient	ξ_{in}	$[-]$
Injector Friction Parameter	ξ_{fr}	$[-]$
Injector Outlet Parameter	ξ_{1-c}	$[-]$
Density	ρ	$\left[\frac{kg}{m^3}\right]$
Injector Ambient Density	ρ_A	$\left[\frac{kg}{m^3}\right]$
Ablator Density	ρ_{abl}	$\left[\frac{kg}{m^3}\right]$
Chamber Density	ρ_c	$\left[\frac{kg}{m^3}\right]$
Coolant Density	ρ_c	$\left[\frac{kg}{m^3}\right]$
Tank Fluid Density	ρ_{fl}	$\left[\frac{kg}{m^3}\right]$
Pressurant Gas Density	ρ_g	$\left[\frac{kg}{m^3}\right]$
Nozzle Throat Density	ρ_t	$\left[\frac{kg}{m^3}\right]$
Chamber Wall Density	ρ_w	$\left[\frac{kg}{m^3}\right]$
Tank Wall Density	ρ_w	$\left[\frac{kg}{m^3}\right]$

Continued on next page

Roman Symbols – continued from previous page

Parameter	Symbol	Default Unit
Stefan-Boltzmann Constant	σ	$\left[\frac{W}{m^2 \cdot K^4}\right]$
Stress (generic)	σ	$[Pa]$
Yield Strength	σ_y	$[Pa]$
Hoop Stress	σ_θ	$[Pa]$
Maximum Hoop Stress	$\sigma_{\theta_{max}}$	$[Pa]$
Combustion Gas Dwell Time	τ	$[s]$
Catalyst Porosity	ψ	$[-]$

Abbreviations

Abbreviation	Meaning
AIT	Auto-ignition Temperature
HTP	High-test Peroxide

1

Introduction

Sounding rockets are a type of rocket that typically follows a sub-orbital trajectory and are utilised for various research purposes, such as atmospheric studies, microgravity research, and technological experiments [1]. Depending on the rocket's size, design, and mission requirements, they are usually launched to altitudes ranging from about 100 to 1,000 kilometres [2]. The term "sounding" originates from their initial purpose of probing the Earth's atmosphere, with one of their earliest applications being atmospheric research. Sounding rockets are also employed for technology demonstrations and testing new spacecraft components and systems, such as reentry vehicles, propulsion systems, and new materials for space use [3], [4]. Additionally, they serve educational and outreach purposes, offering hands-on experience for students in science and engineering fields [5].

Since sounding rockets are employed for various experiments, these diverse applications necessitate a wide range of requirements for each type of experiment. Some experiments, for instance, would benefit from increased control over the rocket's trajectory, such as extended time in specific atmospheric layers or sustained hypersonic flight. A steerable upper stage could provide significant advantages, such as longer experiment duration and more accurate simulation of real-world conditions. Currently, no such system exists in the field of sounding rocketry; upper stages are typically unguided and powered by uncontrollable solid rocket motors.

In the field of sounding rocketry, continuous advancements are being made to improve vehicle capabilities and performance. As a player in this industry, T-Minus Engineering is committed to enhancing its existing launch vehicles. Following the recent successful launch of the T-Minus Barracuda and earlier achievements with the T-Minus 216mm rocket motors, the next phase for this family of rockets is the development of an upper stage.

To leverage the benefits of an upper stage for the Barracuda sounding rocket beyond just increased apogee and velocity, T-Minus Engineering has decided to develop a controllable upper stage. This development is supported by emerging technologies within the company that could be integrated into such a system. Introducing a steerable upper stage would position the Barracuda at the cutting edge of innovation in the sounding rocketry industry. While there are already existing technologies within T-Minus Engineering that can be used for this upper stage like the recently developed staging mechanism or telemetry systems, one of the major points to be addressed for this upper stage is the propulsion system, which this work will focus on.

Based on a previous review of the current state of the sounding rocket industry, propulsion systems, and the technologies in T-Minus Engineering [6], a hydrogen peroxide decomposition-based propulsion system should be used for the steerable upper stage of the Barracuda rocket. This system offers decent efficiency while maintaining low complexity, fitting within the operational capabilities of T-Minus Engineering. Leveraging the technology demonstrator from the HyProp project will further reduce developmental complexity by utilising existing systems. Preliminary system requirements and research questions have been defined based on this approach.

Integrating this technology into a launchable upper stage will require design optimisation for performance and mass, guided by a numerical model. This model will be verified and validated to inform the detailed design. Ultimately, implementing a hydrogen peroxide decomposition-based propulsion system in the Barracuda's steerable upper stage will significantly benefit T-Minus Engineering, enhancing both current and future payloads and contributing to advancements in the sounding rocket industry.

1.1. Research Objective

Based on the previously introduced goals, the main research objective was derived as follows:

> *"Design, model, and mass-optimise a propulsion system for the steerable upper stage for the T-Minus Barracuda using hydrogen peroxide that falls within the operational and technological envelope of T-Minus Engineering"*

The objective firstly defines three aspects that need to be considered and thus defines the scope of this thesis project. The design of the propulsion system in this work will be advanced from the system-level conceptual stage to a subsystem-level detailed design. This work will not include the subsystem-level critical design, i.e. the stage required before entering manufacturing and testing of the first prototype system. This design then will be represented in a numerical model such that a design optimisation can be performed that optimises the design for the lowest mass.

Next to this, the objective also defines two high-level constraints for the design of the propulsion system. Firstly, since the preceding literature study [6] has shown that hydrogen peroxide provides significant benefits for these systems and that hydrogen peroxide is becoming more and more commonplace in propulsion systems of all types, the objective specifically stipulates the use of hydrogen peroxide as the oxidiser for this system. Next to this, the unique nature of the operations of T-Minus Engineering sets certain constraints on the design, which will elaborated in section 3.2. In order to gain tangible benefits from this system, these constraints must be accounted for in the design of this system.

1.2. Research Questions

Based on the previously established research question, four research questions were derived. Each of these four main questions has also been subdivided into three sub-questions to clarify the scope of the research further. The following section elaborates on the reasoning behind each question. The main questions and sub-questions are in table 1.1.

These questions will be re-addressed in chapter 8 to establish whether these questions can be answered based on this work, and if not chapter 9 will describe further future work to answer the research questions more clearly.

1.3. Approach

In order to answer the research questions and work towards the research objective, an approach to the thesis project needs to be defined. In this case, this will be done in 7 phases. These phases have been derived from the research questions and objectives. These phases follow each other sequentially.

1. **Analyse the design of the HyProp technology demonstrator:** To evaluate which of technologies from the HyProp technology demonstrator can be adapted for the Barracuda steerable upper stage, its design needs to be evaluated. The ultimate goal of this phase is to determine the technologies from the HyProp project, whose transfer into this upper-stage propulsion is beneficial to the design of the system. This phase is described in chapter 2.
2. **Generate a system architecture:** Based on the insights of the previous step, a concept architecture for the upper-stage propulsion system will be generated. This will include the layout of subsystems of the propulsion system as well as preliminary design choices or pre-selection of design choices for each of the subsystems. Ultimately, the preliminary design and architecture need to be developed up to the point that all remaining can reasonably represented in the numerical model. This phase is described in chapter 3.
3. **Develop a numerical model:** Once the system architecture and preliminary design are known, a numerical model of the upper-stage propulsion system will be created. This will be used to evaluate

Table 1.1: Research Questions and their Identifiers

Identifier	Requirement
RES-Q-1	*How can hydrogen-peroxide be used as a basis for the propulsion system of the Barracuda upper stage?*
RES-Q-1A	Can it be used in a bi-propellant system?
RES-Q-1B	Is a bi-propellant system advantageous over a mono-propellant system?
RES-Q-1C	Which technologies can be used to achieve decomposition?
RES-Q-2	*How can multiple parameter design optimisation methods be used to maximise the performance of the Barracuda upper-stage propulsion system?*
RES-Q-2A	How can such a propulsion system be numerically modelled?
RES-Q-2B	How can such a propulsion system be numerically optimised?
RES-Q-2C	Which parameters should it be optimised for?
RES-Q-3	*How can the Barracuda upper-stage propulsion system be integrated and interfaced with the existing Barracuda system?*
RES-Q-3A	Which constraints does the existing Barracuda system impose?
RES-Q-3B	Can the propulsion system provide the necessary performance?
RES-Q-3C	Can the propulsion system leave sufficient payload mass margin?
RES-Q-4	*How can the Barracuda upper-stage propulsion system be constructed and operated by T-Minus Engineering?*
RES-Q-4A	What are the technical limitations of T-Minus Engineering?
RES-Q-4B	What are the operational limitations of T-Minus Engineering?
RES-Q-4C	How does this technology require T-Minus Engineering to expand its capabilities?

the system performance and characteristics based on varying sizing parameters. This model primarily focuses on how the sizings of different subsystems affect each other and how they affect the propulsion system as a whole, especially the mass of the entire system. For each subsystem, a custom modelling approach will used. This phase is described in chapter 4.

4. **Verify the numerical model:** Once the numerical model has been constructed and before it can be used to optimise the design, the numerical model needs to be verified. The approach for this will include various unit testing as well as a comparison of certain modules to reference systems. This phase is described in chapter 5.
5. **Optimise the design:** The previously developed model will be used to optimise the design based on the requirements set out in chapter 3. This will be done using a suitable multi-disciplinary design optimisation method. The exact method will also be selected in this phase, based on the characteristics of the numerical model. This phase is described chapter 6.
6. **Validate the outcome:** After the design has been optimised, it needs to be validated. An approach for this will be determined at the beginning of this phase, and will ultimately determine how well and to which extent the design can be validated during this project. This phase is described in chapter 7.
7. **Conclusions and Recommendations:** Finally, the research questions will be revisited and answered based on the work performed in all the previous phases. This will be done in chapter 8. In case one or more questions cannot be conclusively answered, recommendations for future work will made in chapter 9 which will then ultimately allow these remaining questions to be answered. Additionally, chapter 9 will also include further recommendations on additional work and research which became evident throughout the project.

1.4. Scope

To keep the project within the defined limits, a scope should be defined for this work. Otherwise, there is a reasonable risk that the project will creep on while adding more and more analysis, while no conclusion or outcome is reached.

The literature study leading up to this research [6] defined the preliminary objective of the thesis based on the analysis of various key aspects and also determined the overall concept used for the propulsion system. This ultimately culminated in the research questions which were previously defined. Furthermore, this work resulted in preliminary propulsion system requirements, which will later on be refined into the system-level requirements and constraints.

The thesis work itself is defined by the phases in the previous section. This work is finalised when the design outcome of the work is analysed, and when based on revisiting the research questions conclusions are drawn and recommendations are made.

Deriving a critical design as well as a more in-depth and higher fidelity analysis of each subsystem is explicitly not part of the scope of the thesis project. Performing this work for each subsystem of the propulsion system would grossly exceed the scope of a thesis project. Rather this thesis project allows the opportunity to find an optimised design point in the highly multi-dimensional design space, by taking into account crucial characteristics of the system and requirements of the propulsion system. Future work like detailed subsystem design analysis (such as e.g. CFD of the chamber-nozzle gas flow), as well as detailed construction and validation testing, should be performed as part of future work on this propulsion system. The scope is visualised in figure 1.1.

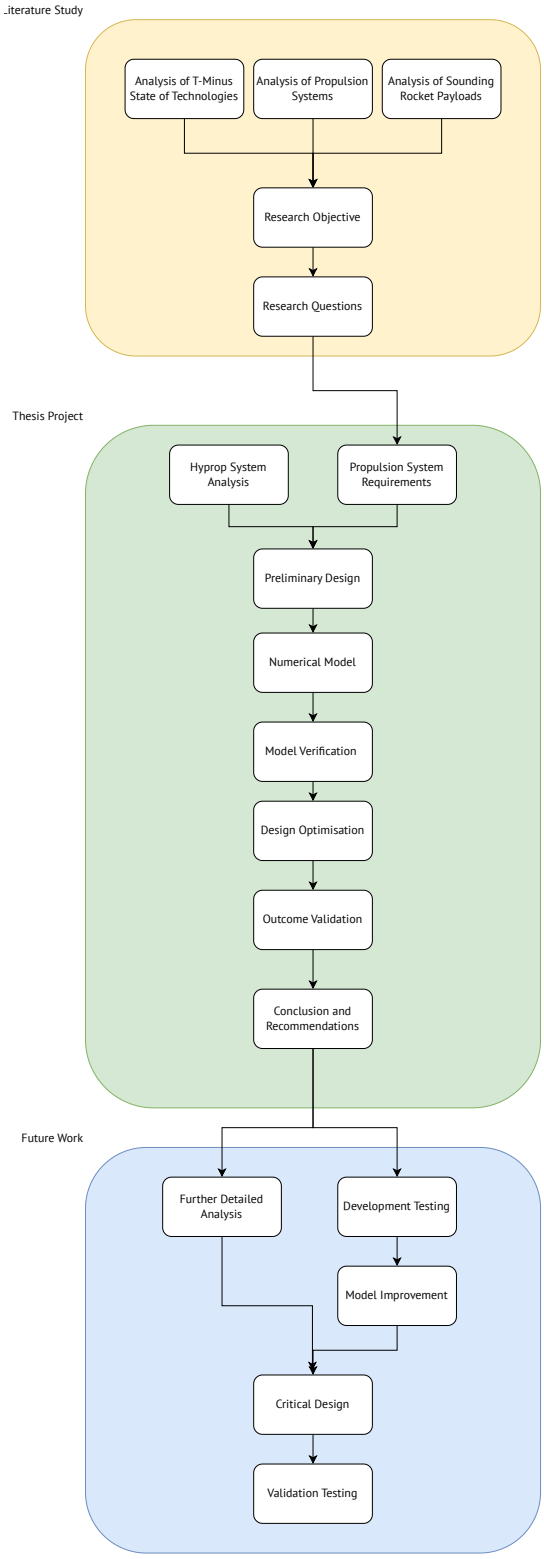

Figure 1.1: Scope of the Literature Study, Thesis Project, and Potential Future Work

2

HyProp System

The HyProp project is a collaboration between T-Minus Engineering and SolvGE. The project's goal is to develop a set of technology demonstrator thrusters based on the decomposition of high-concentration (>85%) hydrogen peroxide (also referred to as high-test peroxide or HTP). Since the HyProp project will deliver a large amount of fundamental insights into how an HTP-based propulsion system fits within the operational and technical constraints of T-Minus Engineering, the Barracuda Upper Stage Propulsion System's design will utilise as many of HyProps insights as possible.

2.1. Project Objectives

The HyProp project primarily functions as a research and development project to demonstrate the feasibility of T-Minus Engineering to develop liquid rocket engines and to advance the technology readiness level of key systems used in liquid rocket engines such as feed systems, control systems, manufacturing, propellant handling etc. Based on this, the HyProp project has the following objectives:

- **Gain experience with HTP handling:** The handling of HTP is associated with certain risks. While T-Minus Engineering is experienced in handling hazardous substances, this experience is mostly limited to the risks surrounding composite solid rocket propellants and pyrotechnics. The risks associated with HTP handling fundamentally differ from the previously mentioned risks, and the HyProp project provides an opportunity to familiarise with the operational requirements of HTP in a controlled environment.
- **Gain experience with designing for HTP compatibility:** HTP is a strong oxidiser. This quality makes it an excellent rocket propellant oxidiser, however, it also makes it prone to react with and degrade other materials. Therefore, the materials which come into contact with the HTP such as tank walls, feed lines, and seals need to be carefully selected for this. The HyProp project allows T-Minus to gain experience with which materials are well-suited and how these materials are processed and used in manufacturing.
- **Gain experience with producing HTP catalysts:** One of the major advantages of HTP is its ability to be catalysed into decomposition by various types of catalysts. To ensure consistent behaviour of the catalysts, the process of producing the catalysts needs to be thoroughly characterised and documented. Since the HyProp project provides a good opportunity for this, this has been deemed one of the major objectives of the project.
- **Gain experience with liquid rocket engines:** Before the start of the HyProp project, T-Minus Engineering has only developed solid rocket motors. Both the HyProp technology demonstrator and all systems derived from it will be liquid rocket engines which fundamentally differ from solid rocket motors. Since the HyProp technology demonstrator is the first liquid rocket engine developed by T-Minus Engineering, the project will also serve to provide T-Minus Engineering with practical first-hand experience on how to design, manufacture, construct, and operate a liquid rocket propulsion system.
- **Lay groundwork for future applications:** Ultimately, the goal of the HyProp technology demonstrator

(a) Initial Decomposition **(b)** Fully Developed Decomposition

Figure 2.1: HTP Decomposition Drip Test on Nickel-Manganese-Oxide Catalyst

is to lay the groundwork for future uses of this technology onboard sounding rocket. While the HyProp technology demonstrator will remain a ground-based test bed, the experiences gained from it described above as well as various other minor insights will allow for the technology developed in this project to be utilised in future systems such as an upper stage for the Barracuda rocket.

2.2. Project Plan

The HyProp project is divided into three major development phases:

1. Catalyst Development and Testing
2. Monopropellant Thruster Development
3. Bipropellant Development

During the first phase, the catalyst design was determined and production methods were trialled and optimised. The catalyst design was based on previous in-depth research into catalyst types [7]. Based on this, the selected catalyst design is made from a nickel sponge, which is coated with a Manganese Oxide coating. This catalyst type has been shown to produce decomposition temperatures above 700 ° C. With the first in-house produced prototypes of the catalyst beds, drip tests were performed to verify its ability to decompose HTP catalytically. These tests are shown in figure 2.1.

Once this phase is completed, the next phase is the development of a set of monopropellant thrusters. This will allow the characterisation of catalyst characteristics under various catalyst bed loading, pressure and catalyst geometries. Next to this, this monopropellant thruster system will also include the first pressurised propellant feed system using HTP design and used by T-Minus Engineering. These phases can thus also be used to gain experience with the design, construction and operation of feed systems. The preliminary design for the smaller size monopropellant thruster can be seen in figure 2.2.

This thruster will especially characterise pressure drop and temperature gain over the catalyst bed. This information can be implemented in the numerical model to more accurately model the behaviour of the flow through the catalyst. Next to this, it can also be used to validate the injector model and After this thruster, another thruster will likely be designed. It will be sized according to the catalyst size required for the propulsion system of the Barracuda upper stage. This system can then be used to validate the decomposition chamber design of the propulsion system design for the Barracuda upper stage.

Finally, a bipropellant engine will be developed based on the second monopropellant. While this thruster will be intended as a ground testing system, it will incorporate as many design characteristics from the propulsion system design of this project as possible. This will ultimately allow for near-complete validation of the entire numerical model.

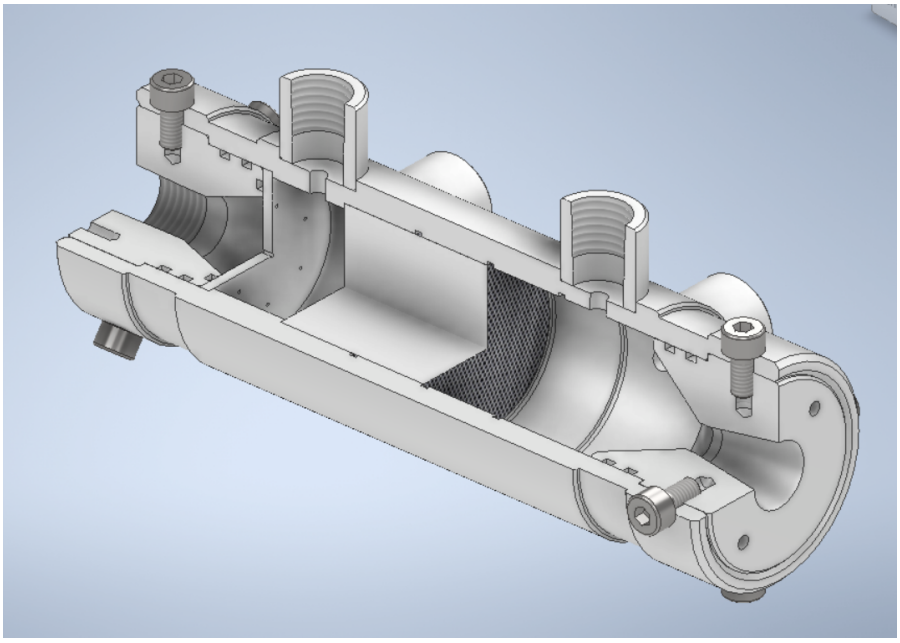

Figure 2.2: HyProp Monopropellant Catalyst Characterisation Test Bed

2.3. Current Status

Currently, the project is in the second phase, constructing the prototype small-scale monopropellant thruster for catalyst bed characterisation. Unfortunately, the first testing will likely only occur after the conclusion of this thesis project. Therefore, its insights cannot be used in this work, but once the catalyst has been characterised, this data can be used to make a model which can be substituted into the numerical model.

2.4. Conclusion

From this phase, three major conclusions can be drawn for the following work on this project. First of all, analysing the HyProp project has shown that there are existing technologies in T-Minus Engineering for the manufacturing of catalyst beds capable of catalysing the decomposition of HTP. This means that choosing HTP as an oxidiser for this propulsion system is preferable as the existing technology strongly supports this compared to other oxidisers. Next to this, the existing catalyst technology should be taken advantage of by using the auto-igniting properties between the decomposition products of HTP and a low-AIT fuel.

Next to this, it can also be concluded that not only is the design of the Barracuda upper-stage propulsion system influenced by the HyProp, but in the same manner, this project influences design decisions in the HyProp project. Especially for later stages of the development of the Barracuda upper-stage propulsion system, the HyProp project should be extensively used as a test-bed for the work of this project, also later outside the scope of the thesis project work.

Finally, due to the delays in the HyProp project, it is not possible to implement the results of the small-scale monopropellant thruster into the numerical model of this thesis project. Therefore, a surrogate model will have to be found for this, which can be replaced by the custom-built model based on experimental once this data becomes available.

The HyProp project has strongly guided the conceptual design of the upper stage and will be used in the development of this propulsion system as a test bed and validation platform.

3

Propulsion System Preliminary Design

The primary goal of this project is to design and size the propulsion system for the upper stage of the Barracuda sounding rocket and to optimise the design to maximise payload capacity. Since it is unfeasible to generate a propulsion system model that can consider all possible design choices, some preliminary and/or higher-level design choices need to be made. More intricate lower-level design choices can then be made during or after the design optimisation process. Hence, this chapter will describe the preliminary design process for the propulsion system of the Barracuda Upper Stage.

Sections 3.1 and 3.2 will define and elaborate on the requirements and constraints of the propulsion system. After this, section 3.3 describes the conceptual design of the propulsion system. Section 3.4 contains the oxidiser selection and fuel pre-selection. Section 3.5 will lay out the chosen propulsion system architecture and subsystem division. Finally, section 3.6 will define the preliminary design for each subsystem to the extent required for the numerical model.

3.1. Requirements

Based on the preliminary requirements of the propulsion system [6], T-Minus Engineering defined the requirements for the propulsion system. These can be found in table 3.1.

Table 3.1: Propulsion System Requirements [6]

Identifier	Requirement
PROP-REQ-1	The propulsion system shall provide at least 600 N of peak thrust.
PROP-REQ-2	The propulsion system shall provide peak thrust for at least 60 seconds.
PROP-REQ-3	The propulsion system shall be extinguishable.
PROP-REQ-4	The propulsion system shall be re-ignitable.
PROP-REQ-5	The propulsion system shall be optimised to minimise mass.
PROP-REQ-6	The propulsion system shall utilise existing technologies within T-Minus Engineering.
PROP-REQ-7	The propulsion system shall be produced by T-Minus Engineering.
PROP-REQ-8	The propulsion system shall integrate into the existing Barracuda rocket system.
PROP-REQ-9	The propulsion system shall interface with the other subsystems on the Barracuda steerable upper stage.

Each of the requirements derives from the needs and constraints that T-Minus Engineering imposes on the propulsion system. Each of them is justified as follows:

- **PROP-REQ-1:** The peak thrust is determined based on high-altitude hovering being one of the primary applications. Barracuda can launch 40 kg to approx. 100 km. This means that at its earliest stage, the Barracuda upper stage will need to be able to hover this weight (approx. 400 N). However, to still be able to perform corrections, the peak thrust should be higher than this weight. Hence 600 N was selected as the minimum peak thrust to allow for these corrections.
- **PROP-REQ-2:** This is based on similar order of magnitude hovering times which can be seen in the trajectory development for the DLR High Altitude Soarer [8], [9]. When assuming a propellant mass of 10 kg, this would require a specific impulse of roughly 185 s from the propulsion system, which is realistically attainable.
- **PROP-REQ-3:** Since the propulsion system might need to be extinguished at precise times before all the propellant is used up, e.g. for precise hypersonic flight conditions.
- **PROP-REQ-4:** Similarly, since the propulsion system might be used to both boost apogee and hover or for more complex hypersonic trajectories, re-ignition capabilities are required.
- **PROP-REQ-5:** To maximise the performance of the propulsion system, and by extensions of the upper stage, the design should be optimised to fulfil the requirements while being as light as possible.
- **PROP-REQ-6:** To accelerate the development process and to keep developmental complexity low, the propulsion system should use as many existing technologies as possible.
- **PROP-REQ-7:** This requirement ensures that any design decision made for this propulsion system will keep in mind the production constraints of T-Minus Engineering.
- **PROP-REQ-8:** The propulsion system must be able to integrate with the already existing technology of the Barracuda sounding rocket. This includes physical, but also performance and operational constraints.
- **PROP-REQ-9:** The propulsion system must be able to interface with the other subsystems onboard the Barracuda sounding rocket. This includes e.g. electronics subsystems, structural subsystems, etc.

It should be noted that these requirements are not solely defined for the work in this thesis project, but also serve as system requirements for the remainder of the development of the upper-stage propulsion system. This also means that not all requirements may be validated at the end of this project. However, if this is the case, then recommendations will be presented for the future validation of these requirements.

3.2. Constraints

The propulsion system for the Barracuda Upper Stage must interface with the other subsystems of the Barracuda Upper Stage and the Barracuda sounding rocket itself. Additionally, the propulsion system must also fit within the operational constraints of T-Minus Engineering. This imposes specific constraints on the propulsion system, which need to be considered both when generating a preliminary design and later when defining the envelope in which the propulsion system can be optimised.

3.2.1. Constraints from Barracuda

The design of the Barracuda rocket is the primary source for all design constraints that revolve around the integration of the propulsion system in an upper stage for this rocket. This subsection discusses and summarises the relevant constraints on the propulsion system.

Most fundamentally, the propulsion system must physically fit inside the airframe of the rocket. In the current design specification, the Barracuda rocket's payload section consists of a composite-material tube and supports an internal diameter of 0.2 [m]. Thus any internal layout of the propulsion system must fit within this constraint imposed by the internal diameter. Furthermore, this airframe tube is currently not designed to be a pressure vessel and is not compatible with HTP. Hence, the actual tanks for fuel, oxidiser, and pressurant must be independent of this airframe tube. This ultimately means that the available internal diameter does not directly translate into e.g. fuel tank internal diameter, but must take into account tank wall thicknesses, feed lines, etc.

On top of this, the propulsion system must also withstand the launch loads during the first stage burn before the upper stage takes over. As a sounding rocket, Barracuda can sustain acceleration beyond 15 g for the majority of its burn time. Next to this, since the first stage of the Barracuda is propelled by a solid

rocket motor, there are immense vibrational loads during the initial first stage powered flight phase. Finally, the propulsion system should not be sensitive to the thermal environment of the rocket during burn-out.

3.2.2. Operational Constraints

The Barracuda rocket can be launched from any location that allows for rocket launches. This is one of the unique selling points of the system and is enabled by the high agility of the mobile launching infrastructure. Therefore, the upper stage for Barracuda should fit within this framework and should be designed with this in mind.

The propulsion system for the upper stage therefore cannot require extensive ground support infrastructure, and the infrastructure that is required needs to be fully mobile like the remainder of the launch installation. Next to this, the propulsion system should be assembled and operated by as few personnel as possible, since the small size of T-Minus Engineering does not allow for large numbers of personnel at a launch campaign.

Finally, the design should always consider the manufacturing envelope of T-Minus Engineering. This does not mean that the system must be fully in-house manufacturable, but the impact of design decisions on manufacturability in-house or externally should be factored in if appropriate.

3.2.3. Propulsion System Design Constraints

Gathering the hardware and operational constraints described in sections 3.2.1 and 3.2.2, a set of design constraints for the propulsion system for the Barracuda Upper Stage can be defined. Some of these were also derived from the preliminary propulsion system requirements [6]. These can be found in table 3.2.

Table 3.2: Propulsion System Constraints

Identifier	Requirement
PROP-CON-1	The propulsion system cannot exceed 0.2 [m] in diameter
PROP-CON-2	The propulsion system must withstand the launch loads of the Barracuda first stage
PROP-CON-3	The propulsion system must withstand the thermal environment during the launch
PROP-CON-4	The propulsion system must not require any permanent ground support infrastructure
PROP-CON-5	The propulsion system shall require no more than 3 personnel to prepare and operate during a launch

- **PROP-CON-1:** The propulsion system must physically fit within the launch vehicle. While it is possible to adjust the length of the upper stage to accommodate e.g. longer tanks, it is not possible to increase the launcher diameter without creating an unacceptable amount of design uncertainty.
- **PROP-CON-2:** Since this upper stage propulsion system is launched on the Barracuda first stage, it needs to withstand the acceleration, rotational, and vibrational loads of the launch.
- **PROP-CON-3:** Especially during hypersonic flight (which is one of the proposed applications for this system [6]), thermal loading can often become the more critical load case over mechanical loading. Therefore, it is important to consider this in the design of the propulsion system and if necessary, define a safe envelope.
- **PROP-CON-4:** To fit into the T-Minus' philosophy of requiring minimal launch infrastructure and being able to launch wherever the mission requires, all the ground support equipment for the propulsion system needs to be mobile.
- **PROP-CON-5:** Limiting the operational personnel required allows the propulsion system to be operated within the operational envelope of T-Minus Engineering. With launch campaign personnel usually around 6-8 personnel, 3 personnel dedicated to the upper stage system was decided to be the constraint imposed by T-Minus Engineering.

Similar to the requirements, some constraints might not be validated as part of this thesis project. If this is the case, then recommendations will be presented to ensure their future validation.

3.3. Conceptual Design

One of the key aspects of this upper-stage propulsion system for the Barracuda rocket is the utilisation of the high-test peroxide (HTP) as an oxidiser. HTP generally refers to hydrogen peroxide with a concentration of above 85%. While higher concentrations could feasibly be used in the future, the current design of the propulsion system is planned to use a concentration of 80%, mostly due to limitations from the supplier. **PROP-REQ-9** requires that the propulsion system shall built upon and/or utilise existing or emerging technologies from T-Minus Engineering since this will reduce development time and project complexity. This becomes especially relevant when considering that this propulsion system in conjunction with the HyProp project is T-Minus Engineering's first venture into the field of liquid rocket engines.

The HyProp project, described in chapter 2, has already been advancing the experience and knowledge of utilising HTP for rocket propulsion. Furthermore, this oxidiser has relatively good handleability, compared to other oxidisers like nitrous oxide, nitrogen tetroxide, or liquid oxygen while still retaining good performance as an oxidiser [10]. Apart from this, the major advantage of the use of HTP is its ability to decompose into water (in the form) and gaseous oxygen exothermically.

Theoretically, the products of the HTP decomposition reaction can already be used to produce thrust, without adding any form of fuel. The reaction produces steam and gaseous oxygen and when catalysed using a Manganese-oxide-nickel catalyst bed, the products can reach a temperature of roughly 700° C [7]. Expanding these gases through a nozzle will already produce a specific impulse of 150-160 s [11].

However, the addition of fuel can drastically increase the release of energy through the decomposition-combustion process, thus improving specific impulse and reducing the required propellant mass for a given thrust level and burn time. Usually, however, this comes with the drawback of needing to create a source of ignition for the propellant mixture, which can limit re-ignitability. When using the HTP decomposition process, however, this need can be circumvented by utilising a fuel with an auto-ignition temperature below 700° C. If fuel is injected into the hot, oxygen-rich environment created by the products of the HTP decomposition, it will combust and release even more energy, ultimately increasing chamber temperature and thus specific impulse. If this is achieved, it makes the selected propellant combination quasi-hypergolic. For this mechanism to work, the fuel must be carefully selected. This process will described in section 3.4.2.

Since reducing complexity is one of the main drivers behind the system requirements [6], using this mechanism in the Barracuda Upper Stage propulsion system will greatly help reduce design and operational complexity while still benefiting from a liquid bi-propellant propulsion system. Similar systems have been already developed for static test applications [12]–[14], but no system like this has been designed for the use on a sounding rocket or launcher upper stage yet.

3.4. Propellant Pre-Selection

One of the earliest design decisions made for a rocket propulsion system is the propellant selection. This selection must be made early on in the design process since the design of nearly all subsystems of the propulsion system is at least to some extent dependent on this selection. A liquid rocket engine utilises a liquid oxidiser and a liquid fuel, which together make up the propellant. This section discusses the process of selection for the oxidiser and fuel as well as a brief overview of the main characteristics of both fuel and oxidiser.

3.4.1. Oxidiser

A primary aspect of this research is utilising the technology around HTP currently emerging within T-Minus Engineering. This propulsion system will be the first liquid bi-propellant rocket engine made by T-Minus Engineering and given the operational and developmental constraints, HTP is the preferred oxidiser for this system since it comes with several advantages because of this. While the oxidiser is thus already selected, the main benefits of the use of HTP for this application should be determined to confirm that using HTP for this purpose is a viable solution. Therefore, this subsection will list the key advantages of using HTP in this application.

Previous Experience

Firstly, the HyProp project will provide important groundwork for the HTP handling and supply infrastructure within T-Minus Engineering and the experience from the project can be used in later-on designs. Additionally,

the results of the project will allow for accurate validation of design tools, so utilising HTP in the upper stage of the Barracuda rocket harnesses the maximum benefit from this previous work. This is further elaborated in chapter 2.

Catalytic Decomposition
The catalytic decomposition of HTP will enable the leveraging of the auto-igniting properties so long as a suitable fuel is selected. This can significantly simplify the construction and operation of the engine and allow for a large number of re-lights without a specialised ignition system. Another aspect that is simplified by this property is valve timings. This is notoriously one of the most challenging aspects of liquid rocket engines. However, when utilising these auto-ignition processes, the engine can simply be run first as a monopropellant thruster, and fuel can be added once the monopropellant flow has stabilised [13]. This mitigates the likelihood of a hard start.

Operational Advantages
Firstly HTP is liquid at room temperature atmospheric conditions (298 [K], 1 [atm]) and non-cryogenic. This significantly simplifies operations around propellant handling and loading. The non-cryogenic nature allows for simplified transport at room temperature rather than complex cryogenic containers and management systems used for e.g. Liquid Oxygen. Similarly, since HTP is liquid at atmospheric conditions, it can be loaded de-pressurised which requires less automated systems than e.g. loading Nitrous Oxide. Finally, its high density of HTP (see table A.17) HTP is more compact in storage than many other oxidisers.

Environmental Benefits
Finally, because the Hydrogen Peroxide is chemically close to water, a large mass fraction (>65%) of the exhaust gas is composed of gaseous water. This of course has benefits from an environmental point of view, since the pollution created is very low. When pure hydro-carbon is used as fuel, the other major component of exhaust gasses is carbon dioxide. Therefore, using HTP likely produces no toxic exhaust products, which is a major advantage compared to systems using hypergolic propellants such as e.g. hydrazine-dinitrogen tetroxide.

3.4.2. Fuel

One of the key points of the chosen propulsion system concept is to utilise the unique properties of the decomposition of HTP and its products. In the case of the fuel selection, this means that the exothermic decomposition can be used to auto-ignite the fuel-oxidiser mixture. To achieve this, the auto-ignition temperature (AIT) of the selected fuel should be lower than 400-500° C. This requirement must be fulfilled for the chosen system concept to be functional. Apart from this, there are also other secondary constraints and considerations to be taken into account such as inherent handling complexity, hazards, cost, sourcing, and existing thermo-chemical models.

Thus the chosen approach is to compile a list of fuels with the adequate AIT and then reduce the number of options based on the other constraints. The initial list of potential fuels was collected from substances typically used as rocket fuels and other hydro-carbons that are used in combustion reactions. The list can be found in table 3.3.

While all of these fuels could theoretically be used for this application, there are some additional criteria by which the list of applicable fuels can be shortened. It should be noted that the chemical formula representations of Jet A, Kerosene and Gasoline are based on their average molecule composition. In reality, they are composed of various long-chain carbon molecules. The representation is equivalent to the representation in their thermo-chemical model.

Firstly, the auto-ignition temperature of each fuel candidate should be below 400-500° C. While the decomposition products of HTP usually have a temperature of around 700° C or more, the temperature drop during the mixture must be taken into account. While the steam/GOX mixture is injected at above 700° C, the fuel is assumed to be injected at 25° C. Thus the mixture will have some equilibrium temperature. If this equilibrium temperature is below the AIT of the fuel, then the fuel might not be ignited, requiring an ignition system and thus removing one of the major advantages of this concept. The exact limit temperature depends on the fuel since it is affected by the thermodynamic properties of the fuel as well as the ideal O/F ratio of the propellant combination.

Table 3.3: Initial list of fuel candidates [15]

Fuel Name	Formula	AIT [° C]	Liquid at 1 bar, 298 K	Thermo-chemical Model
Ethanol (100%)	C_2H_5OH	363	Yes	CEA
Methanol (100%)	CH_3OH	464	Yes	CEA
Butanol	C_4H_9OH	343	Yes	RPA
Triethylamine	$C_6H_{15}N$	312	Yes	RPA
Heptane	C_7H_{16}	204	Yes	RPA
Jet A	$C_{12}H_{23}$ (in CEA)	210	Yes	CEA
Anniline	$C_6H_5NH_2$	615	Yes	RPA
Benzene	C_6H_6	429	Yes	RPA
1-butene	C_4H_8O	385	Yes	RPA
Ethylene Oxide	C_2H_4O	429	Yes	RPA
Isopropyl Nitrate	$C_3H_7NO_3$	300	Yes	RPA
Kerosene	$C_1H_{1.9532}$ (in CEA)	210	Yes	CEA
Acytelene	C_2H_2	305	No	CEA
Ethylene	C_2H_4	543	No	RPA
Ethane	C_2H_6	515	No	RPA
Propylene	C_3H_6	458	No	CEA
Butane	C_4H_{10}	405	No	RPA
Acetonitrile	CH_3CN	523	Yes	RPA
Nitromethane	CH_3NO_2	418	Yes	CEA
Gasoline	C_8H_{18} (in CEA)	280	Yes	CEA
Ammonia	NH_3	651	No	CEA
Diborane	B_2H_6	38	No	CEA

Next to this, each fuel candidate should be liquid at room temperature atmospheric conditions. This requirement predominantly stems from the added operational complexity of fuels which require pressurisation to be liquid. This means fuel loading would need to occur under pressurisation. This adds complexity in terms of ground system requirements and presents an added risk to the system. Thus is it advantageous if the fuel, like the HTP oxidiser, can first be loaded under atmospheric conditions, and then be pressurised after the propellant loading. This also loosens requirements on ground support infrastructure. Additionally, using a liquid at atmospheric conditions fuel allows for a wider range of pressures and pressure drops without risking encountering two-phase flow, where the fuel changes state from liquid to gaseous as it passes through the feed system or injector. This is especially useful in light of throttling the propulsion system.

Finally, in order to perform an optimisation, the fuel should have an existing thermo-chemical model. Ideally, this model exists in the RocketCEA fuel library [16], since this model is used. Since the primary goal is to create a model that can be optimised, the design of the propulsion should be such that the modelling of said system falls within the scope of this project.

Based on the above-described logic, a pre-selection of 6 fuel candidates was made. This can be found in table 3.4. The upper part of the table shows the pre-selected fuels, namely Ethanol, Jet A, Kerosene, Gasoline, Methanol, and Nitromethane. These were selected based on each of them fulfilling the three primary requirements outlined previously for the fuel selection. Some additional characteristics can be found in table 3.5 and more detailed information used in their modelling can be found in appendix A.2.

3.5. System Architecture

At this point, the overall concept for the propulsion system has been defined. The propulsion system will utilise the decomposition properties of HTP to auto-ignite the propellant mixture and thus remove the need for any form of ignition system. This means a reduction in system complexity and a reduction in operational restrictions since there is no restriction on the number of ignitions performed. The propulsion system requires multiple subsystems which serve various purposes such that the propulsion system can

Table 3.4: Pre-selected list of fuel candidates [15]

Fuel Name	Formula	AIT [° C]	Liquid at 1 bar, 298 K	Thermo-chemical Model
Ethanol (100%)	C_2H_5OH	363	Yes	CEA
Jet A	$C_{12}H_{23}$ (in CEA)	210	Yes	CEA
Kerosene	$C_1H_{1.9532}$ (in CEA)	210	Yes	CEA
Gasoline	C_8H_{18} (in CEA)	280	Yes	CEA
Methanol (100%)	CH_3OH	464	Yes	CEA
Nitromethane	CH_3NO_2	418	Yes	CEA
Butanol	C_4H_9OH	343	Yes	RPA
Triethylamine	$C_6H_{15}N$	312	Yes	RPA
Heptane	C_7H_{16}	204	Yes	RPA
Anniline	$C_6H_5NH_2$	615	Yes	RPA
Benzene	C_6H_6	429	Yes	RPA
1-butene	C_4H_8O	385	Yes	RPA
Ethylene Oxide	C_2H_4O	429	Yes	RPA
Isopropyl Nitrate	$C_3H_7NO_3$	300	Yes	RPA
Acytelene	C_2H_2	305	No	CEA
Ethylene	C_2H_4	543	No	RPA
Ethane	C_2H_6	515	No	RPA
Propylene	C_3H_6	458	No	CEA
Butane	C_4H_{10}	405	No	RPA
Acetonitrile	CH_3CN	523	Yes	RPA
Ammonia	NH_3	651	No	CEA
Diborane	B_2H_6	38	No	CEA

Table 3.5: Details of pre-selected fuels

Fuel Name	Formula	AIT [° C]	Density $\left[\frac{kg}{m^3}\right]$	Cost $\frac{\$}{kg}$
Ethanol (100%)	C_2H_5OH	363	789	5.06
Jet A	$C_{12}H_{23}$ (in CEA)	210	775	1.55
Kerosene	$C_1H_{1.9532}$ (in CEA)	210	820	3.05
Gasoline	C_8H_{18} (in CEA)	280	690	2.90
Methanol (100%)	CH_3OH	464	792	14.52
Nitromethane	CH_3NO_2	418	1137	75.64

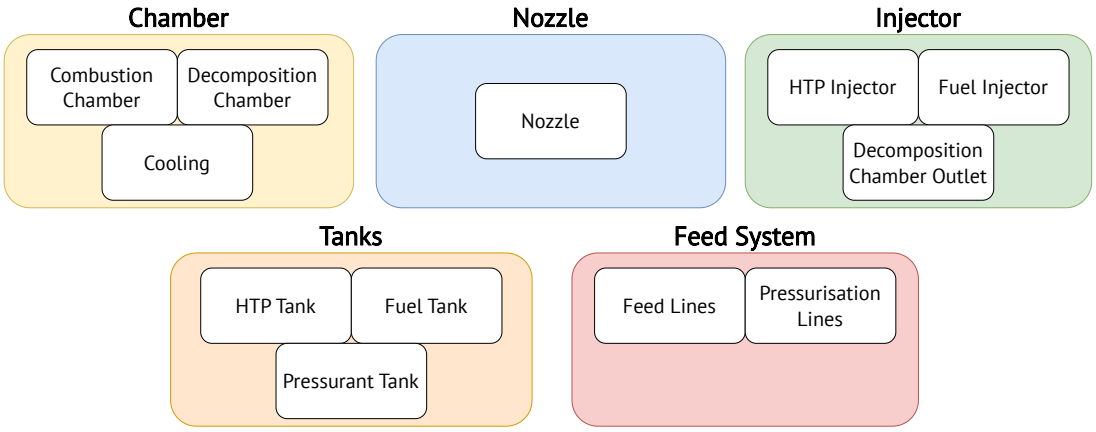

Figure 3.1: Subsystem Architecture

ultimately be functional and fulfil the previously defined requirements.

Since the propulsion system utilises the HTP decomposition process, it will require both a decomposition and combustion chamber. The decomposition chamber will contain the catalyst as well as an injector for the HTP and an outlet that leads the decomposition products of the HTP into the combustion chamber. Downstream of the decomposition chamber will then be the combustion chamber. The combustion chamber contains the fuel injector and once the fuel is injected, it can mix and auto-ignite with the decomposition products. Since the combustion temperatures and expected to be more than 2000° C, the combustion chamber will require some form of thermal management. Finally, the chamber will directly lead into the nozzle of the propulsion system.

Next to this, the design of the propulsion system also entails the design of the overall feed system, this being the system that stores and feeds the propellants into the chamber. This includes tanks, valves, feed lines and propellant feeding systems. In the propulsion system, this will be split between the feed subsystem and the tank subsystem, the former contains all the feed hardware such as feed lines or valves, and the latter will contain the tanks for fuel, HTP, and pressurant.

The distribution of the subsystems is visualised in figure 3.1.

3.6. Subsystem Preliminary Design

The goal of this research is to design, model, and optimise an upper-stage propulsion system. To perform an optimisation, a model is required that can be optimised. An optimisable model entails that there are some design decisions which can be adjusted to find the optimum design according to the defined fitness function. However, since it is impractical to model every propulsion system layout imaginable, certain design decisions need to be made before a model of the system can be created.

3.6.1. Chamber

The chamber subsystem contains the decomposition chamber, the combustion chamber, and the cooling solution applied to both of these chambers. The chamber subsystem is the part of the propulsion system where the actual chemical reactions that ultimately produce thrust take place. This section will address the preliminary design of each of these three components of the chamber subsystem.

Decomposition Chamber

The decomposition chamber contains the catalyst which catalyses the exothermic decomposition of the HTP into gaseous oxygen and steam. This section will treat its layout as well as the catalyst type selection.

To determine the design of the catalyst chamber, the design of it can be treated similarly to a monopropellant thruster. The only difference between the decomposition chamber in this propulsion system and a conventional monopropellant thruster is that instead of a nozzle, this system will have an outlet that does not choke the flow and instead directs it into the combustion chamber. For HTP, generally, cylindrical

Figure 3.2: Initial Production Test Items of the Manganese-Oxide coated Nickel catalyst bed

Table 3.6: Catalyst Bed Properties

Property	Value
Pores per inch	$17 - 23\ [ppi]$
Average Pore Diameter	$0.9\ [mm]$
Average Density	$0.3 - 0.6\ \left[\frac{kg}{m^3}\right]$
Average Porosity	$95.2\ [\%]$
Specific Surface	$1600\ \left[\frac{m^2}{m^3}\right]$

catalyst beds are used [11]. The catalyst bed is then primarily defined by its diameter and its length. The diameter is generally sized by sizing for a certain catalyst bed loading, which is the HTP mass flux on the catalyst. The length is then determined through a length-over-diameter ratio which ensures complete decomposition.

Next to this, the major design choice that needs to be made to model this subsystem of the propulsion system is the choice of the catalyst bed type. Commonly, monopropellant engines use catalyst beds made from pellets or foams made from Silver [11] or metals like Palladium, Platinum, and Rhodium [17].

However, another material that is commonly used for catalysts is Nickel [7]. Through the HyProp project, T-Minus Engineering has developed a method to produce a Manganese-Oxide coated Nickel catalyst. This catalyst has been proven to decompose HTP to temperatures sufficient for the auto-ignition with the fuels selected. Initial production test items of this catalyst type can be seen in figure 3.2.

Since one of the primary goals of the project is to utilise existing technologies within T-Minus Engineering, especially from the HyProp project, the Manganese-oxide-coated Nickel catalyst should be used, since it is able to decompose the HTP to the required extent and the supply and production lines for this component are already well established. Some of the properties of this catalyst bed can be found in table 3.6.

Combustion Chamber

This combustion chamber is part of the propulsion system where the fuel and the HTP decomposition products are mixed and combusted. The main high-level design decisions include the geometry of the chamber. There are various shapes of thrust chambers that have been used in the past, a selection of these can be seen in figure 3.3. The most common one out of all of these is the cylindrical chamber. It provides the simplest geometry for manufacturing and integration and is readily used, thus there is a large array of sizing and modelling methods for this chamber.

The conical and tubular chamber designs were disregarded since they are mostly intended for rocket engines without a nozzle. However, this engine is intended to be optimised for performance and low mass, a nozzle-less engine would waste the opportunity to harness some of the thermal energy in the combustion gases for improved specific impulse, therefore increasing the size/mass of the propulsion system. Because of these factors, these two chamber geometries are not feasible to be used in this propulsion system.

The pear-shaped chamber design is most commonly used on high-thrust rocket engines such as the Space Shuttle Main Engine (SSME) [19]. Following requirement **PROP-REQ-1**, the propulsion designed in this work falls much closer to a low-thrust rocket engine, and thus considering this combined with the increased geometry complexity, this thrust chamber geometry is also discarded

Finally, only the spherical and cylindrical thrust chambers as design options. The spherical chamber uses the least material for a given volume and is the most efficient at carrying the pressure loads of the combustion process. The cylindrical chamber meanwhile can integrate better into a cylindrical rocket fuselage and is simpler to manufacture and integrate with other systems.

The combustion chamber in this propulsion system needs to integrate with the decomposition chamber, which is also cylindrical. Additionally, **PROP-REQ-7** stipulates that the propulsion system design should account for the operational and manufacturing constraints of T-Minus Engineering. While this does not mean that all manufacturing of the flight system needs to be done in-house (e.g. if metal additive manufacturing techniques are used), it is advantageous to have the capability of in-house manufacturing for the ground testing version system, to allow for quick iteration.

Therefore, the chosen chamber geometry is a cylindrical chamber. The exact sizing methodology for the chamber geometry will be elaborated in section 4.4.4.

Cooling

Liquid rocket engines are some of the most challenging rocket engine types when it comes to their thermal management. Unlike solid rocket motors which can be operated with relatively few thermal considerations, a liquid rocket engine (especially one with sustained burnt times) needs to have precautions to direct the heat that is fed from the combustion chamber gases into the chamber walls. Ultimately, the goal of the cooling system is to ensure that the maximum rated temperature of chamber wall materials is not exceeded to ensure that the engine can withstand the combined thermal and mechanical loading.

Various cooling methods are commonly used in rocket engines which are considered for this propulsion system:

- **Uncooled System:** The simplest cooling system is no cooling system. For short burn times, cool combustion temperatures, or very small engines, this technique offers the least complexity while still keeping the engine in a thermal range that ensures the structural integrity of the engine. The choice of material for the chamber will have a large influence on how well this cooling method can work in a given system
- **Heat-sink Cooling:** This cooling method uses the chamber walls as a heat-sink. This means that the entire thermal energy (or heat) of the burn gets stored in the chamber walls. This means that especially for long burn times, the chamber wall thickness will be constrained by the thermal loading instead of the mechanical loading. For heat sink cooling, it is advantageous to use a chamber wall material that has a high specific heat capacity c_p and secondarily a high thermal conductivity k to distribute the heat more equally.
- **Ablation Cooling:** A rocket engine combustion chamber can also be cooled using ablative material. In this case, the inside of the combustion chamber is lined with an ablative liner. The liner does not carry the pressure loads but it does absorb the thermal loads. This is achieved by charring the material in

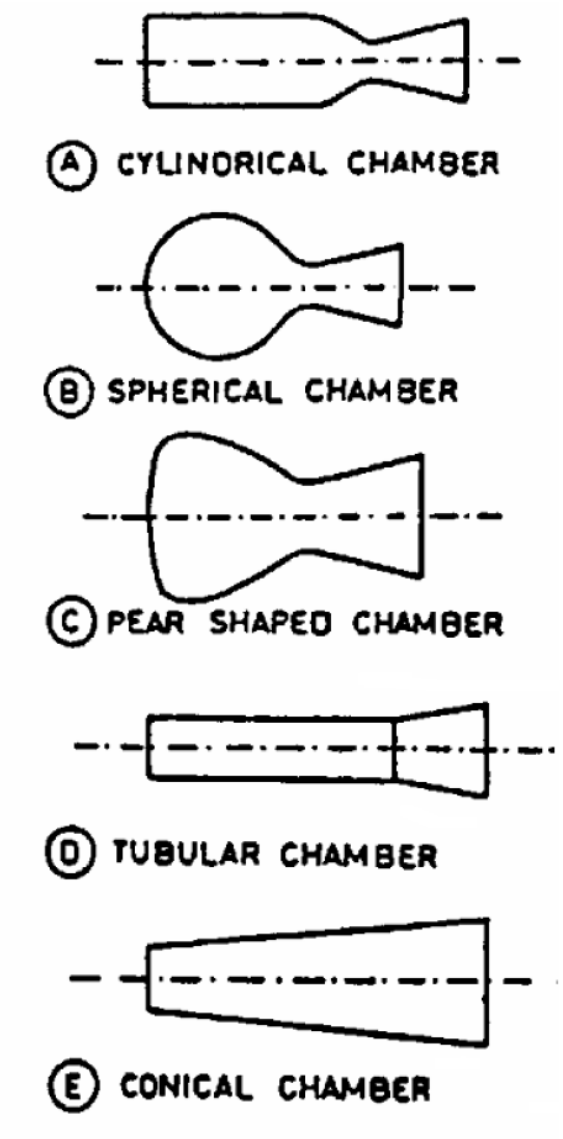

Figure 3.3: Various Combustion Chamber Geometries [18]

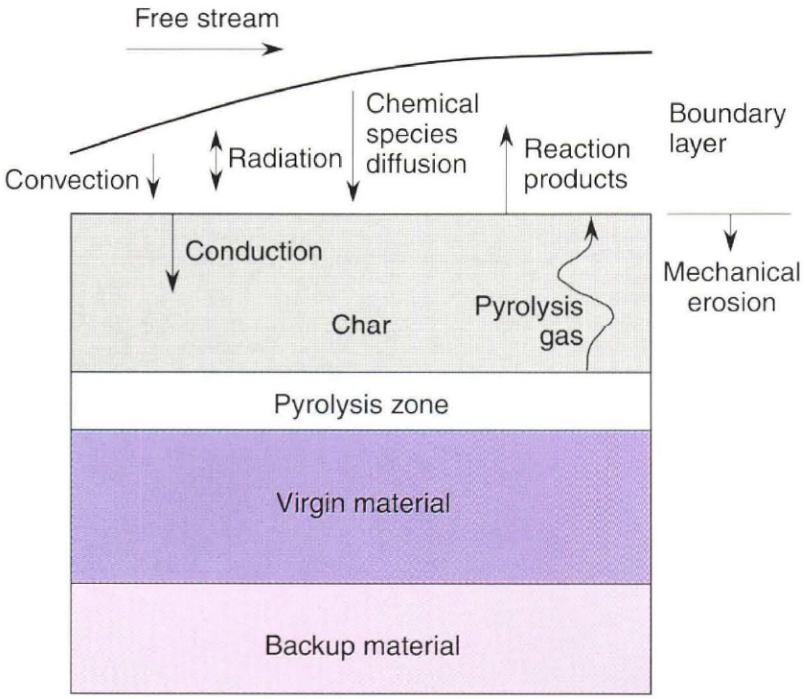

Figure 3.4: Schematic Representation of the Ablation Cooling Process [21]

an endothermic process called pyrolysis. Furthermore, the charred material as well as the remaining virgin material act as an insulation to the structural chamber wall. A schematic representation of this process can be found in figure 3.4.

- **Radiation Cooling:** Black body radiation can also be used to cool a rocket engine. This method however only realistically works in the vacuum of space with its low environmental temperature (≈3K). The radiated heat follows the Stefan-Boltzmann-Law $q = \epsilon \cdot \sigma \cdot T^4$, as can be seen in figure 3.5. This means that the chamber wall temperature can quickly approach temperature above 1000° C. Therefore, advanced refractory materials and/or coatings need to be used to sustain these high temperatures. Apart from this, radiative cooling is often used on high-expansion-ratio nozzle extensions, which will be relevant for this propulsion system.
- **Film Cooling:** The walls of a combustion chamber can also be cooled by injecting a film of propellant (usually fuel) at the wall of the chamber. As this film travels along the chamber wall towards the nozzle exit, the film will absorb heat by getting vaporised and heated to the chamber temperature. This cooling method does require additional fuel to be injected which means that this additional fuel needs to be stored in the fuel tank as well. Film cooling is often used as a supplementary cooling method to other cooling methods such as regenerative cooling.
- **Regenerative Cooling:** This method is the most commonly used cooling method on large rocket motors, but it can also be used on smaller scale systems with the wide spread of metal additive manufacturing techniques [20]. Regenerative cooling works by routing one of the propellants through cooling channels with are embedded in the chamber walls. The chamber walls will transfer heat into the cooling fluid before the fluid is injected into the combustion chamber.

Each of these methods comes with its advantages and disadvantages. These are listed in table 3.7. Based on these, a selection will be made on which cooling methods are taken into the numerical model and which ones are discarded.

Based on these advantages and disadvantages, certain methods can be excluded from the design options that will be implemented into the numerical model. Firstly, due to the 60 s operation time of the propulsion system following **REQ-PROP-2**, it is not feasible to operate the propulsion without any form of cooling considerations. With all of the chosen fuels, the combustion temperature will run above 2000 ° C. This

Table 3.7: Advantages and Disadvantages of various cooling methods

Cooling Method	Advantages	Disadvantages
Uncooled	• Low system complexity • Simple to manufacture • Most mass-efficient option	• Unfeasible on sustained burns • Unfeasible on larger engines
Heat-sink	• Low system complexity • Simple to manufacture	• Low Mass-efficiency on sustained burn times • Requires high heat capacity and high conductivity
Ablation	• Low system complexity • Supports sustained burn times • Separation of structural wall and insulation	• Mediocre Mass-efficiency on sustained burn times • Requires special ablator material • Low dimensional stability on chamber-nozzle contour
Radiation	• Low system complexity • Supports sustained burn times (if steady state is reached) • Good mass-efficiency • Good option at lower temperatures (e.g.nozzle extension)	• Only feasible in vacuum • Requires expensive, heavy refractory materials
Film	• Lower pressure drop (compared to regenerative cooling) • Can be injected at injector face and/or at hot spots (in multiple stages) • Good mass-efficiency • Can be used with gaseous and liquid propellants	• Causes performance deficits in chamber • Requires additional propellant • Mediocre chamber construction complexity • Can only used fuel for cooling
Regenerative	• Can improve efficiency by recycling waste heat back into combustion chamber • Allows for the use of more affordable, otherwise unfeasible materials • Good mass-efficiency • Both oxidiser and fuel can be used for cooling	• Causes additional pressure drop before injector • High chamber construction complexity

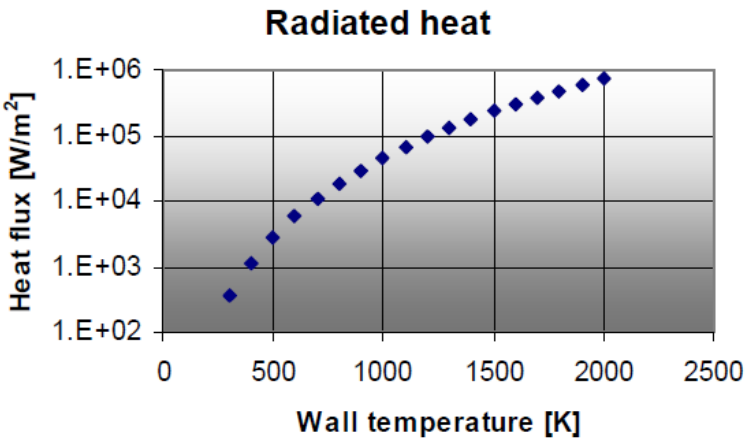

Figure 3.5: Radiated Heat from Chamber Wall (using emissivity $\epsilon = 0.8$) [18]

makes this cooling method unsuitable for any configuration of a propulsion system of this type. Finally, the film cooling will not be directly taken up in the numerical model. This is mostly because it is almost always used in combination with regenerative cooling [22] and generally takes up more of a supplemental role to other cooling methods. Therefore, this cooling method will not be used in the sizing of the propulsion, but instead can later be added as a supplemental cooling method if the validation testing shows that this would be beneficial.

Therefore, the final list of modelled cooling methods is:

- Radiative
- Heat-sink Cooling
- Ablation
- Regenerative (Oxidiser)
- Regenerative (Fuel)

Note that the regenerative cooling will be treated twice, once while using the HTP as the cooling fluid and once while using the fuel as the regeneration fluid. This is because HTP has superior cooling properties over all of the fuels, but using HTP as the cooling thermally catalyses the decomposition reaction of the HTP. If this is the case, then the regenerative cooling also needs to be evaluated for the fuel. On top of this, if the fuel is used for regenerative cooling, it might lead to a more even distribution of pressure drops over the feed system. Otherwise, the HTP pressure drop from the combustion chamber to the tank would include the GOX/steam chamber inlet, the catalyst bed, the HTP injector and the regeneration channels.

Materials

Material selection is a crucial design point in the design of subsystems of a propulsion system or rockets in general. However, given the extreme mechanical and thermal loading by the combustion chamber of the propulsion system, the material choice becomes especially important for this application. Since the material choice will be one of the optimisation variables, a list of possible materials needs to be defined.

For the chamber of small rocket motors, a common baseline choice is stainless steel. Stainless steel has the capability of resisting oxidisation and having decent mechanical stability at elevated temperatures. Especially the AISI 304L and 316L alloys offer great resistance against HTP and oxygen-rich environments. Additionally, steel is relatively cost-effective and readily available.

Another material used in small rocket motor thrust chambers is Titanium. Specifically, the Ti6Al4V alloy has been used in thrust chamber application [23]. Titanium has a superior strength-to-weight ratio and good thermal behaviour, albeit less than that of steel. Titanium is also more expensive compared to steel.

Another set of materials commonly used in the thrust chambers of liquid rocket motors are so-called refractory metals. These are characterised by their extreme resistance to heat and wear. For the application

in a rocket engine, the former characteristic especially becomes a relevant trait. These include elements such as Niobium, Molybdenum, Tungsten or Rhenium. All of these have a melting point above 2200° C. Additionally, these materials usually have extreme mechanical strength. Their major drawback is on the one hand their cost which is commonly 10-15 times higher than the cost of steel, and on the other hand, their high densities, meaning parts made from these materials tend to be heavy. There are also refractory metal alloys such as TZM (a Tungsten-Zirconium-Molybdenum alloy) that fall under this category.

Finally, there are also so-called superalloys such as Inconel, Monel, Waspaloy or Incoloy, most of which are nickel- and/or chromium-based. Commonly, these are alloyed with refractory metals to achieve thermal capabilities similar to those of the refractory metals (albeit not to the same extent). Especially Inconel, Waspaloy and Incoloy have a long tradition of being used in high-temperature applications.

Based on this overview, the following list of possible materials for this propulsion system's thrust chamber has been compiled:

- AISI 304L
- AISI 316L
- Ti6Al4V
- Inconel 600
- Inconel 617
- Inconel 625
- Inconel 690
- Inconel 718
- Inconel X750
- TZM

The decomposition chamber is thermally far less loaded than the combustion chamber. With the decomposition temperature only ever reaching around 700° C, even the least thermally resistant material, stainless steel will withstand this temperature without issue. This means that any choice of material for the combustion chamber will also be sufficient for the decomposition chamber. Therefore, it will be considered as one singular material choice for the combined chamber.

The detailed information and properties of each of these materials can be found in appendix A.1.

3.6.2. Nozzle

The nozzle of a rocket engine is used to turn the heat energy in the combustion gases into kinetic energy in the exhaust flow, thereby raising exhaust velocity and thereby improving the efficiency of the engine. This section lays out which nozzle types will be compared in the numerical model, what design limitations are imposed on them, and how the nozzle material is selected.

Design Options

The goal of a rocket engine nozzle is to expand the combustion gas to ambient pressure outside the rocket engine or to as close to vacuum in the case of an engine in a vacuum application. There are various nozzle design options which can achieve this, which can be seen in figure 3.6. In section 3.6.1, it was already concluded that propulsion should use some form of convergent-divergent nozzle. Each of them has their characteristics:

- **Conical Nozzle:** The conical nozzle is the simplest of the convergent-divergent nozzle. It is comprised of a conical convergent section and a conical divergent section. This nozzle type is more commonly used in solid rocket motors because of solid, superheated particles present in their exhaust flow, but they can also be found on small liquid thrusters. Their primary advantage is their simple construction since the nozzle does not have any major double-curved surfaces, which simplifies manufacturing. The disadvantage of this nozzle type is its long length and the flow divergence loss at the nozzle exit due to lack of curvature. The most common divergent angle on conical nozzles is 15° [24].
- **Bell/Parabolic Nozzle:** The bell nozzle follows a parabolic profile (hence it is also referred to as a parabolic nozzle) which is sized to expand the flow of a shorter distance compared to a conical nozzle

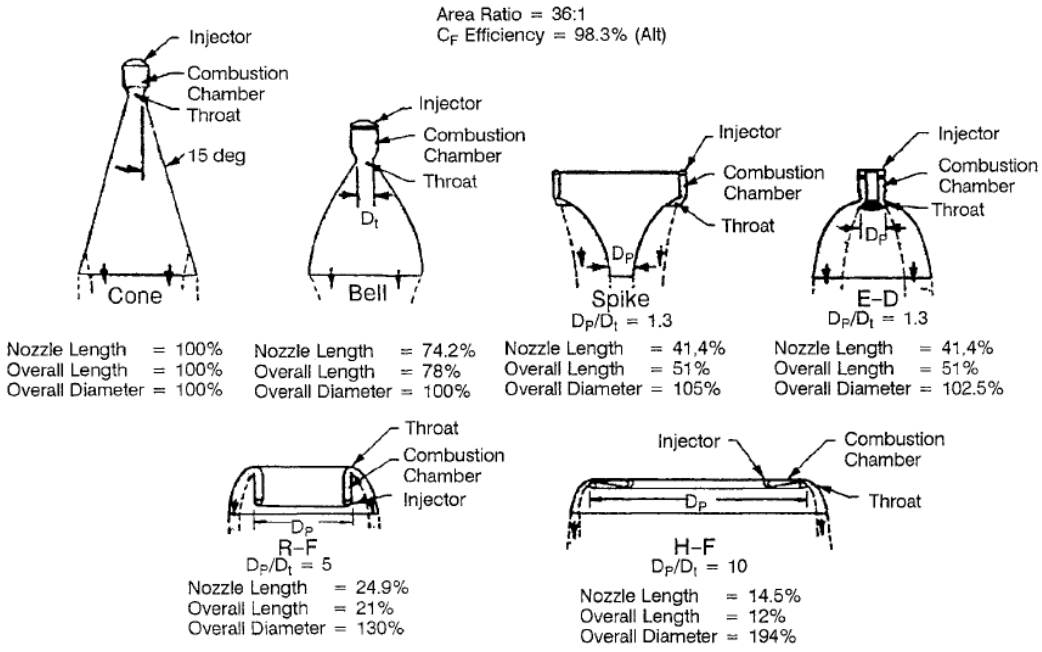

Figure 3.6: Rocket Nozzle Types [24]

and simultaneously reduce the flow divergence losses. Compared to the conical nozzle, parabolic nozzles have a larger initial divergence angle (30-60°), but then due to the parabolic profile, this reduces to around 5° at the exit [24]. This is possible due to the higher pressure closer to the throat. The main advantages of this nozzle type are the reduction of the flow divergence loss and nozzle length compared to a conical nozzle. The disadvantage is the more complex geometries which impose additional challenges on manufacturing.

- **Annular Nozzles:** Conventional nozzles like the previous two examples are designed with a specific area expansion ratio. This ratio expands the exhaust gasses to a desired pressure. If the pressure is lower than this design pressure, the nozzle is under-expanded and if the pressure is higher than this design pressure, then the nozzle is over-expanded. This can be seen in figure 4.4. Especially over-expansion of the nozzle can lead to instabilities and violent vibrations in the nozzle divergent and either type of incorrect expansion leads to efficiency losses. Annular nozzles can counteract this since their flow is not just expanded outwards but also inwards. There are two basic types of annular nozzles: radial-inflow (spike nozzle) and radial-outflow [Expansion-Deflection (E-D), Reverse-Flow (R-F), and Horizontal-Flow (H-F)]. Fundamentally they allow the flow to over- or under-expand more easily, which improves efficiency over a larger range of ambient pressures. The primary disadvantage is the required annular combustion chamber shape which is less conventional and might not be interfaceable with e.g. a decomposition chamber. The

Since the design includes a cylindrical decomposition and combustion chamber, the integration of an annular nozzle would be challenging at best. Additionally, Since the system operates at altitudes beyond 50 km, the pressure can be parasitically considered a vacuum at all times, which makes the large ambient-pressure-range capability of annular nozzles less relevant in this application.

Hence the nozzle types that will be considered in the design model are:

- Bell Nozzles
- Conical Nozzles

The optimisation algorithm will iterate through various design parameter combinations for both of these nozzle types in order to adequately quantify their effects on the overall system performance.

Design Limitations
Ultimately, the propulsion system needs to be integrated into the upper stage of the Barracuda sounding rocket. This imposes design limitations on the nozzle in the form of a limited nozzle expansion. As the ambient pressure goes towards the vacuum, the ideal expansion ratio for any nozzle reaches infinity. This is impractical in real life. Since the propulsion is on the upper stage of the rocket, it needs to fully fit within the separation interface between the first and second stages. Therefore, the expansion ratio will be based on the targeted altitude ambient pressure but will be limited to the available internal diameter in the separation interface.

Materials
The nozzle is one of the most thermally and mechanically loaded parts of the propulsion system after the combustion chamber. In order to simplify the modelling and construction of the propulsion system, the nozzle will be modelled with the same material as the one selected for the combustion chamber. This is because smaller rocket thrust chambers and nozzles are often made out of a single part (often using additive manufacturing [20]).

In later design iterations of this subsystem, this decision can be revisited and a multi-material nozzle can implemented if this brings major benefits.

3.6.3. Injector
The injector of the propulsion system is responsible for injecting the propellants into the decomposition or combustion chamber. Their goal is to inject the fluid into the respective chamber in such a manner that the injected fluid achieves adequate coverage of the catalyst bed or allows for a sufficient mixture of the other propellants. Next to this, the injectors also ensure a sufficient pressure drop from feed lines to the chamber which aids in ensuring stable combustion.

Most liquid bi-propellant systems utilise an injector which atomises the fuel and oxidiser and mixes them such that they can be combusted efficiently. Hence the injectors for fuel and oxidiser are often combined into one unit, where both fuel and oxidiser are injected through the same injector face (though not through the same manifold).

In this propulsion system, however, due to the staged nature of the decomposition and combustion of the HTP, the injectors are all separated and thus cannot be treated as one unit. Therefore, the design options and considerations for the numerical model will be treated for each injector separately instead.

HTP
The HTP Injector sprays the HTP onto the catalyst bed in the decomposition chamber. Thus there a two key objectives for this injector: Firstly, the HTP needs to be atomised sufficiently, and secondly, sufficient catalyst bed coverage needs to be achieved.

In section 3.6.1, the design of the decomposition chamber was treated similarly to an HTP monopropellant thruster. The same holds for the HTP injector. Injector design choices from HTP monopropellant thruster can therefore be used as a basis for the design of this injector. HTP monopropellant engine commonly uses plain-orifice injectors [11], [13], [25]. These can either have the form of a single orifice injector such as the one in figure 3.7 or in the form of a shower head injector such as the one in figure 3.8.

While there are various other injector types such as swirl injectors, pintle injectors, or impinging injectors [24], the single plain-orifice and shower head injectors are the most commonly used types for monopropellant thrusters, and thus these are the two types that will be considered during the design optimisation for this propulsion system.

The primary advantage of the single orifice variant is the construction and manufacturing simplicity. The single orifice can be directly integrated into the injector manifold which reduces the number of parts. Additionally, a single orifice will be larger compared to multiple orifices for a given mass flow, which will simplify manufacturing further. The main advantage of the shower head injector is that the multiple orifices can produce better catalyst bed coverage at a shorter distance from the injector to the catalyst bed. Additionally, smaller injector orifices can improve atomisation [26]. For both injectors, a sufficient pressure drop is crucial to ensure that the decomposition cannot back-travel up the feed line and cause thermal decomposition of the HTP in feed line tanks, which could lead to a catastrophic over-pressurisation.

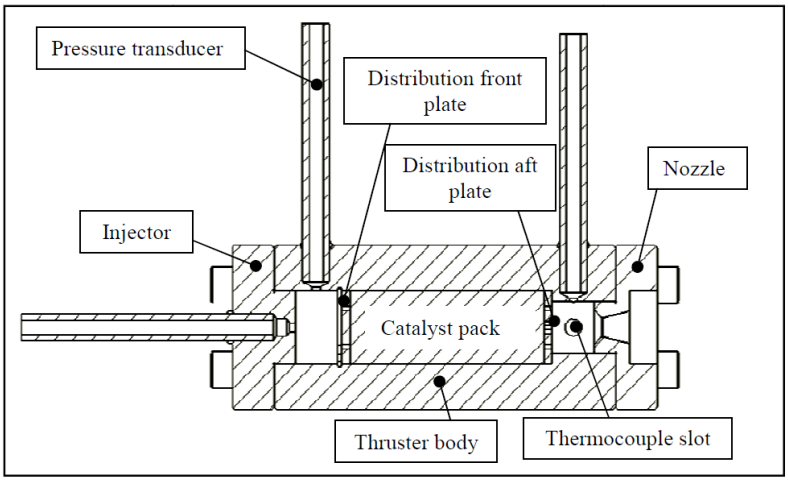

Figure 3.7: An exemplary 50N HTP monopropellant thruster with a single plain-orifice injector [25]

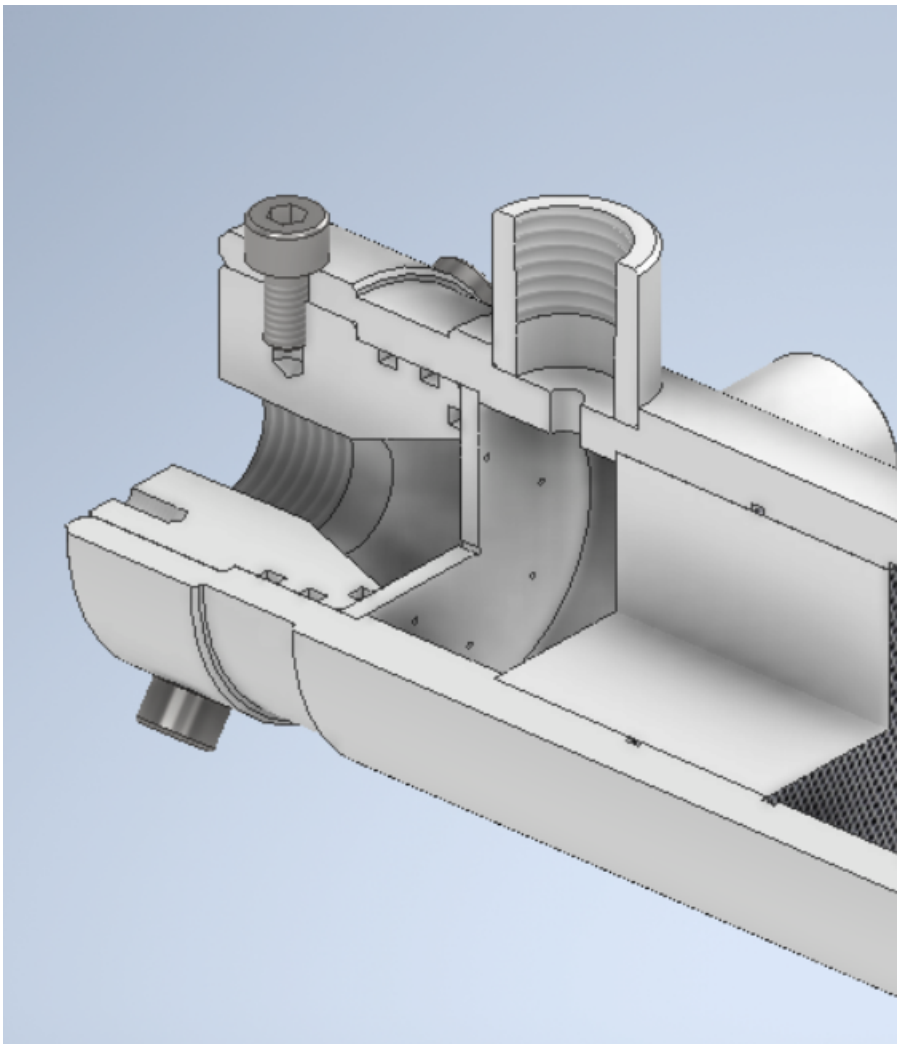

Figure 3.8: 7-element shower head injector on the HyProp catalyst characterisation test bed

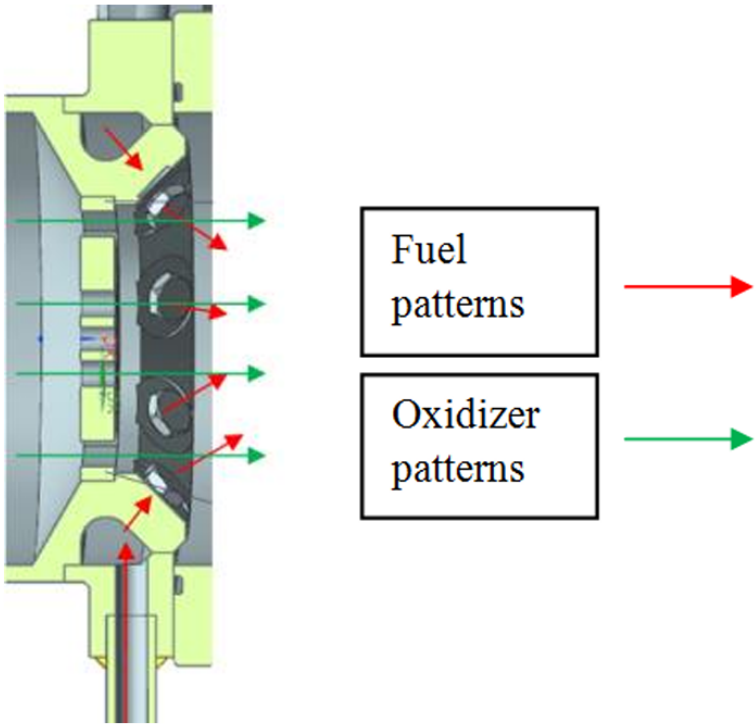

Figure 3.9: Fuel injector pattern on TMPDA-HTP staged bipropellant engine [13]

Since both of the potentially viable injectors can be modelled using the same methods (a single plain-orifice injector can be considered a shower head injector with one orifice), both these types will be modelled in the numerical optimisation. Based on this, the optimisation algorithm can then determine the ideal injector geometry and spacing from the injector to the catalyst bed based on the design parameters of the injector.

In the design of this propulsion system, these elements will be sized as comparatively large circular orifices between the decomposition and combustion chamber.

Fuel

The fuel injector injects the fuel into the combustion chamber and mixes it with the super-heated steam and gaseous oxygen. Next to this, like the HTP injector, the most important characteristics of this injector are the coverage of the chamber as well as the atomisation performance.

Multiple approaches for this type of injector have been used in previous comparable systems. One option is to use a radially inward impinging injector array, as can be seen in figure 3.9.

An alternative arrangement of the centrally located, the radially outward impinging injector was also tested for the same system, but has been shown to result in a lesser combustion efficiency than the radially inward impinging injector, hence the outward impinging option is not considered. Next to this, the other injector with previous use history in this type of liquid bi-propellant engine is the shower head injector integrated into the decomposition outlet/combustion inlet. An example of this can be seen in figure 3.10.

The advantage of the radially inward impinging injector is the relatively simpler construction since the fuel injector manifold does not have to pass through the decomposition outlet/combustion inlet plate or the catalyst itself as is the case in figure 3.10. The primary disadvantage is that the injected fuel may struggle to reach the centre of the combustion chamber without additional precautions. This is also the main advantage of the shower head injector in this situation. It can ensure a more uniform distribution of the fuel injected into the combustion chamber. Conversely, the main disadvantage of this injector is the more complex construction required to inject the fuel equally over the chamber while also allowing the super-heated steam and gaseous oxygen to pass into the combustion chamber.

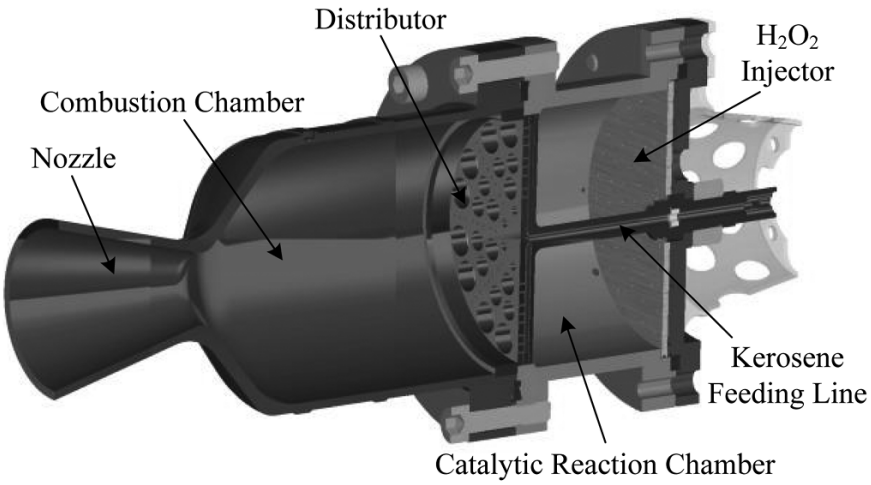

Figure 3.10: Fuel Injector integrated in decomposition outlet/combustion inlet for Kerosene-HTP staged bipropellant engine [14]

Ultimately, the decision is made that the benefits of the radially inward impinging outweigh those from the shower head injector since the drawback of the fuel distribution can be mitigated by varying the injector element angle concerning the chamber axis as well as adjusting the decomposition outlet/combustion inlet orifice arrangement to ensure better mixing. Finally, the radially inward injecting arrangement is more prevalent [12], [13], [27] than the integrated shower head injector [14].

3.6.4. Feed System

The feed system feeds the propellants from the tanks to their respective injectors. Next to this, the feed system also needs to ensure that the propellants are fed into the decomposition and combustion chamber at the correct pressures throughout the entire burn time of the propulsion system.

This section will cover the selected pressurisation/feed method, and discuss the layout of the feed system and the required components.

Pressurisation

Fundamentally, when considering the pressurisation method of an engine's feed system, there are two options: Pressure-fed or pump-fed. Pressure-fed systems use a pressurant gas in the propellant tanks that force the propellants out of the tank down the feed lines to the chamber. This means that tank pressure needs to be higher than the chamber pressure since the tank pressure is derived from the chamber pressure summed with all pressure losses from injectors, lines, valves etc. between the chamber and the tank. Meanwhile pump-fed system uses pumps to increase the pressure in the feed lines between the tank and the chamber of the engine. This makes the chamber pressure mostly independent of tank pressure. However, this comes at the cost of higher developmental and system complexity.

Pressure-fed systems are beneficial due to their simplicity compared to pump-fed systems. Pump-fed systems are beneficial for engines with high mass flow and/or high combustion chamber pressure. Both of these would require the tank pressure to be unacceptably large or would require large volumes of pressurant gas, which would make the use of the gas pressure-fed system unfeasible. However, for this propulsion system, the chamber pressure will likely not exceed 30-40 bar and the mass flow of the system will likely remain below 0.5 kg/s. These values are within typical operating ranges for pressure-fed systems [18].

In order to avoid the large developmental cost of pump hardware, a pressure-fed system will be used for this propulsion system. Pressure-fed systems themselves can be differentiated into two sub-categories: Blow-down and regulated. A simplified schematic overview of both can be seen in figure 3.11.

Blow-down systems come with the advantage of not requiring a pressurant tank or a pressure regulation system. The tank can be externally pressurised before launch. The disadvantage of this system is that as the propellants are forced out of the tank, the tank pressure will decrease. Since as previously mentioned,

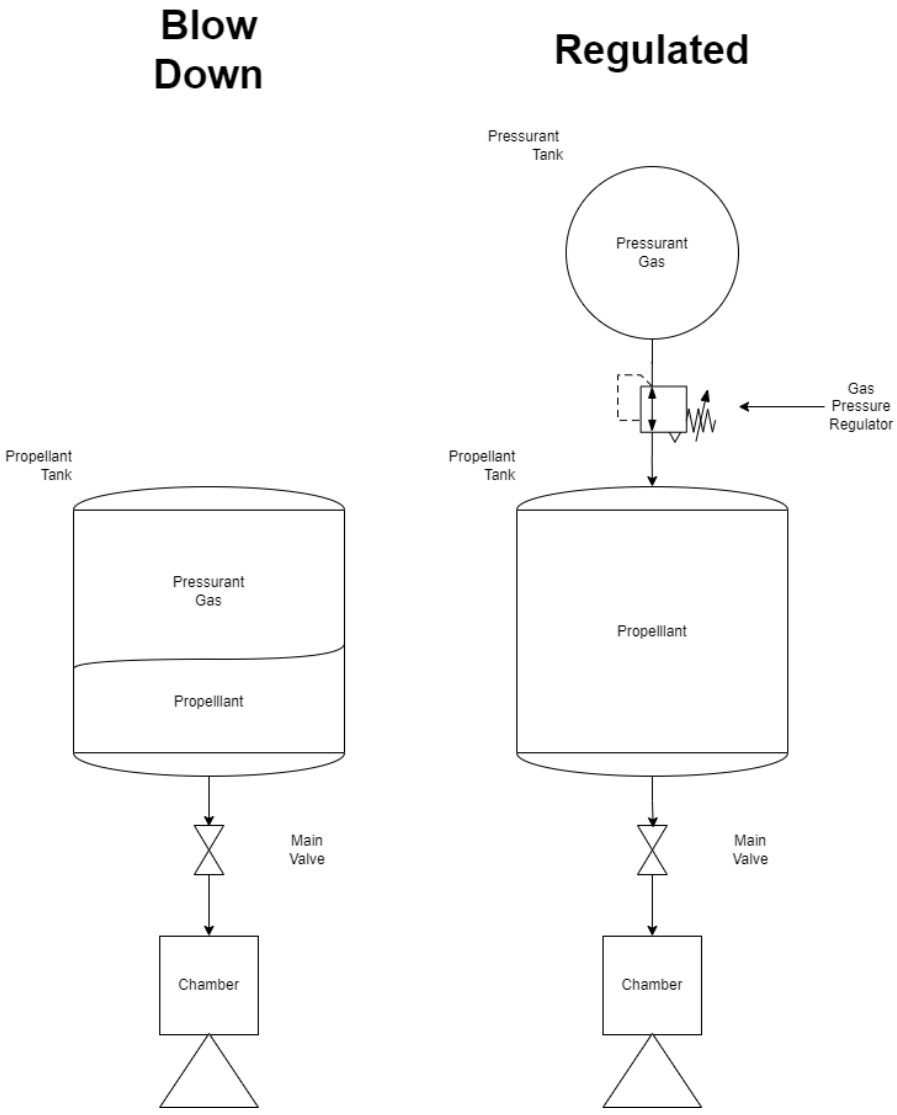

Figure 3.11: Blow-down (left) compared to Regulated (right) pressure-fed system

the tank pressure and chamber pressure are linked in a pressure-fed system, this will also cause a reduction in chamber pressure and thus thrust. Therefore, while this can be somewhat counteracted by increasing the initial volume fraction of gas-to-propellant, blow-down systems are unable to provide consistent performance over long burn times.

Regulated systems utilise a separate pressurant tank where the pressurant is stored at high pressures (150+ bar). A regulator is then placed between the pressurant tank and the propellant tank. It will regulate the inflow of pressurant gas into the tank throughout the burn such that the tank is always kept at the same pressure. A constant tank pressure results in consistent engine performance.

Since **REQ-PROP-2** requires that the engine should provide the peak thrust for at least 60 seconds, a regulated pressure-fed system is chosen for this system.

Feed System Layout

Based on the previous design decisions, a feed system layout can be drawn up. Laying out this overview is important to determine the required valves and feed lines between the chamber, tanks and pressurant tank. This layout can be found in figure 3.12. Based on this layout, table 3.8 describes the function of each feed system component. The leading letter indicates what fluid/gas the component is regulating: **O** is the oxidiser, **F** is the fuel, and **P** is the pressurant. In table 3.8, this leading letter is replaced with X.

Appendix B contains a description of the feed system symbols used in figure 3.12. It should also be noted that the location of the oxidiser and fuel tanks can be switched if the resulting change in CG location and shift is more beneficial for the rocket as a whole (including the first stage).

3.6.5. Tanks

The chosen propulsion system design requires three tanks: The fuel tank, the oxidiser tank and the pressurant tank. The former two tanks will be constructed using the same design methodologies. The pressurant tank will be treated separately since it needs to withstand pressures an order of magnitude larger than the propellant tanks.

Propellant Tanks

With the limited diameter and a conservatively estimated propellant mass of around 15 kg, the propellant tanks will have to be cylindrical, since a spherical fuel tank with an outer diameter of 0.2 metres will not be able to contain the propellants. Among the cylindrical tanks, there are two options: A tank with flat end caps and a tank with spherical end caps, an example of each can be found in figure 3.13.

Each type of tank comes with its own set of advantages and disadvantages. The Flat end cap design is much simpler in terms of manufacturing and thus the costs associated with it are lower. It also utilises the space in the rocket fuselage more effectively than the spherical end cap design. Finally, this tank design has been validated for use with HTP in this application. The advantages of the spherical end caps are mainly the improved structural design of the end caps and thus some mass savings related to this. Next to this due to the spherical end caps, it has better draining behaviour.

A common bulkhead design has been ruled out in this case since this would lead to additional challenges with propellant line routing and in this design, it would only lead to marginal mass savings, since this would impose additional constraints on the design e.g. both tanks having the same wall thickness and/or diameter.

For this propulsion system, no clear ideal option between the two tank designs is apparent. Therefore, both cylindrical tank designs will be modelled in the numerical model, and the decision of which type is used will be based on which one is more ideal option in accordance with the chosen fitness function.

Pressurant Tanks

Where the propellant tank pressure will likely not exceed 40-50 bar, the pressurant tank can easily reach 200-250 bar. This means that a different design approach is to be used for this tank.

For any given volume, a sphere will always produce the most efficient surface area per volume. This means that a sphere will always produce the most efficient pressure vessel for a given volume. Next to this, a spherical pressure vessel only requires half of the thickness to withstand a given pressure when compared to a cylindrical pressure vessel. Because of the high pressures in this tank, this means that if the pressurant

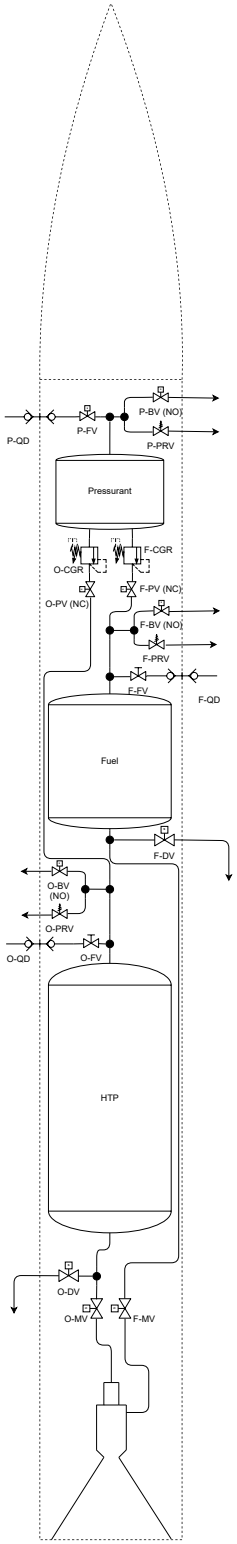

Figure 3.12: Feed System P&ID Diagram

Table 3.8: Feed System Components

Component	Symbol	Purpose
Fill Valve	X-FV	This valve is used to open/close the filling port for its assigned fluid. It should be normally closed. For fuel and oxidiser, these can also be manually operated.
Bleed Valve	X-BV	This valve is used to bleed pressure from the tank. Each tank is equipped with one since the regulator between the tank and the pressurant tank will prevent bleeding the whole system through the pressurant bleed valve. This valve should be normally open, such that the system is safed in case of loss of power.
Pressure Relief Valve	X-PRV	This valve is an automatic pressure relief valve designed to break open at a certain pressure. This valve avoids over-pressurisation in case of an uncontrollable pressure rise in the tank (e.g. thermal decomposition of HTP). This valve is passive and cannot be controlled.
Compressed Gas Regulator	X-CGR	This regulator lower the pressure from the current pressurant tank pressure to the set propellant tank pressure. There is one regulator for each propellant tank such that the propellant tanks can be held at different pressures. A regulator design capable of dynamic pressure regulation (output pressure independent of input pressure) needs to be used for this system to function.
Pressurisation Valve	X-PV	This valve allows for the controlled pressurisation of the propellant tanks. It should be normally closed such that in case of power loss, the propellant tanks will vent without new pressurant flowing in.
Quick Disconnect	X-QD	The quick disconnect is used to connect propellant and pressurant loading systems to the upper stage.
Drain Valve	X-DV	This valve allows the removal by gravity of propellants from the propellant tanks. This valve should be normally closed. Alternatively, the fill valve can also take the place of both the drain valve and the fill valve, but then the fill valve must be remotely operable.
Main Valve	X-MV	This valve control the flow of propellants to the injectors. This valve should be normally closed. To enable precise operations, this valve should have a fast response time.

(a) Cylindrical Tank with Flat End Caps **(b)** Cylindrical Tank with Spherical End Caps [28]

Figure 3.13: Both types of propellant tanks in the fluid tank module

tank can at all be sphere, it should be constructed as such. Only if a spherical pressure vessel is not able to fit inside the rocket fuselage, a cylindrical tank with spherical end caps should be used. In this case, the flat-end cap cylindrical pressure vessel will have too high stress concentrations around the interface between the cylinder and end cap at these elevated pressures for this design to still be feasible.

Hence, the chosen design for the pressurant tank is preferably a spherical tank, and in case this design cannot be integrated into the fuselage, a cylindrical tank with spherical end caps.

The pressurant gas is used to keep a constant pressure in the propellant tanks and thus force the propellant through the feed lines into the combustion/decomposition chamber. To determine which gas can be used, multiple options can be considered:

- Nitrogen N_2
- Helium He
- Carbon Dioxide CO_2
- Argon Ar

The properties of these gasses can be found in appendix A.3. Nitrogen and Helium are commonly used as pressurants in rocket propulsion systems [29]. Meanwhile, Carbon Dioxide and Argon are readily available alternatives which can also be considered. However, it should be noted that Carbon Dioxide can only be used up to a tank pressure of around 55 [bar], since the vapor pressure of CO_2 is around 57 [bar] [30]. This means that at room temperature at this pressure it will condense into a liquid. This is undesirable for a pressurant. However, this design restriction can be implemented into the numerical model such that the optimisation algorithm accounts for this.

Materials

For all tanks of the propulsion system, there are groups of materials that can be considered: Aluminium, Steel and Titanium. Each of these materials has previously been use for propellant and pressurant tanks in rocket propulsion systems. However, some attention needs to be paid to the material compatibility between HTP and the propellant tanks. Certain materials are not compatible with HTP since they will react with it more or less strongly. An overview of this can be found in appendix C.

Notably, while HTP is compatible with many aluminium alloys, it is not compatible with high-strength 7000-series alloys such as EN-AW 7075T6, which is often used in aerospace applications because of its high-strength nature. However, this material can still be used for the pressurant tank. Similarly, only certain stainless steel alloys can be used in this application like AISI 316L. Based on these restrictions, the following material selections have been made for the tanks:

- Aluminium EN-AW 1060H12

- Aluminium EN-AW 5253H12
- Aluminium EN-AW 6082T6
- Aluminium EN-AW 7075T6 (pressurant tank only)
- Stainless Steel AISI 304L
- Stainless Steel AISI 316L
- Titanium Ti6Al4V

3.7. Conclusion

With the completion of this phase, the preliminary design of the propulsion system has been defined. Based on the previously defined preliminary requirements, the requirements and constraints for the propulsion system were defined.

Based on these requirements, it was decided to utilise the catalytic decomposition of HTP in combination with the auto-igniting property by selecting the correct fuel. The auto-ignition temperature of the fuel was therefore one of the primary selection criteria by which options were pre-selected.

Based on this, preliminary architecture was then defined and fuel candidates were selected based on their auto-ignition temperature, their vapour pressure and existing thermo-chemical representation.

Finally, for each subsystem, a preliminary design was created to the extent that each of them can be modelled and subsequently integrated into the numerical model. Therefore it can be concluded that the design has reached the stage of detail required before it can be numerically modelled and subsequently optimised.

4

Numerical Model

This chapter describes the numerical model. The numerical model is split into modules, each of which models a certain aspect of the propulsion system. This distribution is not directly tied to the subsystem distribution defined section 3.5. First, the required model outputs will be defined, and subsequently, the model inputs will be determined. After this, the model architecture will be defined, and the modelling approach for each module will be described. Finally, the internal modelling logic will be defined.

4.1. Architecture

The numerical model was divided into 11 modules, each of which has their purpose:

- **Decomposition:** Model the HTP decomposition and determine the temperature and other properties of the output gases
- **Combustion:** Model the combustion of the HTP decomposition products and the fuel, determine various parameters of the combustion gasses
- **Nozzle:** Size the nozzle based on diameter restriction and altitude optimisation inputs
- **Chamber:** Determine the geometry of the decomposition and combustion chambers.
- **Contour:** Computes chamber-nozzle contour and provides discretised representation for the transport module.
- **Transport:** Determine the profile of various thermodynamic parameters in the exhaust gasses as a function along the chamber nozzle profile.
- **Cooling:** Based on the selected cooling method, size the cooling elements (e.g. cooling channels, ablator) and determine the mass of the cooling system
- **Injector:** Determine the orifice sizes for the HTP and fuel injector
- **Feed:** Determine pressure drop over feed system based on line length to determine required tank pressure
- **Fluid Tank:** Determine the amount of propellant needed, select the most efficient tank design and determine geometry based on required pressure and propellant volume.
- **Pressurant Tank:** Similar to the fuel tank module, but determines pressurant volume based on other tank sizes, then sizes pressurant tank based on required pressurant mass and initial pressure

The distribution of which modules interface with which subsystem of the propulsion system can be found in figure 4.1.

4.2. Required Outputs

To derive a detailed design from the numerical model and perform verification and validation efforts, the outputs provided need to cover most modules. These can be found in table 4.1.

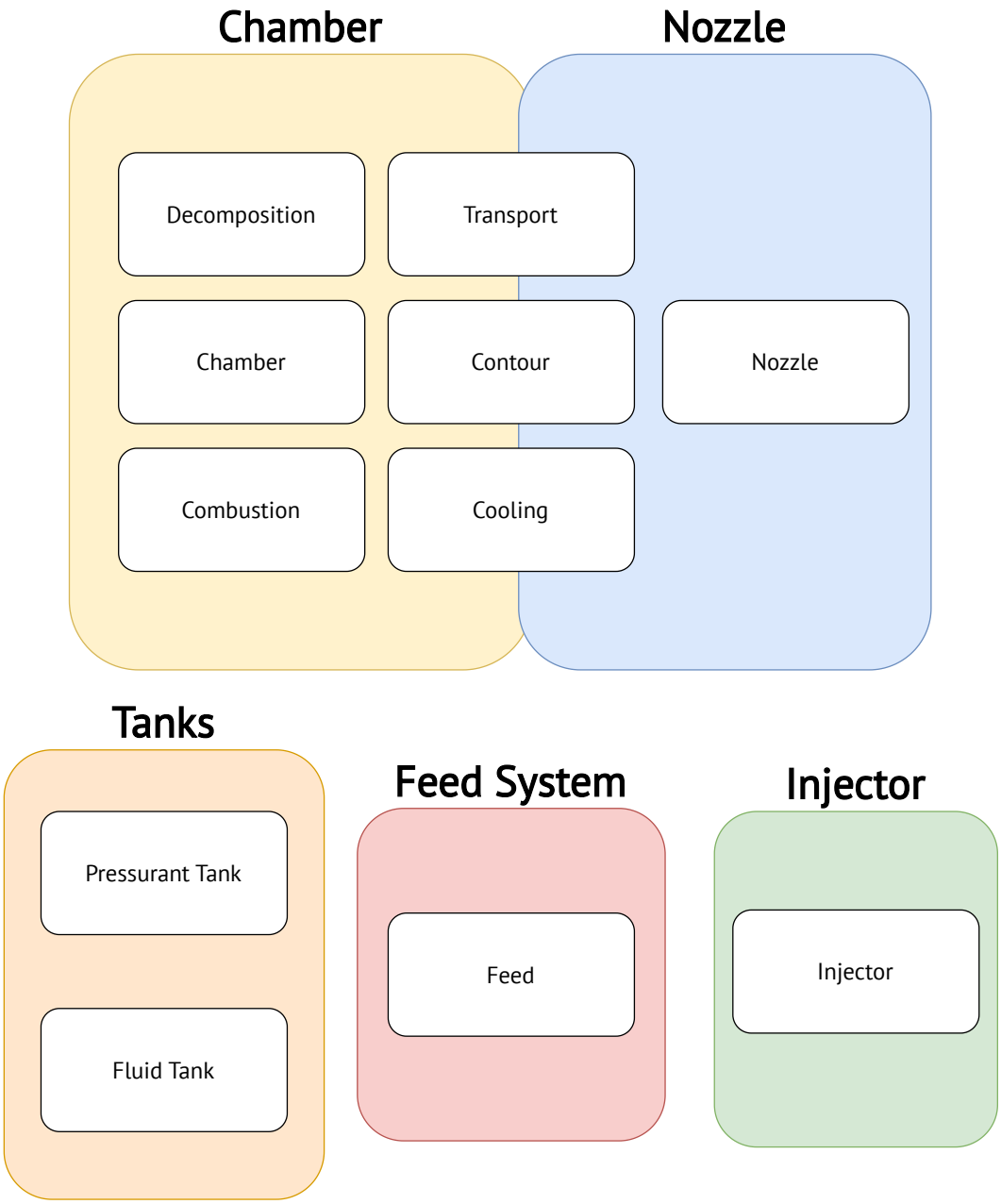

Figure 4.1: Module-Subsystem Assignment in the Numerical Model

Parameter	Purpose
Combustion	
Specific Impulse	Verification/Validation
Characteristic Velocity	Verification/Validation
O/F Ratio	Verification/Validation
Specific Heat Ratio	Verification/Validation
Chamber Density	Verification/Validation
Critical Throat Diameter	Verification/Validation
Chamber	
Length	Detailed Design
Diameter	Detailed Design
Characteristic Length	Verification/Validation
Flow Velocity	Verification/Validation
Chamber Mach	Verification/Validation
Contraction Ratio	Verification/Validation
Sonic Velocity	Verification/Validation
Catalyst	
Length	Detailed Design
Diameter	Detailed Design
Pressure Drop	Verification/Validation
Fuel Injector	
Atomisation	Verification/Validation
Element Number	Detailed Design
Element Diameter	Detailed Design
Element Length	Detailed Design
HTP Injector	
Atomisation	Verification/Validation
Element Number	Detailed Design
Element Diameter	Detailed Design
Element Length	Detailed Design
Nozzle	
Area Expansion Ratio	Verification/Validation
Throat Diameter	Detailed Design
Exit Diameter	Detailed Design
Nozzle Contour Parameters	Detailed Design
Tanks	*(for each instance)*
Content Mass Flow	Verification/Validation
Content Mass	Detailed Design
Volume	Verification/Validation
Type	Detailed Design
Length	Detailed Design
Diameter	Detailed Design
Wall Thickness	Detailed Design

Table 4.1: Numerical Model Outputs

Parameter	Type
Constrained	
Thrust	Continuous
Burn Time	Continuous
HTP Decomposition Temperature	Continuous
HTP Concentration	Continuous
Engine Bay Length	Continuous
Intertank Length	Continuous
Variable	
Chamber Pressure	Continuous
Bell Nozzle Length Fraction	Continuous
Tank Diameter	Continuous
Pressurant Pressure	Continuous
Pressurant	Discrete
Fuel	Discrete
Fuel Injector Pressure Drop	Continuous
Fuel Injector Element Number	Discrete
Fuel Injector Element Length	Continuous
HTP Injector Pressure Drop	Continuous
HTP Injector Element Number	Discrete
HTP Injector Element Length	Continuous
Chamber Material	Discrete
Fluid Tank Material	Discrete
Pressurant Tank Material	Discrete
Feed Line Material	Discrete
Nozzle Exit Diameter Fraction	Continuous
Nozzle Type	Discrete
Cooling Type	Discrete

Table 4.2: Numerical Model Inputs

It should be noted that the construction of the numerical model allows for accessing most variables used, but the ones in table 4.1 are part of the default output functionality.

4.3. Inputs

Like the outputs, inputs have been gathered in table 4.2. They are sorted based on whether they are constrained or variable inputs. Variable inputs will be allowed to vary as part of the optimisation process while the constrained inputs will remain constant.

The boundaries for the optimisation variables can be found in tables 6.1 and 6.2.

4.4. Modules

In this section, figures will be presented at times to clarify the outputs and processes of the various modules of the model. However, due to the nature of the model being subject to an optimisation algorithm at a later stage, placeholder values will be used to provide these outputs. These can be found in

After, define each module and describe in detail how it models the respective subsystem

4.4.1. Decomposition

The main objective of this module is to supply the temperature of the products from the HTP decomposition, such that this can be used in the combustion model to determine the properties of the gaseous oxidiser. Originally, the goal was to use the gathered data from the small-scale monopropellant thruster from the HyProp project to determine the decomposition temperature of the HTP as a function of the catalyst geometry and HTP mass flow.

However, due to the delays in the HyProp project, a surrogate model needs to be implemented. Previous research has shown that the chosen catalyst type provides a consistent decomposition temperature of 700 ° C for various catalyst geometries [7]. Therefore this will be implemented as a constant value. Additionally, no implementable, validated model with a higher fidelity could be found for this specific type of catalyst. Therefore, using a constant decomposition temperature will have to suffice until the insights from HyProp can be implemented.

4.4.2. Combustion

The combustion process is modelled using the NASA chemical equilibrium code CEA (Chemical Equilibrium with Applications) [31], [32]. The program is capable of simulating and computing chemical equilibrium compositions and determining various properties of these compositions. It includes built-in applications such as the calculation of Chapman-Jouguet detonation parameters, shock tube parameters, assigned thermodynamic properties, theoretical rocket performance, and combustion properties. The latter three are used in the modelling of the combustion of the fuel and the gaseous oxygen/steam mixture.

The original CEA program is written ANSI standard FORTRAN. However, since the remainder of the numerical model is written in Python 3.11, the code needs to be wrapped so that the combustion model can be used in the iteration of the model rather than being a fixed input. For this, an existing python wrapping of CEA called "RocketCEA" [16] was used. While it does not allow to use of all the functions of CEA, it is possible to compute combustion properties, assigned thermodynamic properties and transport properties in rocket motors for both infinite- and finite-area combustors. Finite-area combustor models allow for the computation of e.g. pressure drops from the injector face to the start of the convergent section of the nozzle.

All the fuels that were pre-selected in section 3.4.2 are already represented as presets in the CEA thermochemical library. Since for the numerical model it is assumed that the fuel is injected at the standard temperature of CEA (298 K/25° C), these fuel presets do not need to be modified.

While there are presets for both gaseous oxygen and water, these presets are made for the same standard conditions as for the fuel. However, when the fuel combusts with the steam/GOX mixture, this mixture has a temperature of around 700° C [7], so the thermodynamic properties of this mixture will be largely different from a steam/GOX mixture at 25° C and 1 bar pressure.

From a pure thermochemical point-of-view, it would be possible to model the heating of the steam/GOX mixture simply as the direct combustion of HTP and the fuel. However, modelling the combustion of the hot steam/GOX mixture with the fuel instead allows for taking into account efficiency losses and similar effects around the decomposition process and catalyst geometry. Ultimately, this will produce a more exact representation of the propulsion system, which can take into account more than simply modelling a thermodynamically equivalent process. This approach will also allow to modelling of various concentrations of HTP, which can later be used as an additional optimisation variable.

To create an oxidiser preset for CEA, a so-called oxidiser card needs to be constructed. An example can be seen in figure 4.2. This card together with the respective fuel card acts as input to the CEA FORTRAN code. The oxidiser card needs to contain the following information for both steam and GOX:

- Atoms in the specie
- Reference Temperature
- Density
- Enthalpy at the reference temperature
- Relative composition between species in % by weight (%wt)

To model the combustion between the steam/GOX mixture and the fuel, these properties need to be determined. The atoms in each species are already known since the products of the decomposition of HTP are water (H2O) and molecular oxygen (O2), and they are not dependent on any of the model inputs. It is assumed that the HTP fully decomposes into only these two species. Next, the reference temperature will be set as the temperature of the decomposition products and is thus directly taken from the decomposition model.

```
oxid H2O2(L) H 2 O 2  wt%=90.00
h,cal=-44880.0     t(k)=298.15  rho.g/cc=1.407
oxid = WATER H 2.0 O 1.0 wt%= 10.0
h,cal=-68317. t(k)=298.15 rho.g/cc=1.0
```

Figure 4.2: Example CEA Oxidisier Card for 90%(wt) Hydrogen Peroxide [16]

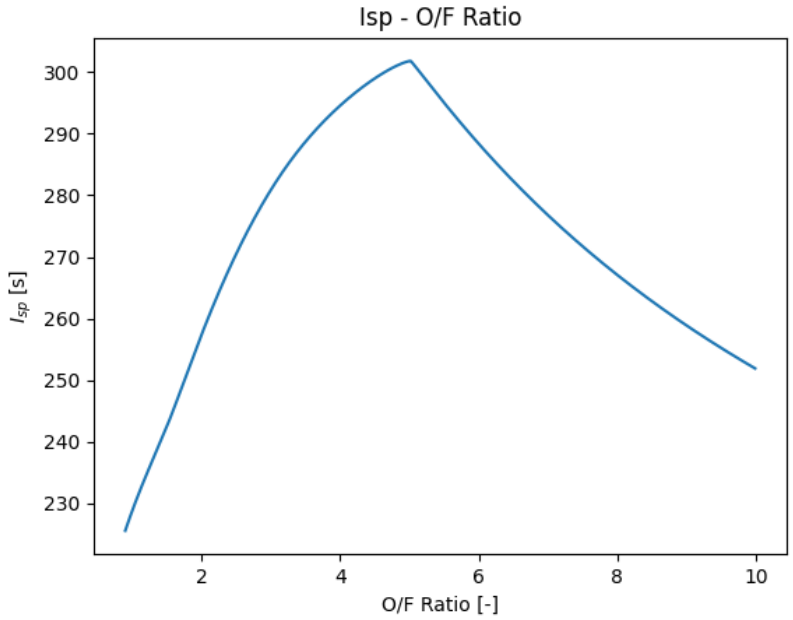

Figure 4.3: Example of an O/F - I_{sp} curve

With the reference temperature and the species known, the density and enthalpy of both steam and gaseous oxygen can be determined. This is done using the Cantera [33] python library. It is an open-source package that can be used for chemical kinetics, thermodynamics, and transport processes. Its strengths lie predominantly in the gas-phase domain. To compute the required properties at the specified conditions, Cantera needs to be supplied with a chemical mechanisms model, for which the GRI-3.0 [34] gas model is used. The Cantera model then determines the required properties based on the species, temperature and pressure. The former two were already determined previously and the pressure is taken as the combustion chamber pressure.

Finally, equation (4.1) for the weight fraction of oxygen can be derived, where n represents the molecular weight of each specie, η describes the concentration by weight of the HTP, and ξ describes the weight fraction of molecular oxygen in the decomposition products.

$$\xi_{O_2} = \frac{\eta n_{O_2}}{\eta n_{O_2} + 2n_{H_2O}} \tag{4.1}$$

All of this information can be used to determine the thermodynamic properties of the oxidiser in the combustion chamber, which defines the oxidiser input for CEA. With the CEA oxidiser input defined, the combustion properties can be modelled. After this, the ideal oxidiser to fuel (or O/F) ratio is determined. The O/F ratio controls various characteristics of the combustion products, but most of these characteristics will ultimately affect the overall fuel efficiency of the rocket engine, which is expressed by specific impulse or I_{sp}. Therefore, the ideal O/F ratio is the one that produces the highest I_{sp}. A typical O/F-I_{sp} curve can be seen in figure 4.3.

It should be noted that the model optimises the O/F ratio for the ideal impulse at the primary operating altitude rather than the ideal specific impulse. To achieve this, the expansion ratio is one of the inputs

for the O/F ratio optimisation algorithm. Since the nozzle expansion ratio can only be determined once the combustion properties are known, an iterative sub-loop is implemented in the model design iteration main-loop to converge the correct nozzle design for the combustion parameters. A more detailed description can be found in section 4.5.

Once the ideal O/F ratio is determined, the model computes various chamber combustion properties such as:

- Characteristic Velocity $C*$
- Chamber Temperature T_c
- Chamber Density ρ_c
- Chamber Mean Molar Mass n_c
- Chamber Specific Heat Ratio γ_c
- Chamber Gas Constant R_c
- Exit pressure P_e

4.4.3. Nozzle

The nozzle module of the numerical model is primarily used to determine the throat area and exit area. This is predominantly done using ideal rocket theory (IRT) [18] using the inputs from the combustion modules (section 4.4.2), fixed design variables and design constraints. The actual nozzle contour based on nozzle type and expansion ratio will be defined in the contour module (see section 4.4.5).

The specific impulse of an ideal rocket engine is defined by equation (4.2a) with T_{nom} representing nominal design thrust, $\dot{m}$ representing propellant mass flow, and g_0 being the standard sea level acceleration due to gravity ($9.80665\ \left[\frac{m}{s^2}\right]$). This can be rearranged to equation (4.2b).

$$I_{sp} = \frac{T_{nom}}{\dot{m} g_0} \tag{4.2a}$$

$$\dot{m} = \frac{T_{nom}}{I_{sp} g_0} \tag{4.2b}$$

Based on this, the fuel and oxidiser mass flows can be computed using equations (4.3a) and (4.3b). These values are used primarily in the feed system, tank, and injector sizing modules.

$$\dot{m}_F = \frac{\dot{m}}{1 + OF} \tag{4.3a}$$

$$\dot{m}_O = \frac{\dot{m}\ OF}{1 + OF} \tag{4.3b}$$

The nozzle throat area is sized using the characteristic velocity. The characteristic velocity in an ideal rocket engine is defined as seen in equation (4.4a) and can be rearranged to equation (4.4b) to determine the throat is A_t. $C*$ represents the characteristic velocity, $\dot{m}$ the propellant mass flow, and p_c the combustion chamber pressure (at the injector face).

$$C^* = \frac{A_t\ p_c}{\dot{m}} \tag{4.4a}$$

$$A_t = \frac{C^*\ \dot{m}}{p_c} \tag{4.4b}$$

For sizing the nozzle exit area, there are two competing constraints. On the one hand, the nozzle expansion should be sized such that pressure at the exit of the nozzle divergent section should equal the ambient pressure at the nominal operating altitude of the rocket engine. This ensures that the expansion work

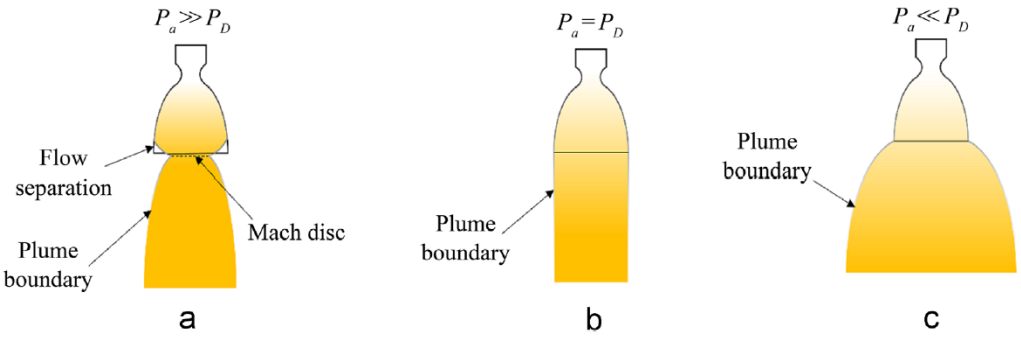

Figure 4.4: Over-expanded (a), correctly expanded (b), and under-expanded nozzle (c) [35]

performed on the exhaust gas is maximised without inducing flow separation losses from an over-expanded nozzle. An example of various nozzle expansions can be seen in figure 4.4.

One of the fixed model inputs is the nominal (or design) operating altitude for the propulsion system. The ambient pressure at this altitude is used to size the exit pressure at the nozzle. To determine, the international standard atmosphere (ISA) model is used to obtain an ambient pressure estimate for a given altitude. The ideal exit area for a certain pressure ratio can be computed using equation (4.5), where A_t is the previously determined throat area, γ is the specific heat ratio of the exhaust gases, $\Gamma(\gamma)$ is the Vandenkerckhove function (see equation (4.6)), p_c is the combustion chamber pressure, and p_e is the targeted expansion pressure.

$$A_e = A_t \frac{\Gamma(\gamma)}{\sqrt{\frac{2\gamma}{\gamma-1}}} \left(\frac{p_e}{p_c}\right)^{\left(\frac{\gamma-1}{\gamma}\right)} \tag{4.5}$$

$$\Gamma(\gamma) = \sqrt{\gamma} \left(\frac{2}{\gamma+1}\right)^{\frac{\gamma+1}{2*(\gamma-1)}} \tag{4.6}$$

This area is then compared to the area constrained by the rocket's internal diameter. Since the propulsion system is an upper-stage propulsion system, the exit diameter of the nozzle needs to fit within the separation interface. Therefore, the nozzle exit diameter cannot exceed this internal diameter. Once the ideal exit diameter is computed, it is compared with the maximum possible exit diameter. If the ideal nozzle exit is larger than this constraint, the nozzle exit diameter is constrained to this maximum possible diameter. The nozzle area expansion ratio ϵ can finally be defined by equation (4.7).

$$\epsilon = \frac{A_e}{A_t} \tag{4.7}$$

4.4.4. Chamber

The chamber module's primary objective is to size the dimensions of the decomposition and combustion chambers. This only includes the internal geometry of the chambers. Transport and thermal considerations will be treated in sections 4.4.6 and 4.4.7.

Decomposition Chamber

The catalyst chamber contains the catalyst used to decompose the HTP into the hot steam/GOX mixture, which is then injected into the combustion chamber to combust with the fuel. The sub-module primarily determines the geometry of the catalyst but also estimates the pressure drop over the catalyst bed. The latter will be required in the injector, feed system and tank sizing modules.

The catalyst used in this propulsion system is a Manganese-oxide-coated nickel sponge. Research has shown that this type of catalyst performs best for a given catalyst bed loading (CBL) [7], with a common

value being $60 - 70\ \frac{kg}{m^2 \cdot s}$. This can be used to determine the cross-sectional area of the catalyst bed using equation (4.8)

$$A_{cat} = \frac{\dot{m}_O}{CBL} \tag{4.8}$$

Similarly, this type of catalyst is commonly used with a length-to-diameter ratio (L/D_{cat}) of 1-2. Since the catalyst bed is designed as a cylinder, the length of the catalyst can be determined using equation (4.9).

$$L_{cat} = L/D_{cat} D_{cat} = L/D_{cat} \sqrt{A_{cat} \frac{4}{\pi}} \tag{4.9}$$

This defines the geometry of the catalyst bed and therefore also the catalyst chamber. To determine the mass of the decomposition chamber, the wall thickness of the chamber needs to be determined. However, this is only possible if the maximum pressure in the decomposition chamber is known. To determine this, the pressure drop over the catalyst bed needs to be known (since the sum of the pressure drop and the chamber pressure will be the maximum pressure in the decomposition chamber).

In future works on this system, this data should be directly sourced from HyProp testing, but as a temporary substitute, an Ergun-type equation, in this case, equation (4.10), can be used to model the pressure drop for a given length in a sponge [36]. ΔL is the length of the catalyst, μ is the dynamic viscosity of the gas flowing through the catalyst bed, d_h is the hydraulic diameter, ρ is the gas density, and u is the flow velocity ahead in the catalyst bed.

$$\Delta p = \Delta L \left(\frac{110\mu}{\psi d_h^2} u + \frac{1.45\rho}{\psi^2 d_h} u^2 \right) \tag{4.10}$$

The porosity ψ was specified in section 3.6.1 as 0.952. The source of equation (4.10) also specifies equation (4.11) as a relation between ppi (pores-per-inch) and the hydraulic diameter.

$$d_h = 0.028 \cdot ppi^{-0.721} \tag{4.11}$$

The viscosity and density of the hot steam/GOX mixture are determined by utilising the same Cantera model used in section 4.4.2. Finally, based on this the flow velocity can be determined using equation (4.12).

$$u = \frac{\dot{m}_O}{A_{cat} \rho} \tag{4.12}$$

Finally, the maximum pressure in the decomposition chamber will be the sum combustion chamber pressure and the catalyst bed pressure drop:

$$p_{d_{max}} = p_c + \Delta p \tag{4.13}$$

With this, the wall thickness of the chamber can be computed. This is done using the thin-walled approximation for circumferential stress in pressure vessels [37], as seen in equation (4.14b). σ_y is the yield stress of the selected material and SF is a safety factor following the ECSS-E-ST-32-02C standard specifying failure mode safety factors for pressure vessels [38].

$$\sigma_y = \frac{p_{d_{max}} \cdot D_{cat}}{2 \cdot t} \tag{4.14a}$$

$$t = SF \frac{p_{d_{max}} \cdot D_{cat}}{2 \cdot \sigma_y} \tag{4.14b}$$

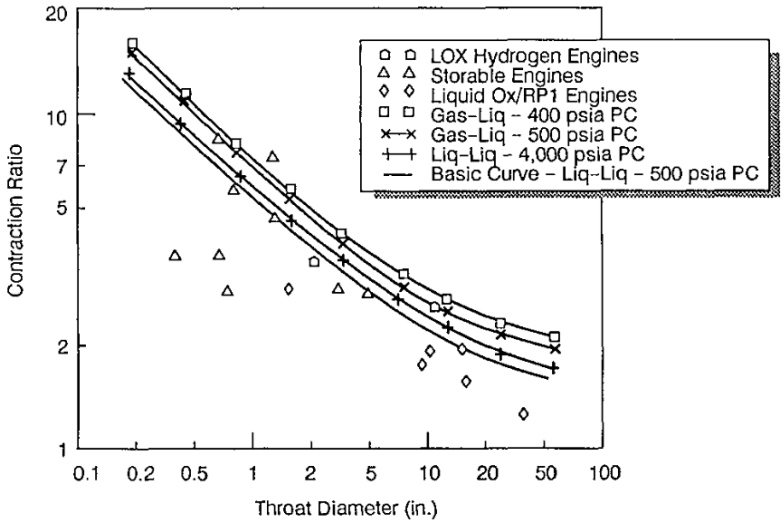

Figure 4.5: Throat Diameter - Contraction Ratio [24]

Based on this, the mass of the decomposition chamber as well as the catalyst is then computed and added to the total mass tally of the model.

Combustion Chamber

Generally, the combustion chamber of a liquid rocket engine is sized by the so-called characteristic length L^* [29]. The characteristic length is defined by equation (4.15), where V_c is the combustion chamber volume and A_t is the throat area.

$$L^* = \frac{V_c}{A_t} \tag{4.15}$$

The characteristic length can also be used to determine the dwell time τ of the mixed, combusting propellants in the combustion chamber. This is expressed in equation (4.16) [18], where $\Gamma(\gamma)$ is the Vandenkerckhove function (see equation (4.6)) and c^* is the characteristic velocity.

$$\tau = \frac{1}{\Gamma(\gamma)^2} \frac{L^*}{c^*} \tag{4.16}$$

The dwell time in the combustion chamber should be sufficiently long such that the propellant mixture can completely combust, but not too long such that fully combusted products start losing heat before expansion work can be performed on the gas through the nozzle. Since both the time to complete combustion and the characteristic velocity are properties of the fuel-oxidiser combination (and thus independent of engine parameters), the characteristic length is also tied to the fuel-oxidiser combination. For common propellants, there is sufficient historical data that a thrust chamber can be sized by comparing to a large enough number of similar systems using the same propellant.

However, due to the unique nature of the combustion process proposed in this work, there are very few historical examples of comparable systems. Additionally, the fuel can change since the type of fuel is one of the optimisation variables. Therefore, a chamber geometry sizing method needs to be chosen that does not immediately rely on the specific propellant type. Another possible method for sizing the chamber geometry is to relate chamber length and contraction ratio to the same throat diameter [24]. Crucially this has been correlated for various pressures and propellant-phase combinations. These correlations can be seen in figures 4.5 and 4.6.

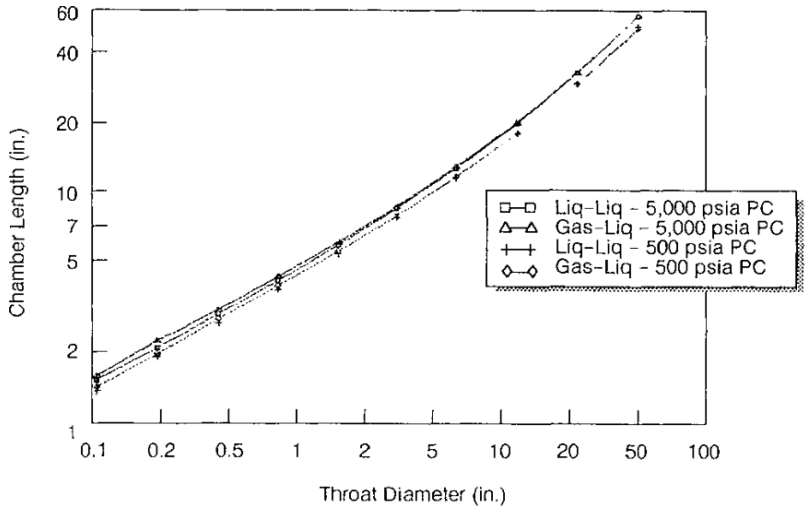

Figure 4.6: Throat Diameter - Chamber Length [24]

One of these correlations is made for one of the propellants being liquid and one of them being gaseous, at around 500 psia (35 bar) chamber pressure. This very adequately describes the type of propulsion system in this work. Thus the estimates for chamber length and contraction ratio are based on the curve-fit in equations (4.17a) and (4.17b) respectively.

$$L_c = 1.51807351 + 0.68061063 \cdot D_t + 0.58795218 \cdot \sqrt{D_t} \tag{4.17a}$$

$$\epsilon_c = 0.02105119 + \frac{0.76570091}{D_t^{0.47232351}} \tag{4.17b}$$

Based on this, the chamber diameter can also be determined using equation (4.18).

$$D_c = \sqrt{\epsilon_c} \cdot D_t \tag{4.18}$$

With this, the combustion chamber geometry has been determined. However, for the verification and validation of this module, additional parameters need to be determined to characterise the propellant flow through the chamber.

4.4.5. Contour

The main purpose of the contour module is to provide a discretised model of the combined combustion chamber and nozzle contour. This contour is used in the chamber transport model (see section 4.4.6) and also for the nozzle and chamber mass estimations. Next to this, the contour module also determines the exact geometry of the nozzle, which is especially important for bell/parabolic nozzles.

Chamber

The representation of the decomposition and combustion chambers is relatively trivial. Due to the cylindrical geometry of both of these sections of the propulsion system, the cross-section remains constant from the injector face to the nozzle entrance. The combustion chamber however is still discretised to allow for the modelling of the pressure drop from the injector face to the nozzle entrance, thus modelling the engine as a finite area combustor rather than an infinite area combustor.

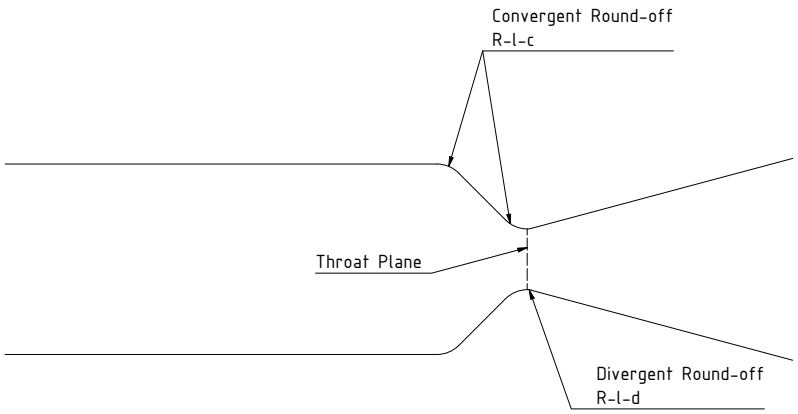

Figure 4.7: Throat Round-offs

Nozzle Convergent/Throat

The convergent of the nozzle is commonly set at an angle of $\beta = 45°$ [29]. Furthermore, the transition from the chamber to nozzle convergent as well as the transition from convergent to throat are rounded off with the round-off radius R_{l_c} defined by equation (4.19), where R_t is the throat radius.

$$R_{l_c} = 1.5 \cdot R_t \tag{4.19}$$

Furthermore, the transition from the throat into nozzle divergent is rounded off with the round-off radius R_{l_d} defined by equation (4.20), again based on throat radius R_t

$$R_{l_d} = 0.382 \cdot R_t \tag{4.20}$$

The location of the round-offs is visualised in figure 4.7, which shows a conical nozzle divergent as an example though the round-offs remain the same for a bell/parabolic nozzle as well.

Nozzle Divergent - Conical

One of the two nozzle types modelled is the conical nozzle. Its main advantage is its simple geometry and thus it is comparatively simple in manufacturing aspects. Conical nozzles are typically used on solid rocket motors (since super-heated solid particles do not allow for a double-curved nozzle contour) and cold-gas thrusters [29]. However, the manufacturing and construction advantages also apply to liquid rocket motors.

Because of the simple construction of a conical nozzle, its contour is also defined by a simple set of parameters. The primary parameters defining the shape of a conical nozzle divergent are:

- Throat Radius R_t
- Exit Radius R_e
- Divergent Angle α

The throat radius is determined via the throat area by the nozzle sizing module (see section 4.4.3) using equation (4.4b). The same module also determines the exit radius via the exit area using equation (4.5). The divergent angle is determined based on historical data. The optimum throat angle according to literature [24], [29] lies in the range of 12°- 18°. Therefore, for this application, a divergence angle α of 15° is used.

The length of the conical divergent can be determined using equation (4.21). This equation also accounts for the throat-divergent transition round-off,

$$L_d = \frac{R_t \cdot (\sqrt{\epsilon} - 1) + R_{l_d} \cdot \left(\frac{1}{\cos\alpha} - 1\right)}{\tan\alpha} \tag{4.21}$$

This divergent section is also discretised to allow for the thermal modelling of the throat and nozzle divergent. Finally, the flow divergence loss at the end of the nozzle is computed.

Finally, the flow divergence loss ε_{div} can be computed using equation (4.22). This is then factored back into the impulse component of the thrust, which is then fed back into the iteration to adjust the thrust setting such that the effective thrust produced still matches the required thrust.

$$\varepsilon_{div} = 1 - \left(\frac{1 + \cos(\alpha)}{2}\right) \tag{4.22}$$

Nozzle Divergent - Bell

Next to the conical nozzle divergent, the contour model can also determine and discretise the shape of a bell/parabolic nozzle. It is shaped so that it has a relatively high initial expansion which gradually decreases. This is possible because of the initial higher pressure in the early phases of the nozzle divergent. Ultimately, the bell nozzle reduces the flow divergence losses while producing an overall shorter nozzle for the same expansion ratio when compared to an equivalent conical nozzle divergent.

The throat contour is based on a parabolic equation. In figure 4.8, the coordinate system can be seen. The parabolic equation defining the shape of the bell nozzle is defined in equation (4.23). The x-axis is the centerline of the nozzle, and the y-axis points radially out of the nozzle. Point P is the point where the throat-divergent round-off transitions into the divergent of the nozzle. Point E (not represented in equation (4.4b)) is the exit of the nozzle.

$$x = a \cdot y^2 + b \cdot y + c \tag{4.23}$$

Thus the coefficients of the parabola need to be defined such that the parabola passes through point P. It should also be tangent to the throat-divergent round-off at Point P and also have the desired final parabola angle at Point E. Based on this, the parameters a, b, and c are defined by equations (4.24a) to (4.24c) respectively [18].

$$a = \frac{\tan\left(\frac{\pi}{2} - \theta_E\right) - \tan\left(\frac{\pi}{2} - \theta_P\right)}{2 \cdot (y_E - y_P)} \tag{4.24a}$$

$$b = \tan\left(\frac{\pi}{2} - \theta_P\right) - 2 \cdot a \cdot y_P \tag{4.24b}$$

$$c = x_P - a \cdot y_P^2 - b \cdot y_P \tag{4.24c}$$

These three curve parameters are defined as the x- and y-coordinates of the throat-divergent round-off transition point x_P and y_P, the y-coordinate at the nozzle exit y_E, and the initial and final parabola contour angle θ_P and θ_E. The coordinates of point P can be determined using equations (4.25) and (4.26) by using the trigonometric relations then can be derived from figure 4.8.

$$x_P = R_{l_d} \cdot \sin(\theta_P) = 0.382 \cdot R_t \cdot \sin(\theta_P) \tag{4.25}$$

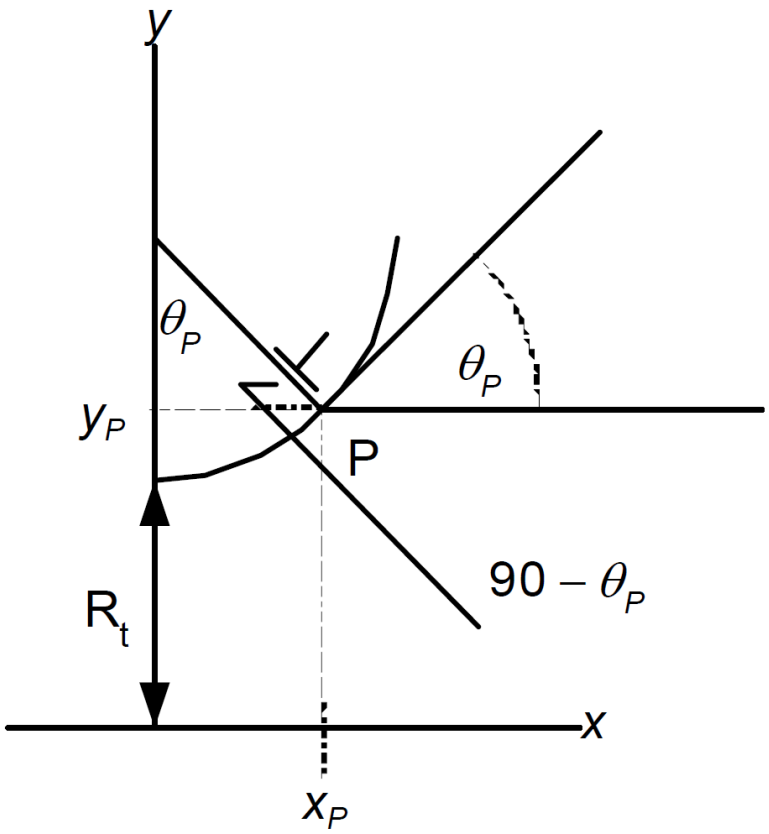

Figure 4.8: Throat Contour [18], [39]

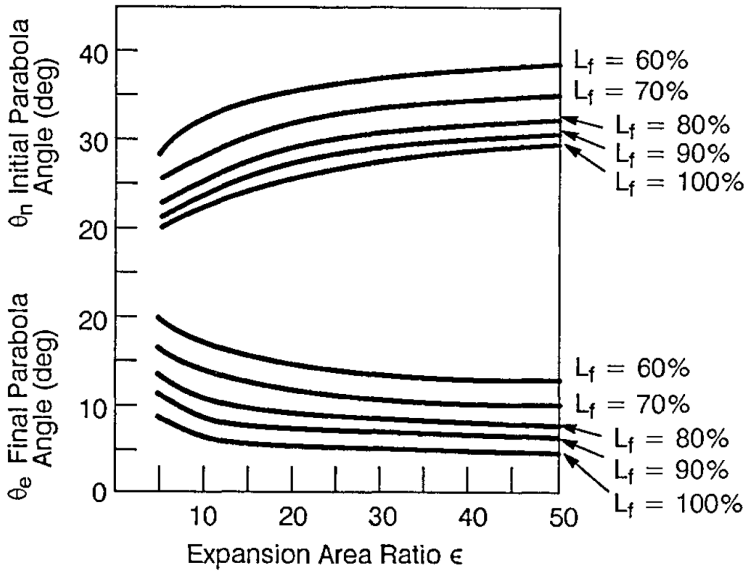

Figure 4.9: Initial and Final Parabola Angle θ_P and θ_E as a Function of Area Expansion Ratio ϵ for Varying Nozzle Length Fractions Lf [24]

$$y_P = R_t + (1 - \cos(\theta_P) \cdot R_{l_d} \tag{4.26}$$

Since the y-coordinate of the parabolic equation represents the radius of the nozzle at any given point, the y-coordinate of the exit point is exactly the nozzle exit radius. This can be derived using equation (4.27) and throat radius R_t and the nozzle area expansion ratio ϵ

$$y_E = R_e = \sqrt{\epsilon} \cdot R_t \tag{4.27}$$

In order to define the parameters defined by equations (4.24a) to (4.24c) as well as equations (4.25) and (4.26), the initial and final parabola angles need to be determined. Since these angles are chosen to optimise the complex flow through the nozzle, these are determined similarly to the chamber geometry by interpolating previously determined relations [24]. In this case, the graphs in figure 4.9 are interpolated into two surfaces, one for the initial parabola angle and one for the final parabola angle. For this, equation (4.28) is used.

$$\theta(\epsilon, Lf) = a + b \cdot \epsilon + c \cdot Lf + d \cdot \epsilon^2 + e \cdot Lf^2 + f \cdot \cdot \epsilon \cdot Lf + g \cdot \ln(\epsilon) + h \cdot \ln(Lf). \tag{4.28}$$

The parameters a - h are determined using a non-linear least-square regression curve fit. One curve fit is performed for the initial angle and one curve fit is performed for the final angle. For expansion ratios beyond 50, the only interpolation is done between varying nozzle length fractions using a parabola, since for higher expansion ratios the ideal angles become practically constant, as can be seen in figure 4.9.

With the initial and final parabola angle determined, all the other previously defined parameters can be computed and the nozzle divergent contour can be defined. In figure 4.10, an exemplary contour can be seen, with dimensions in [m]. It has an area expansion ratio of 108, a length fraction of 80%, an initial parabola angle of 31.81° and a final parabola angle of 7.81°.

Similarly to the conical nozzle, the flow divergence loss can be computed using the empirical relation in equation (4.29) [18], with final parabola angle θ_{final} and the angle of the straight line between throat and nozzle exit α, i.e. the angle of a conical nozzle with the same nozzle length and expansion ratio.

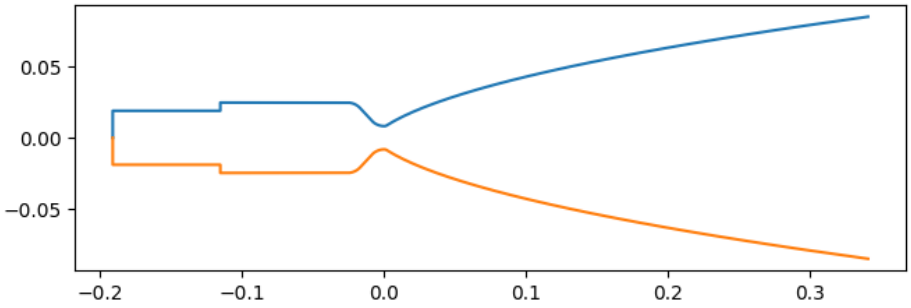

Figure 4.10: Combined Contour of Decomposition Chamber, Combustion Chamber, and Bell Nozzle

$$\varepsilon_{div} = 0.5 \cdot \left(1 - \cos\left(\frac{\alpha + \theta_E}{2}\right)\right) \tag{4.29}$$

4.4.6. Transport

The primary objective of the transport module is to compute various characteristics of the gases in the combustion chamber from the injector face through the nozzle to the nozzle exit. The outputs of these modules are primarily used by the cooling module (see section 4.4.7) to size and optimise various cooling methods. The algorithm also iterates through the solution multiple times to account for variations in specific heat ratio and flow properties. It should be noted that the flow model is a 1-D model, thus it ignores flow variations with a given cross-section from the centre line to the nozzle wall. To represent this would require the implementation of more complex finite element computational fluid dynamics algorithms, which would exceed the scope of this research. For the goal of finding the optimal design parameters in the given design space, this representation will be sufficient.

The transport module primarily relies on the isentropic flow equations. Initially, they are used to determine the Mach number through the combustion chamber and nozzle from the injector face to the nozzle exit. To achieve this, equation (4.30) is solved iteratively for the Mach number in the chamber/nozzle [18].

$$\frac{A}{A_t} = \left(\frac{\gamma + 1}{2}\right)^{-\frac{\gamma+1}{2\cdot(\gamma-1)}} \cdot \frac{\left(1 + \frac{\gamma-1}{2} \cdot M^2\right)^{\frac{\gamma+1}{2\cdot(\gamma-1)}}}{M} \tag{4.30}$$

This equation will always produce two Mach numbers for the same area ratio, one supersonic and one subsonic. Before the throat is passed, the subsonic solution is assumed; after the throat, the supersonic solution is taken. Based on this a Mach number profile through the nozzle can be determined.

This Mach number profile can then be used to determine the pressure, density, temperature and velocities of the hot gas along the chamber, using equation (4.31) for pressure, equation (4.32) for the density, equation (4.33) for the temperature, and equations (4.34) and (4.35) combined for the flow velocity in the nozzle.

$$\frac{p}{p_t} = \left(1 + \frac{\gamma - 1}{2} M^2\right)^{-\frac{\gamma}{\gamma-1}} \tag{4.31}$$

$$\frac{\rho}{\rho_t} = \left(1 + \frac{\gamma - 1}{2} M^2\right)^{-\frac{1}{\gamma-1}} \tag{4.32}$$

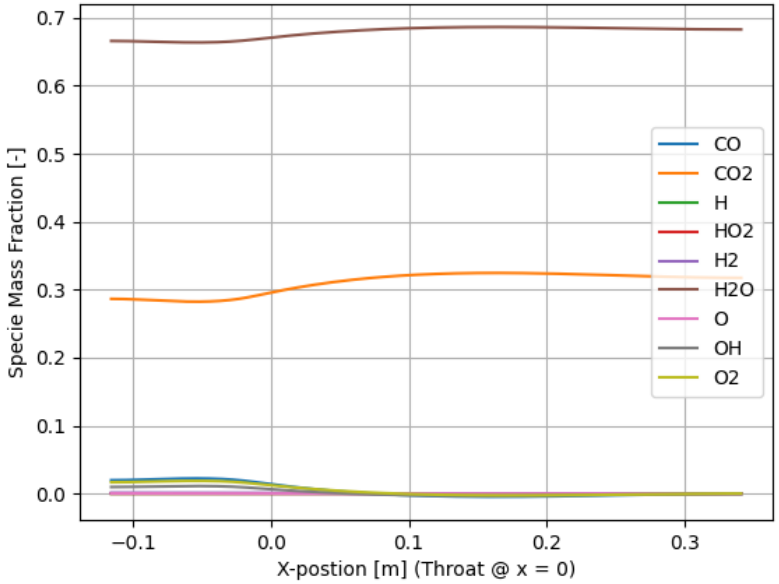

Figure 4.11: Exemplary gas composition along the combustion chamber

$$\frac{T}{T_t} = \left(1 + \frac{\gamma - 1}{2} M^2\right)^{-1} \tag{4.33}$$

$$a = \sqrt{\gamma \frac{p}{\rho}} \tag{4.34}$$

$$u = a \cdot M = \sqrt{\gamma \frac{p}{\rho}} \cdot M \tag{4.35}$$

To determine these for the whole chamber, the throat conditions (subscript t) need to be known first, since they define these conditions for the rest of the isentropic flow process. For this, the chamber conditions can be used, since they are an output of the combustion modules (see section 4.4.2). Equations (4.31) to (4.33) can be solved for p_t, ρ_t, and T_t respectively to determine these values.

For the first iteration of the chamber transport module, the model assumes a constant value of the specific heat ratio γ. However, in reality, the specific heat of a substance changes with temperature, therefore the specific heat ratio can also change. To account for this, an iteration over the specific heat ratio is performed. After the first iteration, a first estimate of the state of the gas along the combustion chamber is known. Next to this, the combustion model provides a mass fraction distribution of the species in the hot gas at the injector face, the nozzle entrance, the nozzle throat, and the nozzle exit. This is then interpolated using cubic splines to obtain a continuous function of gas composition along the chamber. This can be seen in figure 4.11.

This is used to create a Cantera gas model (similar to those in the catalyst and combustion modules sections 4.4.2 and 4.4.4) is used to determine various gas properties at high temperatures. For this, a modified version of the GRI-3.0 [34] is used. Based on the temperature, pressure and composition of the gas, the model determines of the profile of the specific heat ratio γ, viscosity μ, and specific heat at constant pressure c_p throughout the chamber. While the specific heat ratio profile is fed back into the above equations to generate a more accurate estimate of the chamber transport, viscosity and specific heat are used in the heat transfer calculations.

To size various cooling methods modelled by the cooling modules (see section 4.4.7), the heat transfer rate from the hot gas in the chamber into the chamber walls needs to be determined. The main transfer mode of heat in the combustion chamber from the gas to the wall is convective heat transfer. The heat flux from this type of heat transfer is defined by equation (4.36), where T_g is the hot gas temperature, T_w is the wall temperature, and h_α.

$$q_\alpha = h_\alpha \cdot (T_g - T_w) \tag{4.36}$$

The hot gas temperature is known from the previous computations, and the wall temperature is set to the maximal allowable temperature allowed by the selected chamber wall material.

The heat transfer coefficient in this case is determined using the semi-empirical Standard-Bartz relation [40] in equation (4.37). Compared to other heat transfer coefficient relations, the Standard-Bartz allows taking chamber contour variations into account, which allows it to be used throughout the chamber.

$$h_{\alpha_g} = \frac{0.026}{D_t^{0.2}} \cdot \frac{\mu^{0.2} \cdot c_p}{Pr^{0.6}} \cdot \left(\frac{p}{c*}\right)^{0.8} \cdot \left(\frac{D_t}{r_c}\right)^{0.1} \cdot \left(\frac{D_t}{D}\right)^{1.8} \cdot \varphi \tag{4.37}$$

The coefficient is defined by the following variables:

- Throat Diameter D_t
- Local Viscosity μ
- Local Specific Heat at Constant Pressure c_p
- Local Prandtl number Pr
- Local Pressure P
- Characteristic Velocity C^*
- Throat round-off radius r_c
- Local Diameter D
- Boundary Layer Correction Factor φ

The correction factor φ accounts for variation across the boundary layer and is defined by equation (4.38).

$$\varphi = \frac{\left(1 + M^2 \cdot \frac{(\gamma-1)}{2}\right)^{-0.12}}{\left(0.5 + 0.5 \cdot \frac{T_w}{T_g} \cdot \left(1 + M^2 \cdot \frac{(\gamma-1)}{2}\right)\right)^{-0.68}} \tag{4.38}$$

4.4.7. Cooling

The cooling module of the numerical model is tasked with sizing various types of cooling methods which can be used in the propulsion system. In section 3.6.1, five possible cooling methods to be considered in the design optimisation were defined: Radiative Cooling, Heat-sink Cooling, Ablation Cooling, Regenerative Cooling with HTP, and Regenerative Cooling using the fuel.

Each of these options will be modelled in the numerical model such that the optimisation algorithm can select the best cooling method based on the defined fitness function. It should be noted while the two regenerative cooling methods are considered as separate design options (due to changing implications on feed pressure drops etc.), they can be modelled using the same method. Hence these four modelling methods are considered in this section.

It should be noted that for this module, certain assumptions need to be made which limit the scope of this module. Firstly, the cooling model always assumes the specified burn time as part of the numerical model inputs. This means that if throttling is implemented in the future, this is not taken into account especially when considering the heat-sink and ablation cooling, where the burn time is an essential factor in the sizing of the cooling system. Next to this, the modules always only assume cooling mode at the same time.

This means that with e.g. regenerative cooling, potential heat-sink or radiative effects are ignored. The effect of this should be negligible for each case since each of the cooling methods will be sized such that the design mode is the dominant heat transfer mode.

Radiative

Radiative cooling is the most easily modelled cooling method. In section 4.4.6, equation (4.37) defines the hot-gas side heat transfer coefficient h_{α_g} from the combustion gases into the chamber walls. This can be used in equation (4.39) together with the combustion gas temperature T_g and the inside wall temperature T_{w_i}.

$$q_{w_i} = h_{\alpha_g} \cdot (T_g - T_{w_i}) \tag{4.39}$$

Furthermore, it is known that the radiated heat flux is defined by the Stefan-Boltzmann law in equation (4.40), with outer wall temperature T_{w_o}, Stefan-Boltzmann Constant σ and emissivity ε, which is assumed to be 0.8.

$$q_{rad} = \varepsilon \cdot \sigma \cdot T_{w_o}^4 \tag{4.40}$$

Finally, in order to link the inner wall temperature to the outer wall temperature, the equation for conductive heat transfer in equation (4.41) with wall thickness t_w and wall material thermal conductivity k.

$$q_{cond} = \frac{k}{t_w} \cdot (T_{w_i} - T_{w_o}) \tag{4.41}$$

Since the numerical model only considers steady-state conditions, it can be deduced that the three previously determined heat fluxes must be equal for the chamber to be in thermal equilibrium. Therefore, equation (4.42) must hold.

$$q_{w_i} = q_{rad} = q_{cond} \tag{4.42}$$

Combining equations (4.39) and (4.41) can be used to relate the inner wall temperature and the outer wall temperature with equation (4.43).

$$T_{w_i} = \frac{T_{w_o} + \frac{h_{\alpha_g}}{k}}{1 + \frac{h_{\alpha_g}}{k}} \tag{4.43}$$

Finally, the balance between the radiated heat on the outer wall and the convected heat on the inner wall in equation (4.44) can be implicitly solved for the outer wall temperature.

$$h_{\alpha_g} \cdot (T_g - T_{w_i}) = \varepsilon \cdot \sigma \cdot T_{w_o}^4 \tag{4.44}$$

This computation is performed for each step along the discretised chamber-nozzle profile. If for any given point along the profile, the equilibrium temperature of the outer wall exceeds the maximum allowable mechanical temperature of the selected material, the local wall thickness is increased until the the temperature is within acceptable limits or until 10 [mm] wall thickness is reached. In the case of the latter, the primary cooling method will be switched to heat-sink cooling, since a thick-walled chamber automatically leads to this cooling method.

The primary limitation of the radiative cooling model used is that it does not account for heat sink cooling, which is the reason its wall thickness range is limited to 10 [mm]. Next to this, the model does not account for heat conduction along the length of the chamber. Overall this, would likely flatten the curve of the outer wall temperature and spread some of the heat more towards the nozzle exit.

Heat-sink
For the heat-sink cooling model, it is assumed that all heat convected from the combustion gases is stored in the mass of the chamber walls. Hence, any radiation of the heat is ignored.

In section 4.4.5, the contour module discretises the shape of the combustion chamber into cylindrical segments of length dx. Using equation (4.39), the heat rate radiated per segment can defined using equation (4.45) with local segment diameter D_{seg} and segment length dx.

$$Q_{seg} = q_{w_i} \cdot A_{seg} = q_{w_i} \cdot \pi \cdot D_{seg} \cdot dx \tag{4.45}$$

In order to determine, the energy radiated into the chamber wall, the heat rate is multiplied with the burn time. The required thermal mass of a given chamber wall segment can then be determined using equation (4.46) with burn time t_b, chamber wall specific heat c_w, maximum allowable wall temperature T_{max} and initial wall temperature T_{init}. The initial temperature is assumed as 298 [K] and the maximum allowable temperature is based on the material selected.

$$m_{seg} = \frac{Q_{seg} \cdot t_b}{c_w \cdot (T_{max} - T_{init})} \tag{4.46}$$

Since the inner diameter of the chamber is fixed, the required outer chamber diameter is constrained such that the cylindrical section of the segments has the required thermal mass. Based on the equation for the mass of a cylinder, the required outer diameter can be derived using equation (4.47) with wall material density ρ_w.

$$D_{o_{seg}} = \sqrt{\frac{4 \cdot m_{seg}}{\pi \cdot \rho_w \cdot dx} + D_{seg}^2} \tag{4.47}$$

The chamber-nozzle mass can then be determined by summing all mass segments:

$$m_c = \sum^{seg} m_{seg} \tag{4.48}$$

Similarly to the radiative cooling model, which does not account for heat-sink effects, the heat-sink cooling model does not account for radiative effects. Furthermore, it assumes perfect distribution of heat throughout the chamber. The steady-state nature of this model does not allow for the combined modelling of heat-sink and radiation cooling, since the heat transfer through the chamber wall requires the modelling of time-dependent effects [41].

In this step, more exact temperature strength curves should be implemented. At this point, the model limits the temperatures of the material to the point where the mechanical strength properties noticeably decrease. However, especially in the heat sink, the large amount of material can offset some losses in strength, at which point less material might be required. Overall, this method makes a more conservative estimate, which should serve well for determining the best cooling method for this propulsion system. However, for more detailed, final sizing of the propulsion system, this model should be improved if this cooling method is used.

Ablative
For ablative cooling, the modelling approach is rather similar to heat sink cooling. In this, case the heat flux convected into the ablator is assumed to be such that the material would not exceed the temperature limit of the chamber wall, thus it is defined by equation (4.36). The ablator surface is then assumed to be sized to the inner dimension of the combustion chamber. Since this is done in a segmented approach, the local ablator area is given by equation (4.49).

$$A_{abl} = D_c \cdot \pi \cdot dx \tag{4.49}$$

This can then be used in equation (4.50) to determine the thickness of the ablator for each segment. Here, Q_{seg} represents the segment heat flow, and ρ_{abl} and H_{abl} is the ablator density and heat of ablation. Common values for the latter two are 1900 $\left[\frac{kg}{m^3}\right]$ and 2500 $\left[\frac{kJ}{kg}\right]$ respectively [18].

$$t_{abl} = \frac{Q_{seg}}{\rho_{abl} \cdot A_{abl} \cdot H_{abl}} \tag{4.50}$$

Using this, the per-segment-ablator mass can be determined using equation (4.51). Summing this value for each segment will then yield the mass of the ablator.

$$m_{abl} = t_{abl} \cdot A_{abl} \cdot \rho_{abl} \tag{4.51}$$

Regenerative

Both regenerative cooling design methods will use the same modelling method since both HTP and all selected fuels can be represented using the same processes. For the model of regenerative cooling, the model considers three main heat transfer modes: From hot gas to inner chamber wall, from inner chamber wall to cooling channel wall, and from cooling channel wall to coolant. Thus, any heat transfer from radiation is neglected, since this usually makes up less than 5% of the heat transfer [42].

The first heat transfer mode is once again computed using equation (4.39) which is the same equation as for the radiative heat transfer. Similarly, the conductive heat transfer is still defined by equation (4.41) but taking the form of equation (4.52), where T_{w_c} represents the inner wall temperature and t_{w_i} is the inner chamber wall thickness (i.e. the wall between the combustion chamber and cooling channel.

$$q_{cond} = \frac{k}{t_{w_i}} \cdot (T_{w_i} - T_{w_c}) \tag{4.52}$$

However, unlike radiating the heat from the outer chamber wall, with regenerative cooling it instead is transferred into the cooling by another convective cooling process, from the cooling channel wall into the coolant. The heat flux from this process is defined equation (4.53) where h_{α_c} is the coolant-side convective heat transfer coefficient and T_{b_c} is the bulk temperature of the coolant in the coolant channel.

$$q_{cool} = h_{\alpha_c} \cdot (T_{w_c} - T_{b_c}) \tag{4.53}$$

The heat transfer coefficient h_{α_c} can be defined using equation (4.54) [43] using the coolant Nusselt number Nu_c, the coolant thermal conductivity k_c, and the cooling channel hydraulic diameter d_{h_c}.

$$h_{\alpha_c} = \frac{k_c \cdot Nu}{d_{h_c}} \tag{4.54}$$

The Nusselt number of the coolant can be determined using the empirical relation in equation (4.55) [43] using the coolant Reynolds number and Prandtl number Re_c and Pr_c.

$$Nu_c = 0.023 \cdot Re_c^{0.8} \cdot Pr_c^{0.4} \tag{4.55}$$

The coolant Reynolds number and Prandtl number can be determined using equations (4.56a) and (4.56b).

$$Re_c = \frac{\rho_c \cdot u_c \cdot d_{h_c}}{\mu_c} \tag{4.56a}$$

$$Pr_c = \frac{c_{b_c} \cdot \mu_c}{k_c} \tag{4.56b}$$

Finally, the hydraulic diameter of a cooling channel is defined by equation (4.57) using the individual cooling channel area A_c and the cooling channel cross-section perimeter P_c.

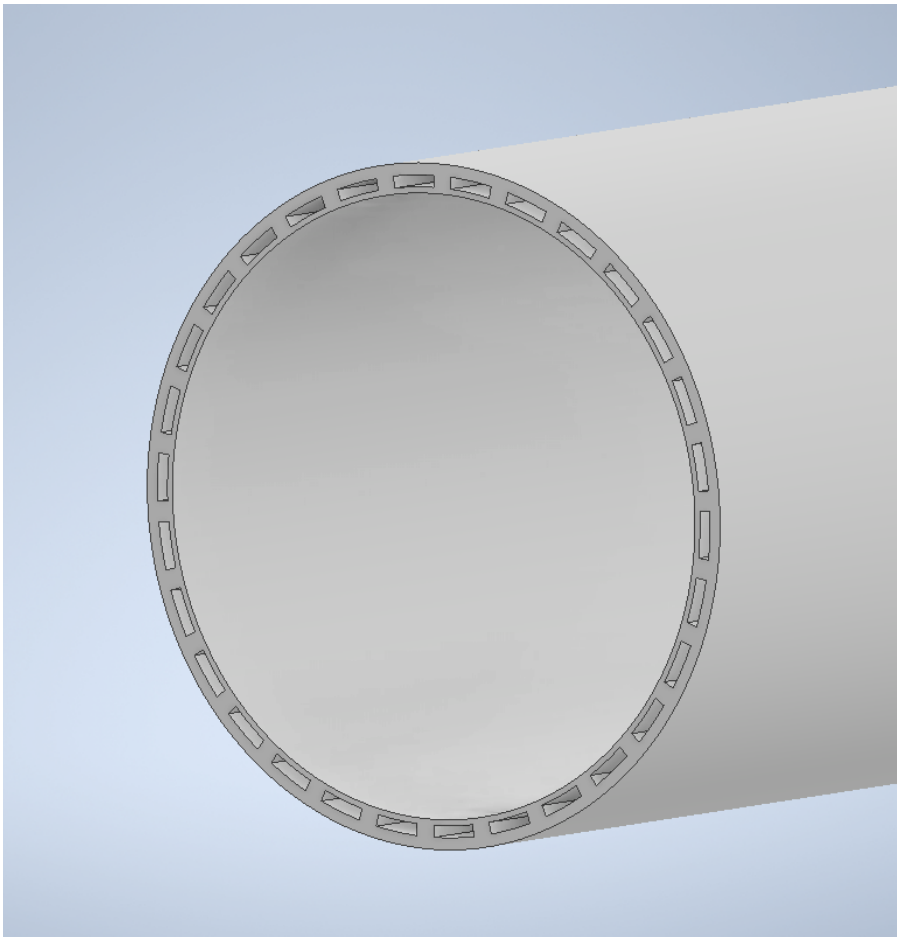

Figure 4.12: Cooling Channel Geometry

$$d_{h_c} = \frac{4 \cdot A_c}{P_c} \tag{4.57}$$

Since the heat transfer between chamber and coolant is dependent on the coolant temperature and some of the relevant coolant properties are temperature dependent, the method used is to start the coolant state computation at the nozzle exit and propagate up the chamber to the injector manifold of the combustion chamber. The coolant is assumed to enter the cooling channel manifold at the nozzle exit at a temperature of 298 [K]. For this model, a relatively simple cooling channel geometry has been assumed in order to simplify the model. This geometry can be seen in figure 4.12. If this cooling method is selected, then in later design iterations various other cooling channel designs can be considered to minimise the pressure drop over the cooling channels.

Similarly to the radiative cooling model, the temperatures are balanced by assuming that all the heat radiated convected into the hot-gas side chamber wall is conducted to the coolant side wall and convected into the coolant. This balance can thus be expressed in using equation (4.58).

$$q_{w_i} = q_{cool} \tag{4.58a}$$

$$h_{\alpha_g} \cdot (T_g - T_{w_i}) = h_{\alpha_c} \cdot (T_{w_c} - T_{b_c}) \tag{4.58b}$$

The goal is to solve this balance for the inner and cooling channel wall temperatures T_{w_i} and T_{w_c} respectively. In order to achieve this, the inner wall temperature can be related to the coolant channel wall temperature using equation (4.59).

$$T_{w_i} = \frac{h_{\alpha_g} \cdot T_g + \frac{k}{t_w} \cdot T_{w_o}}{h_{\alpha_g} + \frac{k}{t_w}} \tag{4.59}$$

With this, equation (4.58) can be solved iteratively solved for the cooling channel wall temperature. Once the solution has converged, the inner wall temperature can be determined using equation (4.59).

At this point, heat flux q_{cool} is known which can be used to determine the coolant temperature increase in a given nozzle segment using equation (4.60) with coolant mass flow $\dot{m}_c$ and coolant specific heat c_{p_c}.

$$\Delta T_{b_c} = \frac{q_{cool} \cdot \pi \cdot D_{seg} \cdot dx}{\dot{m}_c \cdot c_{p_c}} \tag{4.60}$$

Since the cooling channels can cause a significant pressure drop in the feed overall feed line from the tank to the combustion chamber, the coolant pressure drop needs to be estimated. This is done for each segment using equation (4.61), with coolant velocity u_c defined by equation (4.62), and the friction factor f_D implicitly defined by equation (4.63) using channel wall roughness ϵ_{w_c}.

$$\Delta p_{cool} = f_D \frac{dx}{2 \cdot d_{h_c}} \cdot \rho_c \cdot u_c^2 \tag{4.61}$$

$$u_c = \frac{\dot{m}_c}{\rho_c \cdot A_c} \tag{4.62}$$

$$\frac{1}{\sqrt{f_D}} = -2 \cdot \log\left(\frac{\epsilon_{w_c}}{3.7 \cdot d_{h_c}} + \frac{2.51}{Re_c \cdot \sqrt{f_D}}\right) \tag{4.63}$$

The temperature increase and pressure decrease of each segment are then factored into the coolant state before the next segment such that the property estimation of the coolant is accurate for the next segment.

Based on this method, a profile of coolant temperature, hot gas and coolant side wall temperature can be determined. An example of this can be seen in figure 4.13.

If the maximum inner wall temperature lies above the material limit temperature (as defined by appendix A), then the cooling channel geometry is adjusted until the maximum temperature lies below the limit. Similarly, if the maximum temperature is more than 10% below the specified limit, the cooling channel geometry is also adjusted until the temperature falls between these two boundaries. The adjustment is primarily done using the cooling channel height. This ensures that the cooling channels always provide sufficient cooling. Note that there is no safety margin defined since for this model the temperature limit is defined as the temperature where the material begins to lose its mechanical strength. Since the defined chamber geometry already includes safety margins on this strength, no safety factor is required for this.

Finally, the mass of the cooling system is estimated by summing the mass of the inner wall, the cooling channel tabs and the outer wall for each segment of the contour.

4.4.8. Injector

The goal of the injector module is to size and determine the performance of the injector. Since each injector is unique, they are represented differently in the model, but the underlying sizing principle is identical for the two fluid injectors.

For fluid injectors, the primary characteristic used in their sizing is the pressure drop over the injector Δp_i. It is defined by equation (4.64). Since the fluid density ρ and the orifice discharge coefficient C_d can be considered constant, the pressure drop predominantly affects the injection velocity V_{inj}.

$$\Delta p_i = C_d \cdot \frac{1}{2} \rho V_{inj}^2 \tag{4.64}$$

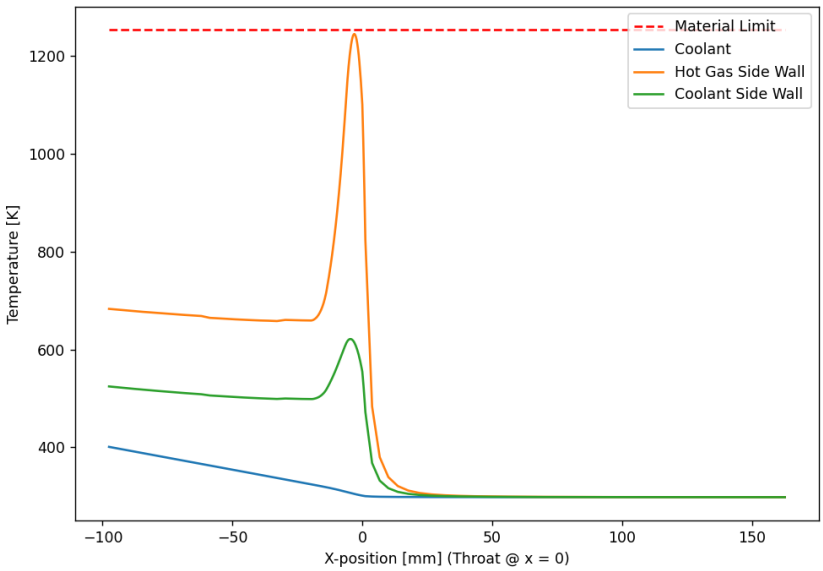

Figure 4.13: An exemplary plot of Hot-Gas Side Wall, Coolant Side Wall, and Coolant Temperature using HTP as coolant and Inconel 718 as chamber material.

However, the pressure drop is usually sized not solely by the injection velocity, but also by other considerations not directly quantified by equation (4.64). On the one hand, a higher pressure drop can lead to improved combustion stability. Additionally, in this case, the exothermic decomposition of HTP can be thermally catalysed, thus it can initiate a runaway decomposition reaction. A higher pressure drop helps to prevent this. On the other hand, a larger pressure drop means a larger required pressure upstream of the injector in the feed system. Especially in the case of a pressure-fed system, high feed pressures can quickly become impractical.

Thus, to determine the injector geometry without relying on cold-flow data, an iterative empirical approach is used [44]. This method has been previously used to size injectors with similar propellants. First, the initial characteristics of the injector need to be specified. These are:

- Injector Pressure Drop Δp_i
- Injector Mass Flow $\dot{m}_i$
- Injector Length l_i
- Fluid Density ρ
- Fluid Viscosity ν

It should be noted that the mass flow $\dot{m}_i$ refers to mass flow through an orifice

Next, the flow parameter μ is determined through equation (4.65). It is defined by the injector inlet coefficient ξ_{in}.

$$\mu = \frac{1}{\sqrt{1 + \xi_{in}}} \tag{4.65}$$

Initially, the injector inlet coefficient ξ_{in} can be determined using figures 4.14 and 4.15. Both figures suggest that for an unrounded, straight injector, ξ_{in} can be assumed to be equal to 0.5.

Once the flow parameter μ is determined, the diameter of the injector passage can be sized using equation (4.66)

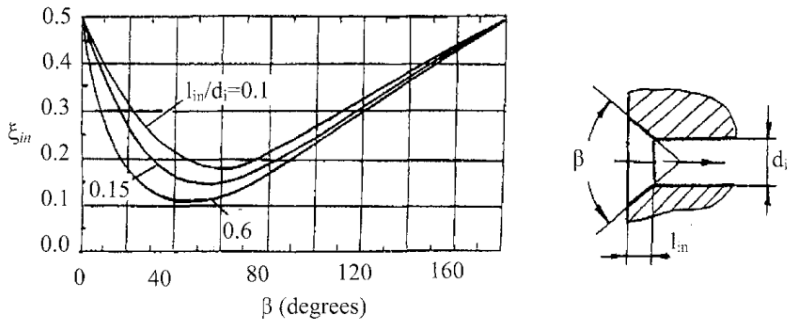

Figure 4.14: Effect of inlet-edge contraction on coefficient ξ_{in} [44]

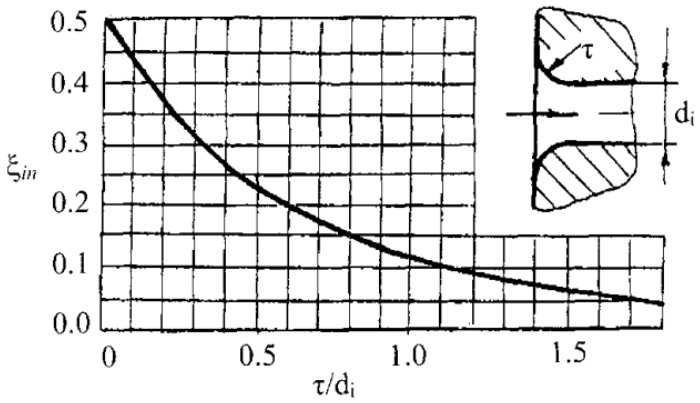

Figure 4.15: Effect of inlet-edge rounding on coefficient ξ_{in} [44]

$$d_i = 0.95 \cdot \dot{m}^{0.5} \cdot \mu^{-0.5} \cdot (\rho \cdot \Delta p_i)^{-0.25} \tag{4.66}$$

After this the injection velocity V_i and subsequently the injector Reynolds number Re need to be determined. The former is needed to determine the injector Reynolds Number and the latter is used to determine the fluid friction drag coefficient λ. The injection velocity is defined by equation (4.67).

$$V_i = \frac{1.273 \cdot \dot{m}_i}{\rho \cdot d_i^2} \tag{4.67}$$

The Reynolds number is then defined by equation (4.68) and it can be used to determine the friction drag coefficient λ using equation (4.69).

$$Re_i = \frac{\rho \cdot V_i \cdot D_i}{\nu} \tag{4.68}$$

$$\lambda = 0.3164 \cdot Re^{-0.25} \tag{4.69}$$

Based on this, the injector friction parameter ξ_{fr} can be determined based on the friction drag coefficient λ, the injector length l_i, and the injector diameter l_i using equation (4.70).

$$\xi_{fr} = \lambda \cdot \frac{l_i}{d_i} \tag{4.70}$$

The overall flow parameter can be updated using the equation (4.71), similar to equation (4.65).

$$\mu = \frac{1}{\sqrt{1 + \xi_i}} \tag{4.71}$$

The injector parameter ξ_i is determined using equation (4.72) and is determined by the parameters ξ_{1-c}, ξ_{in}, and ξ_{fr}.

$$\xi_i = \xi_{1-c} + \xi_{in} + \xi_{fr} \tag{4.72}$$

The latter two have already been previously established, thus only xi_{1-c} remains to be determined. It can be determined using equation (4.73).

$$\xi_{1-c} = 3.55378 \cdot e^{-0.647016 \cdot \log(Re)} - 0.103358 \tag{4.73}$$

Equation (4.73) is a a curve fit for the graph in figure 4.16. With parameter μ determined, the iteration process is looped back to equation (4.66). The iteration finishes once the parameter μ has converged and changes by less than 10^{-6} per iteration.

This method allows for the adequate sizing of the injector geometry without relying on extensive test data. However, this method fails to atomisation and spray behaviour of the injector orifice. The degree of atomisation determines how well the fuel and oxidiser mix in the combustion chamber. Additionally, the spray cone angle can be estimated to ensure uniform catalyst bed loading and improved mixing in the combustion chamber.

To judge the atomisation performance of an injector orifice, the Reynolds number Re from equation (4.68) can be compared with the Ohnesorge number Oh in equation (4.74), where σ represents the surface tension of the fluid. The Ohnesorge number relates viscous forces with surface tension and inertial forces in a fluid.

$$Oh = \frac{\nu}{\sqrt{\rho \cdot \sigma \cdot L}} \tag{4.74}$$

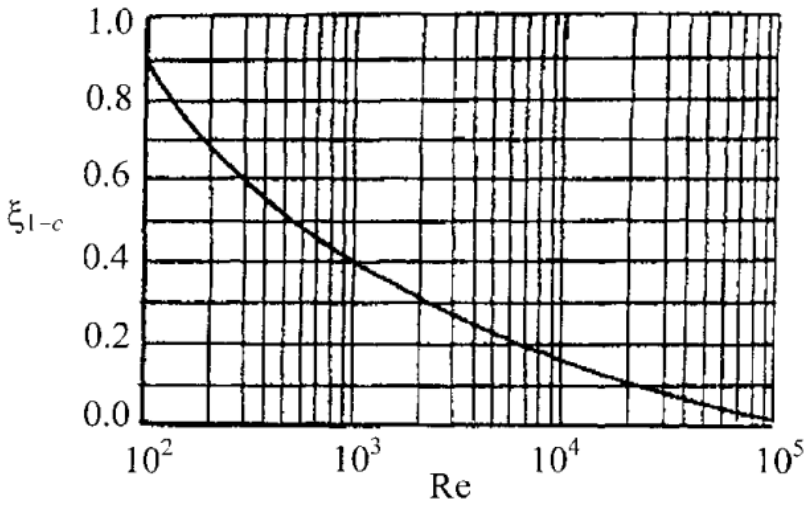

Figure 4.16: Injector parameter ξ_{1-c} as a function of of injector Reynolds number Re_i

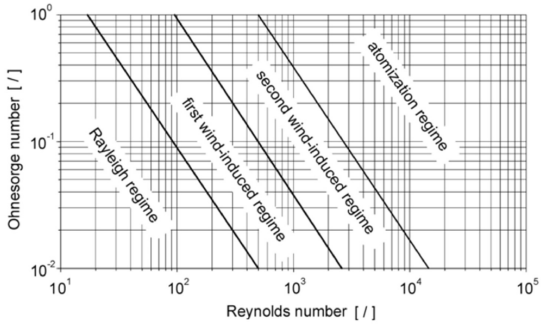

Figure 4.17: Regions of Spray Breakup Characterised by the Ohnesorge and Reynolds number [45]

To determine the spray breakup regime, the Ohnesorge and Reynolds numbers of the injector are compared to figure 4.17. For a rocket engine injector, the desired regime is the atomisation regime. Thus the Ohnesorge and Reynolds numbers must lie in this region for the injector to be a valid design. If this criterion is not met, then the design is discarded and reiterated with new parameters.

Next to this, another characteristic of the injector is the spray cone angle of each injector element as seen in figure 4.18. For the HTP injector, it is used to determine the coverage of the catalyst bed and for the fuel injector, it is used to determine the coverage in the combustion chamber.

The spray cone half angle θ can be determined using equation (4.75), where Re is the injector Reynolds number, l_i is the injector orifice length, d_i is the injector orifice length, ρ_L is the density of the injected fluid, ρ_A is the ambient density in the chamber, and n is a parameter given by equation (4.76). This specific relation for the spray cone angle is well-correlated for high ambient pressures [26].

$$\theta = 0.067 \cdot Re^{0.64} \cdot \left(\frac{l_i}{d_i}\right)^{-n} \cdot \left(1 - e^{0.023 \cdot \frac{\rho_L}{\rho_A}}\right)^{-1} \tag{4.75}$$

$$n = 0.0284 \cdot \left(\frac{\rho_L}{\rho_A}\right)^{0.39} \tag{4.76}$$

This angle can then be used to relate the spray cone radius r_{sc} to the spray cone length l_{sc} using 4.77.

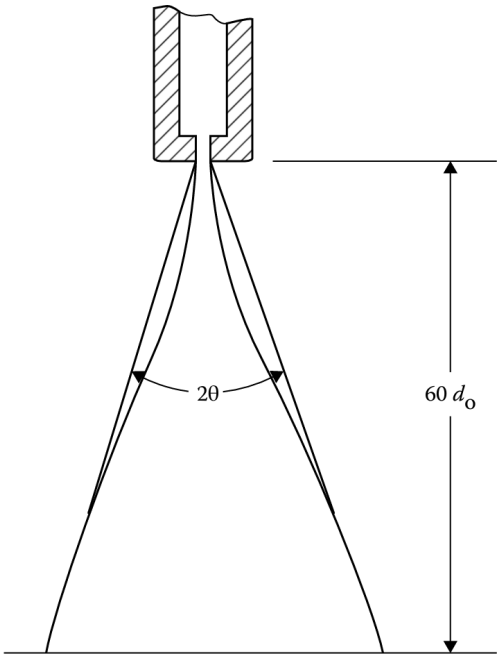

Figure 4.18: Spray Cone Angle on a Plain Orifice Injector [26]

$$\tan(\theta) = \frac{r_{sc}}{l_{sc}} \tag{4.77}$$

The coverage check is ultimately implemented for further improvements to the numerical model where propellant mixing in the combustion chamber will be able to be taken into account for the chamber transport and combustion models. At this stage, this merely serves as another verification and sizing output, which will predominantly be used to determine the sizing of various injector components.

4.4.9. Feed Lines

The Feed Line module represents the feed lines between tanks and combustion chamber/injectors. The primary task is to determine the pressure loss over the feed lines and to a lesser extent the mass of the feed line components. Determining the pressure loss over the feed lines is important for the sizing of the fluid tanks and subsequently the pressurant tank.

The feed line module can determine the effects of three main pressure loss sources:

- Straight Pipe Section
- Curved Pipe Sections
- Valves

The pressure loss over a straight section of pipe with length L is defined by the Darcy-Weisbach equation [46] in equation (4.78). ρ is the fluid density, v is the fluid flow velocity and D_H is the pipe hydraulic diameter. The latter is equal to the pipe internal diameter of pipes with a circular cross-section.

$$\frac{\Delta p}{L} = f_D \cdot \frac{\rho}{2} \cdot \frac{v^2}{D_H} \tag{4.78}$$

To define this equation for the specific application, the Darcy friction factor f_D needs to be determined. This can be done using the Colebrook-White equation [47] in equation (4.79) where ϵ is the pipe surface roughness, which is assumed as a material property of the feed line material.

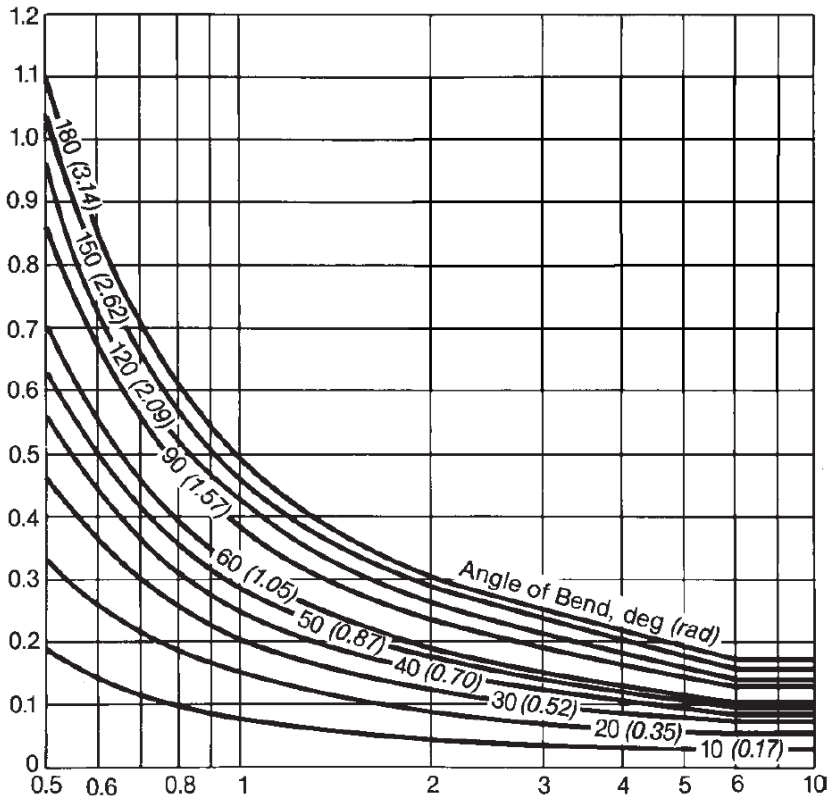

Figure 4.19: Bend loss coefficient k_b (vertical axis) for various bend angles as a function of bend radius to pipe diameter ratio $\frac{R_b}{D}$ (horizontal axis) [49]

$$\frac{1}{\sqrt{f_D}} = -2 \cdot \log\left(\frac{\epsilon}{3.7 \cdot D_H} + \frac{2.51}{Re \cdot \sqrt{f_D}}\right) \tag{4.79}$$

This relation needs to be solved numerically due to its implicit nature. Based on the length of the individual straight sections of the feed lines, their pressure losses can then be estimated. The lengths of the straight sections depend on the length of the tanks, the length of the interstages between them, and their position. Finally, the line mass is computed by a specified mass per unit length.

Since the feed lines need to run next to tanks, there will be several bends in the feed lines. These cause an additional pressure loss on top of the straight section pressure loss. The pressure drop in a curve is defined by equation (4.80) [48], where f_D is the same friction factor as for a straight pipe section derived from equation (4.79). R_b and θ_b are the bend radius and angle respectively.

$$\Delta p = \frac{1}{2} \cdot f_D \cdot \rho \cdot v^2 \cdot \frac{\pi \cdot R_b}{D} \cdot \frac{\theta_b}{180^\circ} + \frac{1}{2} \cdot k_b \cdot \rho \cdot v^2 \tag{4.80}$$

The parameter k_b is the bend loss coefficient and can be determined based on figure 4.19. At this stage, only 90° turns are assumed in the feed lines. Since lines will be rather small in diameter, a high bend radius to pipe diameter ratio is assumed, and thus a value of 0.15 is picked for this parameter.

Finally, valves are also a source of pressure loss in the feed system, and thus they should be accounted for. The pressure loss of a valve is commonly expressed using the so-called Kv value. This expresses the volume in $[m^3]$ that is required to flow through the valve in one hour to cause a pressure loss of one bar ($0.1\ [MPa]$). Thus a Kv value of 15 would mean that a flow of 15 $\left[\frac{m^3}{h}\right]$ would cause a pressure loss of one bar. The definition of the value can be found in equation (4.81).

$$Kv = \frac{Q\ \left[\frac{m^3}{h}\right]}{\sqrt{\Delta p\ [bar]}} \tag{4.81}$$

In this equation, Q represents the volume flow per hour. Because the definition of the Kv value does not use primary SI units, special attention needs to be paid to the units in equations. The pressure drop expressed in $[Pa]$ can be then derived using equation (4.82).

$$\Delta p\ [Pa] = \left(\frac{Q\ \left[\frac{m^3}{h}\right]}{Kv}\right)^2 \cdot 10^5 \tag{4.82}$$

Finally, the volume flow rate Q can be expressed in $\frac{m^3}{h}$ using equation (4.83), with feed line mass flow $\dot{m}$ and fluid density ρ, both in primary SI units.

$$Q\ \left[\frac{m^3}{h}\right] = \frac{\dot{m}}{\rho} \cdot 3600 \tag{4.83}$$

These three sources of pressure loss define the pressure loss over each of the two propellant feed lines from the tank outlet to the injector manifold. While there are three types of sources for pressure losses, there can be multiple instances of each e.g. multiple bends in the line or a separate main valve and throttle valve. The sum of all pressure losses in the feed line is then used to determine the required tank pressure based on the injector manifold pressure.

The pressurant feed lines will be sized in terms of mass, but their effect on pressure drop will neglected since the flow rate of gaseous pressurant through these pipes will be very low which directly links to pressure drop.

4.4.10. Fluid Tank

The Fluid Tank module represents a propellant tank. The goal of the module is primarily to size the tanks in terms of length, diameter and wall thickness, and subsequently determine the mass of each tank. Next to this, the tank module is also responsible for accounting for the propellant mass in the total mass tally in the model. The sizing method is identical between the oxidiser and fuel tank. For the pressurant tank, a slightly altered approach is used which is described in section 4.4.11.

The primary dimension from which the tank is sized is the required volume of the tank. It is comprised of the actual fluid volume V_{fl} and the ullage gas volume V_u. The fluid volume is defined by equation (4.84) using the fluid density ρ_{fl} and the fluid mass m_{fl} which itself is defined by the fluid mass flow $\dot{m}_{fl}$ and the burn time t_b.

$$V_{fl} = \frac{m_{fl}}{\rho_{fl}} = \frac{\dot{m}_{fl} \cdot t_b}{\rho_{fl}} \tag{4.84}$$

The chosen feed system is a dynamically-regulated pressure-fed system. This means that pressure in the fluid tank is kept constant by regulating the in-streaming pressurant. This means that ullage volume does not directly affect the system performance and thus can be kept minimal. Therefore the ullage gas volume is defined to be 10% of the fluid volume by equation (4.85).

$$V_u = 10\% \cdot V_{fl} \tag{4.85}$$

The total tank volume V_t is then defined by equation (4.86) as the sum of both volumes.

$$V_t = V_{fl} + V_u \tag{4.86}$$

Since the outer diameter of the tank is one of the optimisation variables, the inner diameter is dictated by the outer diameter of the tank as well as the internal pressure. Normally, a tank of the size with the size and pressure in this system can be computed using the thin-walled approximation. However, in this case, a subroutine for solving the equation for the stress in a thick-walled pressure vessel already needs to be implemented into the model for the pressurant tank. Therefore, the same subroutine can also be re-used here, which makes all tanks in the system sized by the same algorithm.

The hoop stress σ_θ at radius r in a thick-wall pressure vessel is defined by equation (4.87) [50] using the tank inner radius r_i, the tank outer radius r_o, and the tank pressure p_t.

$$\sigma_\theta = \frac{r_i^2 \cdot p_t}{r_o^2 - r_i^2} \cdot \left(1 + \frac{r_o^2}{r^2}\right) \tag{4.87}$$

Since the material properties are assumed constant throughout the tank wall, the tank needs to be sized using the radius r with the highest stress. Reconsidering equation (4.87), it is clear that this will inner wall of the tank, thus $r = r_i$. Equation (4.87) then simplifies to equation (4.88).

$$\sigma_{\theta_{max}} = p_t \cdot \frac{r_o^2 + r_i^2}{r_o^2 - r_i^2} \tag{4.88}$$

The maximum allowable stress is defined by the yield strength of the tank material. A safety factor according to ECSS-E-ST-32-10C [38] is applied to determine the design stress. With this defined, equation (4.88) can be solved for the tank internal radius r_i. With the inner radius defined, the length of the tank can be determined.

The model is capable of representing a cylindrical tank with either flat or spherical end caps. An example of each can be found in figure 3.13. The masses of both options are computed and the lighter option is selected.

For the cylindrical tank with flat end caps, the length of the tank is defined by equation (4.89) using the length of the required internal volume and the thickness of the flat end caps t_{ec}.

$$L_t = \frac{V_t}{\frac{\pi}{4} \cdot D_i^2} + 2 \cdot t_{ec} \tag{4.89}$$

The mass of the cylindrical tank is then defined by the mass of the cylindrical wall m_w and the circular end cap mass m_{ec} through equation (4.90), where ρ_w represents the wall material density.

$$m_t = m_w + 2 \cdot m_{ec} = \frac{\pi}{4} \cdot (D_o^2 - D_i^2) \cdot L_t \cdot \rho_w \; + \; 2 \cdot \frac{\pi}{4} \cdot D_i^2 \cdot t_{ec} \cdot \rho_w \tag{4.90}$$

To determine the mass of the tank variant with the spherical end caps, the same approach is used for the spherical tank. However, the computation of the tank length needs to be adapted for the spherical geometry.

The volume of the cylindrical tank with spherical end caps is given by equation (4.91) based on the equation for the volume of a cylinder and the volume of a sphere (since the two spherical end caps combined make the full sphere).

$$V_t = V_{cyl} + V_{ec} = \frac{\pi}{4} \cdot D_i^2 \cdot L_{cyl} \; + \; \frac{4 \cdot \pi}{3} \cdot \frac{D_i^3}{8} \tag{4.91}$$

Solving equation (4.91) leads to an expression for the cylindrical section length L_{cyl} in equation (4.92).

$$L_{cyl} = \frac{V_t - \frac{4 \cdot \pi}{3} \cdot \frac{D_i^3}{8}}{\frac{\pi}{4} \cdot D_i^2 \cdot} \tag{4.92}$$

However, the total length of the tank also includes the length of the spherical end caps, thus the total tank length is defined by equation (4.93).

$$L_t = L_{cyl} + D_i \tag{4.93}$$

The total mass of the tank is then defined similarly to the flat end cap tank, but instead of flat disks, the end caps are represented by half-spherical shells instead. This total tank mass is then defined by equation (4.94).

$$m_t = m_{cyl} + m_{ec} = \frac{\pi}{4} \cdot (D_o^2 - D_i^2) \cdot L_t \cdot \rho_w \; + \; \frac{4 \cdot \pi}{3} \cdot \frac{D_o^3 - D_i^3}{8} \cdot \rho_w \tag{4.94}$$

The mass of the lighter of the two tank designs is then added to the total mass tally together with the total mass together with the mass of its contents, including both fluid and pressurant gas.

4.4.11. Pressurant Tank

The pressurant tank module represents the pressurant tank. The propulsion system utilises one pressurant tank which pressurises both tanks. However, each tank uses its own dynamic pressure regulation since the tank pressures are not the same between all tanks. This means that the pressurant tank needs to contain enough pressurant gas at the start of the burn to fill both tanks at their required pressure as well as the pressurant tank at a pressure which is high enough such that it can still pressurise the propellant tanks.

Thus for each propellant tank, the mass of pressurant contained at the end of the burn needs to be determined. Since the pressurant gas is assumed to be an ideal gas, the density of the pressurant gas ρ_g can be expressed using equation (4.95) with tank pressure p_t, pressurant gas constant R_g, and tank temperature T_t.

$$\rho_g = \frac{p_t}{R_g \cdot T_t} \tag{4.95}$$

The tank temperature is assumed to remain constant through the burn of the engine. Due to the relatively short duration from lift-off to upper-stage ignition, the temperature is assumed to remain constant at 15° C. From this, the required pressurant mass for one tank can be derived using equation (4.96) with the previously determined pressurant density ρ_g and the tank volume V_t.

$$m_g = V_t \cdot \rho_g \tag{4.96}$$

This expresses the mass of pressurant per fluid tank. However, the pressurant tank's final pressure needs to remain at the highest tank pressure, with a sufficient margin such that it can keep feeding the fluid tanks until engine burnout. This additional gas needs to be taken into account in order to size the pressurant tank volume correctly.

To determine this, the equation of state for an ideal gas (equation (4.97)) can be used. The amount of substance n must remain constant since no pressurant gas is lost to the outside of the tank system, thus all gas remains in the system. Furthermore, it is assumed that due to the slow process (60 s burn time), the temperature T in the tanks remains constant. In future model improvements, extended implementations of heat transfer in this process can be implemented.

$$p \cdot V = n \cdot R \cdot T \tag{4.97}$$

Based on the above equation and assumption, the following balance can be made between the initial gas state in the pressurant tank and the final gas state in the pressurant tank and propellant tanks. This balance is defined by equation (4.98)

$$\left(\frac{p_t \cdot V_t}{R \cdot T}\right)_{p_i} = \left(\frac{p_t \cdot V_t}{R \cdot T}\right)_{p_f} + \sum^{tanks} \left(\frac{p_t \cdot V_t}{R \cdot T}\right)_t \tag{4.98}$$

From this, the expression in equation (4.99) for the pressurant tank volume V_{t_p} can be derived, defined by the sum of fluid tank pressures p_t multiplied with their volume V_t as well as the difference between the initial and final pressurant pressures p_{p_i} and p_{p_f}.

$$V_{t_p} = \frac{\sum^{tanks} p_t \cdot V_t}{p_{p_i} - p_{p_f}} \tag{4.99}$$

This defines the required volume of the pressurant tank and using the initial pressure of the tank pressure, the pressurant total can be determined using equations (4.96) and (4.97).

Like the fluid tank module, the pressurant tank module represents two types of tanks. However, due to the different applications and higher pressures, the pressurant tank can either be modelled as a spherical tank or a cylindrical tank with spherical end caps. Since the spherical tank design is the preferable option due to its superior load distribution, it is always chosen if the interior constraints of the rocket allow for it.

If the required tank volume allows for a spherical, then the outer tank diameter can be determined based on the equation for the stress in a thick-walled spherical pressure vessel, equation (4.100) [50], defined by the internal pressure p, and the inner and outer radii r_i and r_o.

$$\sigma = \frac{r_i^2 \cdot p}{r_o^2 - r_i^2} + \frac{r_i^2 \cdot r_o^2 \cdot p}{(r_o^2 - r_i^2) \cdot r_i^2} \tag{4.100}$$

This equation is then solved for the outer radius by imposing the failure stress with a safety margin according to ECSS-E-ST-32-10 [38]. In case the pressuring tank outer radius falls outside the available radius within the rocket, the tank type is also switched to the cylindrical tank design.

If the spherical tank design is selected, the tank dimension sizing methodology is the same as the one used for the cylindrical tanks with spherical end caps in the section 4.4.10, using equations (4.87) and (4.93).

4.5. Iteration Sequence

Some of the inputs of some modules are outputs of the other modules. This is a common occurrence in multi-disciplinary design models. However, to create on cohesive model where the inputs can be handed from one module to the next, the correct iteration sequence needs to be determined for this. Only then can the numerical model function as one singular model that can be implemented into the optimisation algorithm. To determine this order, it can be helpful to consider the N2 diagram for the modules in figure 4.20.

Based on this, as well as on the process of assembling the modules into one singular model, the iteration sequence diagram in figure 4.21 can be determined.

This figure however only represents on singular iteration of the numerical model to determine the design output for a given set of input parameters. During the optimisation, the model may run through this sequence several hundred times.

4.6. Conclusion

Based on the preliminary design in chapter 3, a numerical model was constructed which covers all relevant of designing and sizing the various subsystems of the propulsion system. This concludes the numerical model development phases and in the next phase, the model will be verified such that it can later be optimised.

The inputs that were defined in this process allow for the optimisation of the design based on 19 parameters, which can be varied in various ranges. These ranges will be defined in chapter 6. Meanwhile, a large array of output parameters were defined which can be used for verification and validation, or to determine the sizing of various components. Additionally, due to the object-oriented nature in which the numerical model was implemented, nearly all parameters of each module can be accessed.

Figure 4.20: Module N2 Diagram

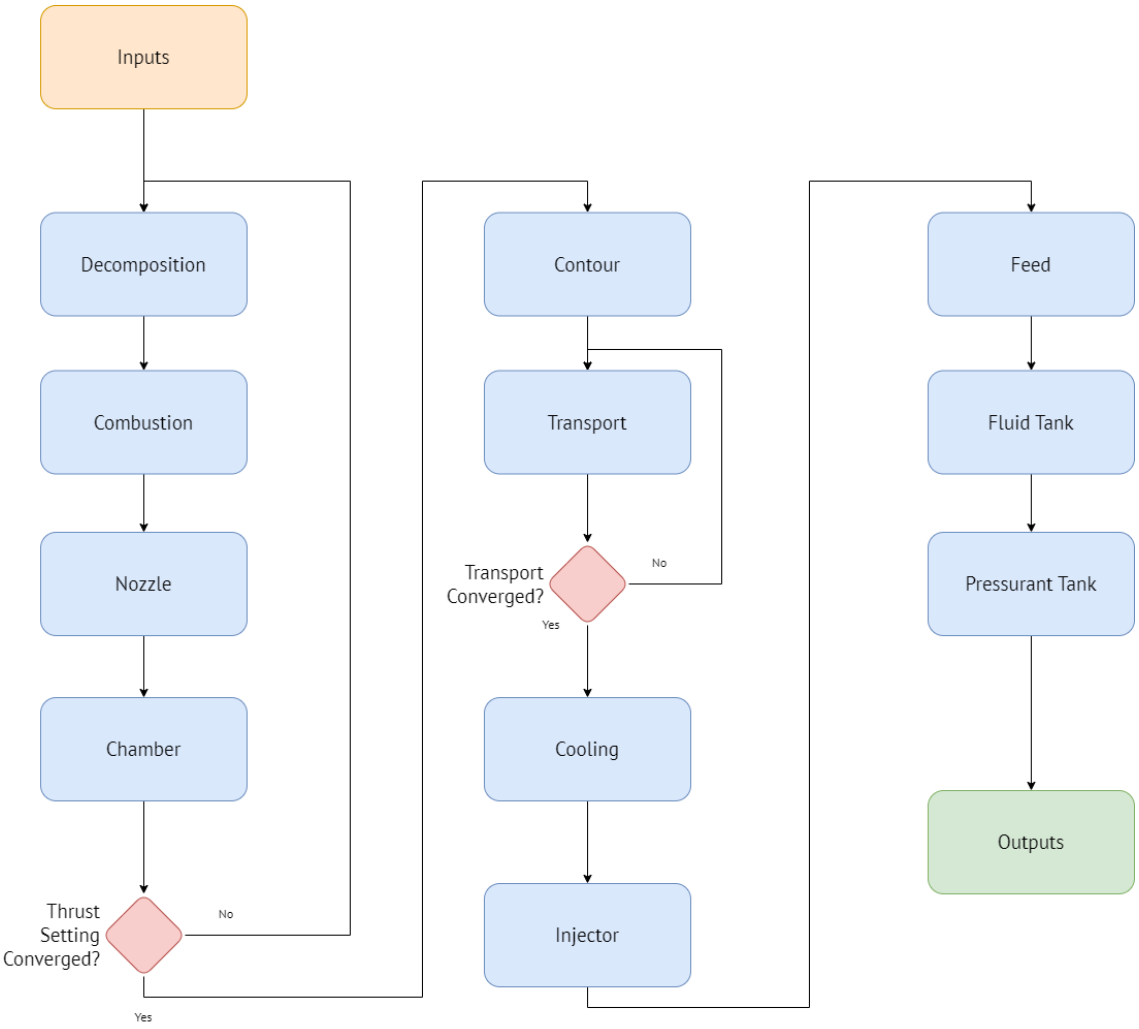

Figure 4.21: Iteration Sequence of Numerical Model

Finally, during the construction of the model, some inherent limitations of the have become apparent. Firstly, the numerical model as a whole only considers the steady-state operation of the propulsion system. This means that no transient effects are captured in the numerical model. Apart from this, one of the more major limitations is the current decomposition model since it is based on a fixed decomposition temperature. Data from future tests of the HyProp project (see chapter 2) will be used to replace this model. Another limitation lies in the chamber transport model since it only considers 1D flow, i.e. the gas properties are assumed constant from the central axis of the chamber to the wall and only vary along the length of the chamber. In reality, however, there are variations over the diameter of the chamber. Finally, the regenerative cooling model only considers a simple cooling channel geometry, as seen in figure 4.12. More complex geometries could offer better cooling performance, but evaluating various geometries and their performances exceeds the scope of this work.

Ultimately, none of these limitations obstruct the original goal of the numerical model. Ultimately, the output of the design optimisation will have to undergo further analysis and potential refinement, and therefore, these limitations can be compensated once the optimised design is refined into a critical design before entering manufacturing and testing.

5

Model Verification

With the completion of the numerical model, the next important step is its verification. The verification of the model will determine whether the model correctly represents real-life processes and systems. The goal of the model verification can be summarised by the following question:

Was the model built correctly?

Compared to this, the goal of the validation of the model, which is covered in chapter 7, can be summarised by the following question:

Was the correct model built?

In this context, verification aims to determine if the model represents reality and how sensible the model outputs are, while validation will determine how accurately the model represents the system it is meant to represent. The model must be verified before the numerical optimisation is performed. If the model does not adequately represent reality, then the optimisation algorithm will also not produce the optimal result.

This chapter describes all model verification efforts undertaken with the numerical model. Section 5.1 will describe the logic behind the overarching approach, section 5.2 will describe the verification of each module of the model on its own, and finally section 5.3 will describe the verification of the numerical model as one cohesive unit.

5.1. Approach

The verification of the model will be performed in two steps. First, each module of the numerical model (see section 4.4) is verified on its own and afterwards, the numerical model is verified as one unit.

This is done to ensure that first all discrepancies within each module are caught before the modules are assembled into one cohesive numerical model. This means that once this is done, each module on its own should be verified and thus adequately represent its subsystem. If any discrepancies arise during the model verification, these must then come from the integration of the modules into one model rather than the separate modules themselves.

Similarly, only once the model verification is completed, the optimisation will be performed. This ensures that if any discrepancies arise during the optimisation, it is highly likely that these come from the optimisation algorithm rather than elsewhere in the model. Generally, this bottom-up verification approach ensures that any discrepancies can be swiftly traced and addressed.

5.2. Module Verification

This section contains the verification of each module of the numerical model. Note that the decomposition model is not treated here since it assumes a constant value from the literature and thus no reasonable verification can be performed on this module.

	Case 1	Case 2	Case 3
Chamber Pressure	10 $[bar]$	20 $[bar]$	30 $[bar]$
HTP Decomposition Temperature	900 $[K]$	800 $[K]$	700 $[K]$
OF Ratio	5.01 $[-]$	5.02 $[-]$	5.02 $[-]$
Fuel	Ethanol	Ethanol	Ethanol

Table 5.1: Combustion Model Test Cases

Table 5.2: Comparison between CEArun and Numerical Model for Case 1

Parameter	CEArun	Numerical Model	Deviation
Characteristic Velocity [m/s]	1549.4	1548.8	−0.039%
Chamber Temperature [K]	2530.9	2519.7	−0.443%
Chamber Density [kg/m³]	1.032	0.9697	−6.03%
Specific Heat Ratio [-]	1.132	1.132	±0
Chamber Molar Mass [g/mol]	21.706	21.716	+0.046%

5.2.1. Combustion

The combustion model is a direct NASA CEA chemical equilibrium simulator. This program is very well-validated for modelling the combustion in a liquid rocket motor. However, modifications had to be made to the oxidiser input to represent the decomposed HTP products and capture the effect of decomposition efficiency. Therefore, some verification efforts should still be undertaken to fully verify this module. Similar to the larger verification approach, a bottom-up approach can be taken for this module.

Comparison with CEArun

To begin, the results of the combustion module can be compared to the results of the same NASA CEA program outside its Python implementation. The comparison between these two is useful to ensure the Python implementation of CEA produces the same results as the standalone program and to ensure that custom inputs made for the oxidiser can be reproduced by the standalone CEA program.

For this, three test cases have been created, with some variation in decomposition temperature and chamber pressure. The fuel type was not varied since the fuel presets in RocketCEA and CEArun are identical and thus they will not cause a difference between the two models. These cases can be found in table 5.1.

Based on this, the following output parameters between RocketCEA and CEArun can be compared using various parameters. For this analysis, the parameters that will be used for the comparison are the characteristic velocity, combustion temperature, chamber density, specific heat ratio, and chamber molar mass. These parameters were chosen as they are the primary outputs of the combustion module that are used by other modules of the numerical model. The comparisons for each case can be found in tables 5.2 to 5.4

For the characteristic velocity, the chamber temperature, specific heat ratio, and chamber molar mass, the variations between CEArun and the RocketCEA implementation in the numerical model are negligible. The chamber density however notably does deviate between the two models. This is likely due to the influence of the property estimation of the super-heated steam and gaseous oxygen in both models. CEArun utilises its built-in thermo-chemical process models to determine the properties of this mixture at the preset conditions, while the numerical model utilises the Cantera thermodynamic model suite using the

Table 5.3: Comparison between CEArun and Numerical Model for Case 2

Parameter	CEArun	Numerical Model	Deviation
Characteristic Velocity [m/s]	1539.4	1539.2	−0.013%
Chamber Temperature [K]	2521.4	2510.5	−0.432%
Chamber Density [kg/m³]	2.081	1.955	−6.05%
Specific Heat Ratio [-]	1.138	1.138	±0
Chamber Molar Mass [g/mol]	21.816	21.821	+0.023%

Table 5.4: Comparison between CEArun and Numerical Model for Case 3

Parameter	CEArun	Numerical Model	Deviation
Characteristic Velocity [m/s]	1527.3	1527.1	−0.013%
Chamber Temperature [K]	2497.4	2486.3	−0.444%
Chamber Density [kg/m³]	3.162	2.970	−6.07%
Specific Heat Ratio [-]	1.142	1.143	+0.088
Chamber Molar Mass [g/mol]	21.885	21.890	+0.046%

GRI-3.0 mechanism [33], [34]. This is likely to cause a discrepancy of this magnitude in the estimation. Ultimately, however, the discrepancy is consistent throughout the cases and it is low enough that safety margins introduced in the later stages of the design will more than account for this.

Hence it can be concluded that based on this comparison, the proposed implementation of the CEA combustion model using RocketCEA and Cantera produces the same results as the CEA base code on its own.

Comparison with RPA

In this next verification step, after determining that the CEA code is adequately implemented, the goal shifts now to determining that the CEA code itself can produce consistent results. In order to do this, it should be compared to a different, industry-standard combustion model, to determine whether the module as a whole produces a reasonable output. For this, the RPA computer program is used.

The RPA (Rocket Propulsion Analysis) combustion simulator is a powerful tool used for the conceptual and preliminary design of chemical rocket engines. Developed by RP Software+Engineering UG, it offers a comprehensive suite of features including engine performance analysis, thrust chamber sizing, nozzle wall contour optimisation, and engine cycle power balance analysis. The simulator is equipped to handle various propulsion system analyses such as monopropellant and bipropellant engines, and it can simulate different engine cycles like staged combustion and gas generator cycles. The software utilises a robust Gibbs free energy minimisation approach to determine combustion compositions and thermodynamic properties, making it highly reliable and industry-accepted [51].

To compare the combustion model, a similar approach to the previous section can be taken for the previous step. However, since the RPA program is capable of nested analyses, a more continuous comparison can be made between the two models. This comparison was made using the chamber temperature, characteristic velocity, molar mass, and specific heat ratio. This can be found in figure 5.1.

This shows that none of the measured deviations noticeably exceeds 1%. It can also be seen that the lines for Ethanol, Methanol and JetA tend to be grouped closely while the Gasoline and Kerosene lines are more separated. This is likely due to the fact the thermo-chemical representations of the latter two fuels have larger deviations between the modelling in CEA and RPA due to these long-chain hydrocarbons naturally showing more deviation depending on the source. However, none of these deviations are large enough to cause any issues in the model that have to be corrected.

The combustion model also determines the ideal fuel mixture ratio or O/F ratio. The nested analysis function in RPA can also be used to determine how well the estimation matches between the two models and thus verify that the numerical model does determine the ideal O/F ratio for a given fuel and chamber pressure. This comparison can be seen in figure 5.2. The figure is made based on a chamber pressure of 15 bar, ethanol as the fuel, and an area expansion ratio of 100.

This figure shows that the match between the two models is near perfect. This shows on the one hand that the model does determine the ideal O/F ratio reliably, but also confirms that the specific impulse estimation (used to size the nozzle and propellant requirements) factors in the area expansion effects of the nozzle correctly.

5.2.2. Nozzle

The nozzle sizing modules determine the throat area, exit area, and by extension area expansion ratio based on the combustion parameters and the required thrust. This module is most easily verified by comparing

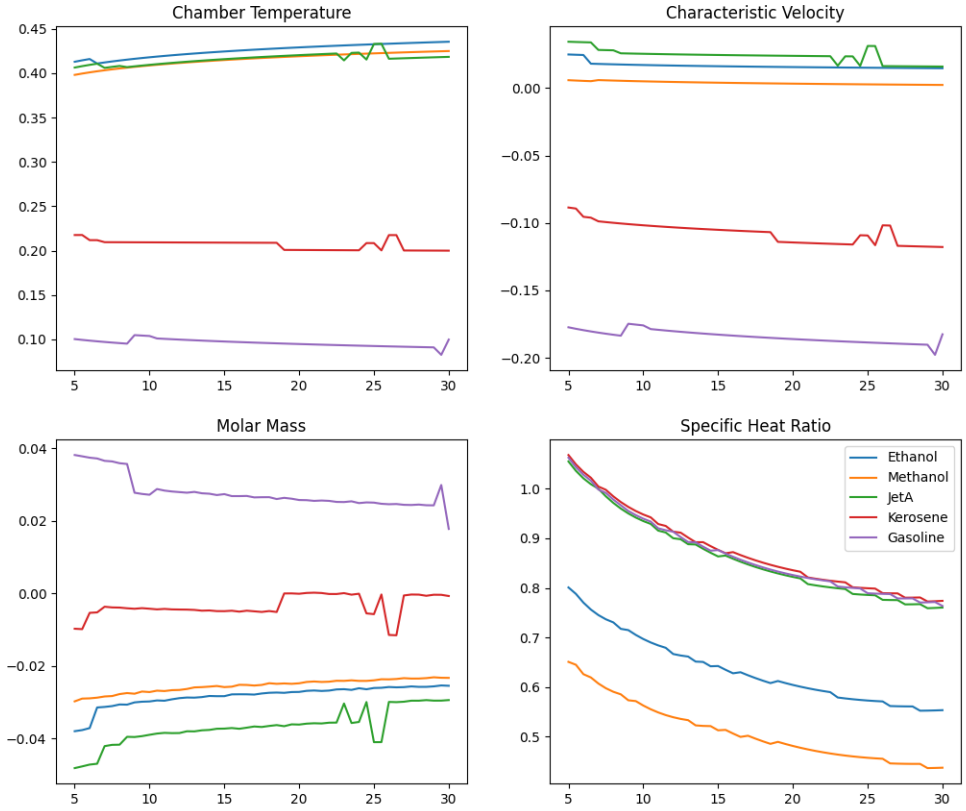

Figure 5.1: Deviation [%] between RPA and Numerical Model for Chamber Temperature, Characteristic Velocity, Molar Mass, and Specific Heat Ratio as a function of Combustion Chamber Pressure

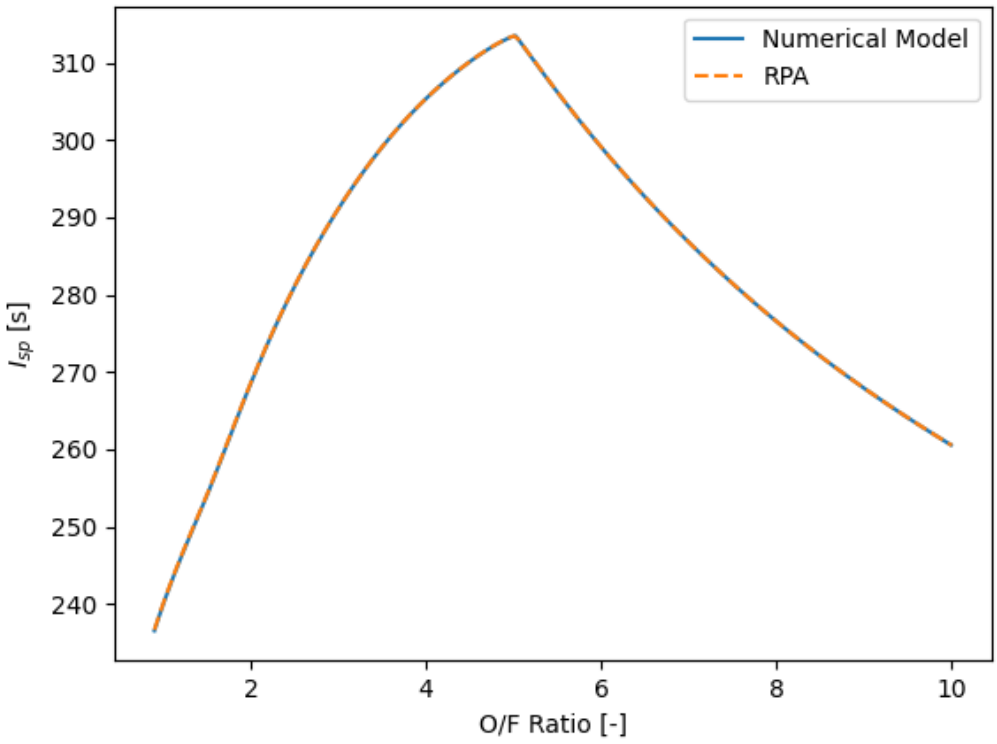

Figure 5.2: Specific Impulse as a function of O/F Ratio with Ethanol as fuel at a pressure of 15 bar from RPA and the Numerical Model

Table 5.5: Comparison between a reference system and the output of the nozzle module

Parameter	Reference System [14]	Numerical Model Output	Deviation
Throat Diameter	16.83 $[mm]$	16.82 $[mm]$	−0.06%
Exit Diameter	37.44 $[mm]$	39.04 $[mm]$	+4.27%
Area Ratio	4.95 $[-]$	5.38 $[-]$	+8.69%

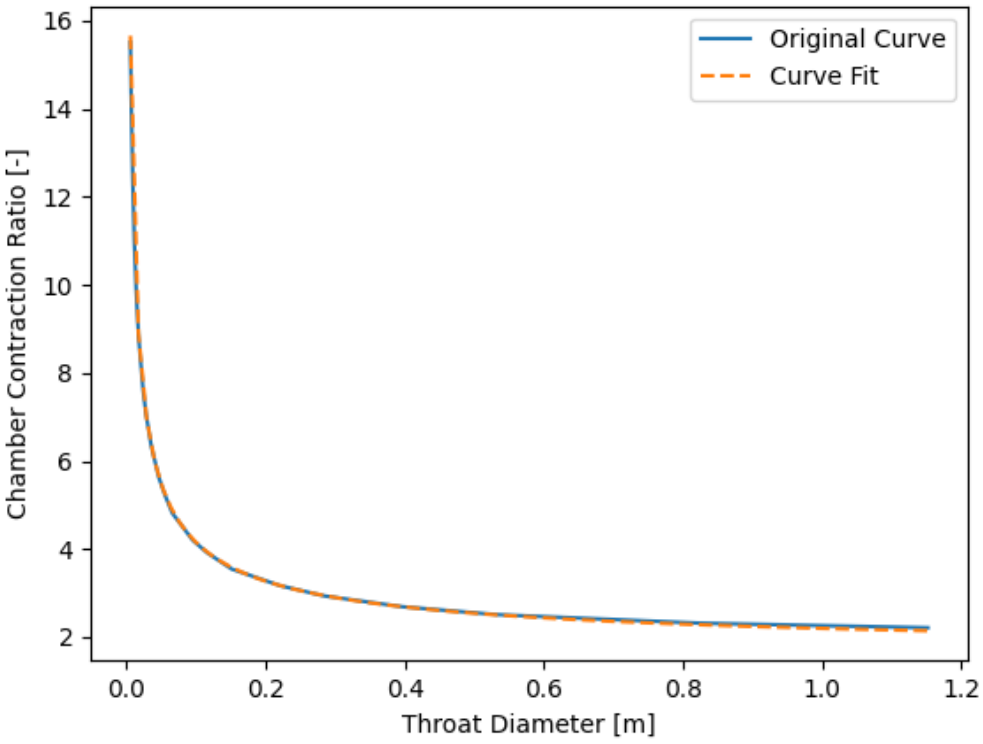

Figure 5.3: Throat Diameter vs Chamber Contraction Ratio: Interpolated Curve and Curve Fit [24]

these parameters for comparable systems based on their design inputs. For this, the reference system used is a staged bi-propellant engine using HTP and Kerosene [14]. This comparison can be found table 5.5.

From this, it can be concluded that the throat area estimation is very accurate. There is some notable discrepancy in the exit diameter between the two compared systems. This likely stems from the nozzle being designed for different exit pressures or a difference in assumptions of the specific heat ratio. Out of these two parameters, the throat area is far more important to achieve the correct thrust level for certain set chamber pressure and propellant combination (see equation (4.4a)). While the exit area is also of importance to accurately achieve the correct thrust and maximise the expansion, these discrepancies can be accepted. Ultimately, this confirms that the module does produce sensible nozzle sizings based on the provided inputs.

5.2.3. Chamber

Since the chamber model was based on interpolating a curve that related the throat diameter to the chamber contraction ratio and the chamber length, the most important step is to verify that the curve fit generated by the module fits the original curve well. An overlay of both can be seen in figures 5.3 and 5.4.

At first sight, both of these curves already demonstrate a decent curve which can be used to determine. The utilised curve fit algorithm [52] also supplies the covariance matrix for the parameters used in equa-

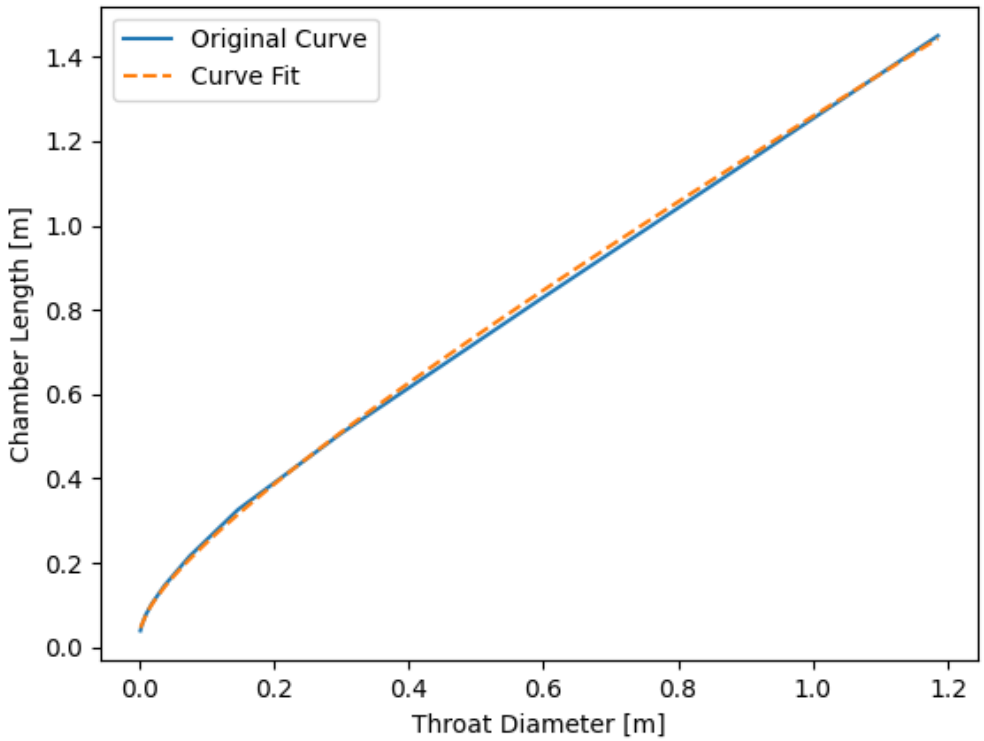

Figure 5.4: Throat Diameter vs Chamber Length: Interpolated Curve and Curve Fit [24]

Table 5.6: Throat Diameter vs Chamber Contraction Ratio: Parameters and their deviations

Parameter	Value	Standard Deviation	Relative
a	1.518	±0.0471	±3.10%
b	0.681	±0.0215	±3.16%
c	0.588	±0.00586	±0.997%

Table 5.7: Throat Diameter vs Chamber Length: Parameters and their deviations

Parameter	Value	Standard Deviation	Relative
a	0.0211	±0.00631	±29.9%
b	0.766	±0.0305	±3.99%
c	0.472	±0.0338	±7.16%

tions (4.17a) and (4.17b). The diagonals of this matrix are the variances for each parameter, which means that the standard deviation can be determined for 1σ. These deviations can be found in tables 5.6 and 5.7.

The majority of parameters show very little standard deviation for the supplied data points. The only exception for this is the parameter a for the chamber length curve interpolation, a deviation of 30% can be observed. This is likely due to the nature of the interpolated curve which is quasi-linear in some ranges and rather non-linear in other ranges. Due to a lack of a better implementable model for the chamber length of the gaseous-liquid combustion chamber, this error is accepted and should be monitored in the model.

Finally, the output can be used to determine the characteristic length of the chamber, using equation (4.15). This parameter is used for the sizing of chamber geometry and is generally a characteristic of the propellant combination [29]. This can be compared to the reference system [14] from table 5.5. When supplying the constraints of the reference system, the chamber module determines a chamber which has a characteristic length of 0.86 [m]. The reference system itself was designed with a characteristic length of 0.96 [m]. While these values differ, they are located in the same order of magnitude. It should also be noted that the characteristic length usually is defined as a range rather than one exact value for any given specific propellant combination. Therefore, this result is acceptable, especially when considering the scope of the design of this research.

5.2.4. Contour

Next to various unit testing, the most important verification step for the contour module is to determine the 3-D curve fit accuracy for determining the parabolic nozzle initial and final parabola angles. This will be done similarly to the previous section. The interpolated data as well as the fitted curve can be found in figures 5.5 and 5.6.

Due to the large number of parameters, the variances of each parameter are less meaningful than in the previous section, so this will not be considered in this section. However, the plots in figures 5.5 and 5.6 show a good correlation between the fitted surface and the original data. It should also be noted that considering the scope of this research, further analysis will have to be performed on each of the subsystems to determine the final sizing before entering production, but for exploring the design space and determining certain design choices based on this analysis, this sizing accuracy for the nozzle is considered sufficient.

5.2.5. Transport

The chamber transport model can be verified using once again the RPA combustion simulator. Given the correct inputs, it can provide chamber transport information that can be compared with the outputs of the model. Since the transport model requires many pre-requisite inputs from the other modules, a test case is defined for the verification of the transport module. It is based on the characteristics in table 5.8.

These inputs are gathered based on the inputs required to fully define the transport model of RPA. One major disadvantage of the RPA version used for verification is that it is only able to supply chamber transport characteristics at the injector face, the nozzle throat, and the nozzle exit. However, in the scope of verifying the transport module, this information should be sufficient to confirm the correct implementation of the

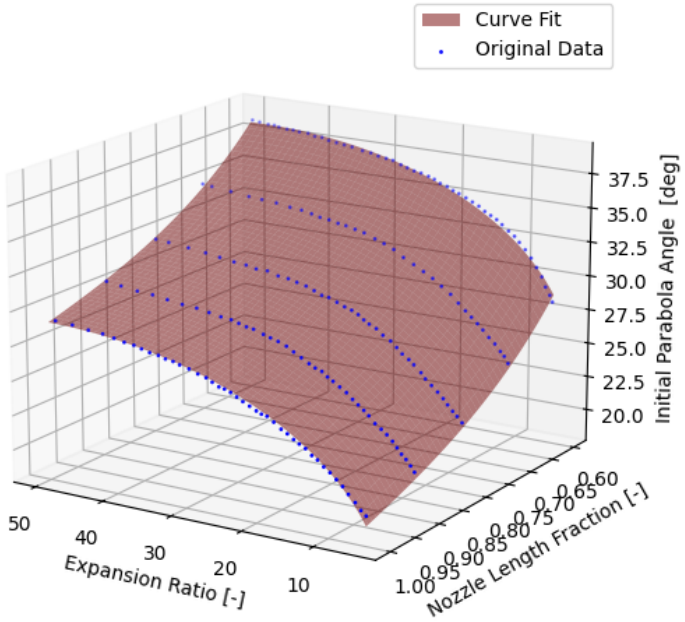

Figure 5.5: Nozzle Initial Parabola Angle: Interpolated Data and Curve Fit

Table 5.8: Test Case for the Transport Module used in the Numerical Model and RPA

Parameter	**Value**
Chamber Pressure	30 $[bar]$
Nozzle Exit Pressure	0.054 $[atm]$
Fuel	Ethanol
Contraction Ratio	10.9 $[-]$
O/F Ratio	5.02 $[-]$
HTP Concentration	80 $[\%]$
HTP Decomposition Temperature	900 $[K]$

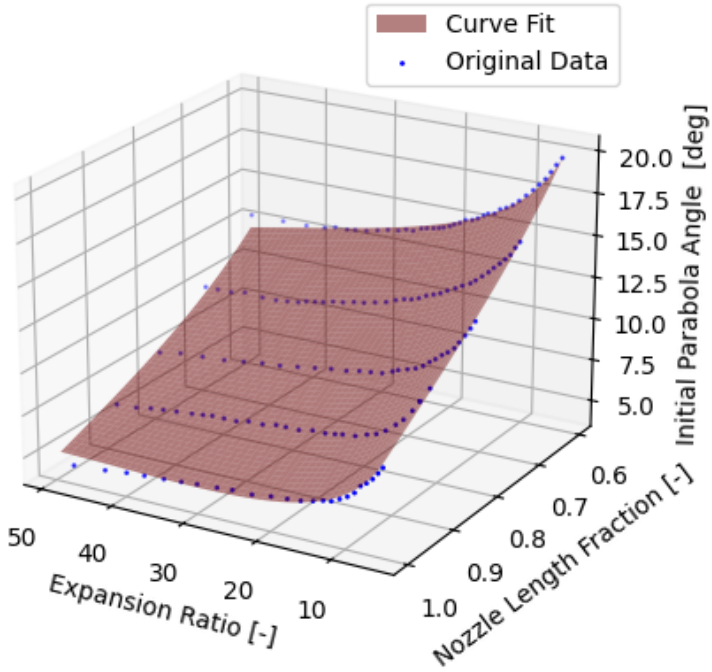

Figure 5.6: Nozzle Final Parabola Angle: Interpolated Data and Curve Fit

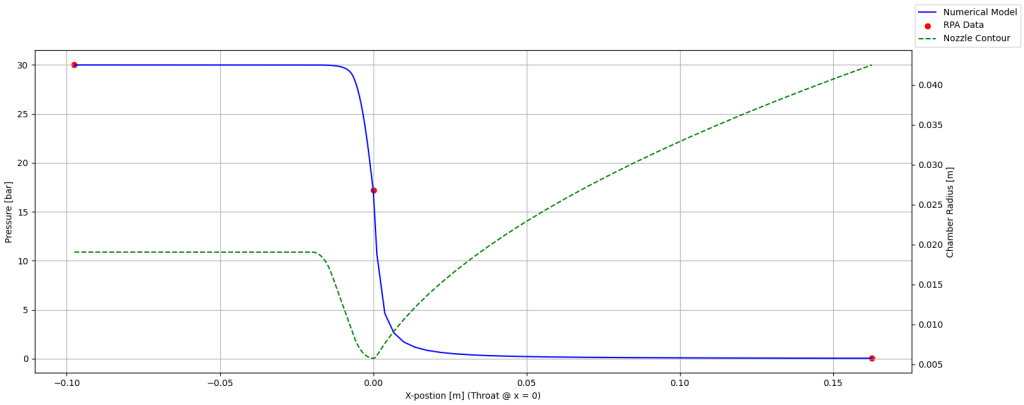

Figure 5.7: Combustion Gas Pressure along the Nozzle: Numerical Model and RPA

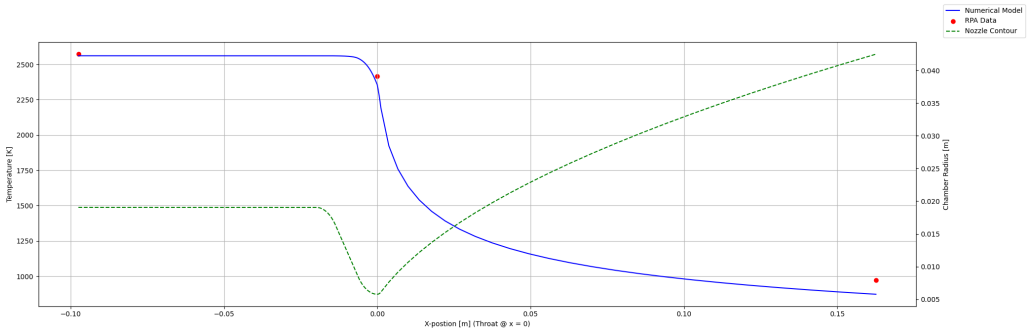

Figure 5.8: Combustion Gas Temperature along the Nozzle: Numerical Model and RPA

process defined in section 4.4.6.

Figures 5.7 to 5.10 show the pressure, temperature, Mach number and flow velocity as a function of the chamber length from the numerical model with the three data points from RPA overlaid.

The aforementioned plots show a good correlation between the numerical model and RPA. There is some discrepancy in the temperature (figure 5.8) and subsequently velocity plot (figure 5.10). This likely stems from slight deviations between the RPA and CEA thermo-chemical databases.

Next to this, the numerical model also generates a mass fraction profile of the species in the combustion gas as a function of chamber length. The same output from RPA can be found in figure 5.11 while the numerical model output can be found in figure 5.12.

Comparing these two outputs, they are again adequately correlated. Thus it can be assumed that the chamber transport model has been implemented correctly for the use of optimising this propulsion system. The primary discrepancies are also only found at the nozzle exit, where the lesser thermal loading means that deviations in the thermal conditions will have a lesser impact on the design, as other constraints such as manufacturing considerations will dictate the optimal design here.

5.2.6. Fluid and Pressurant Tank

Most parts of the fluid and pressurant tank modules are constructed relatively simply such that apart from unit testing and other low-level verification during implementation, there are very few major verification efforts that can be meaningfully undertaken to implement the model. One of the possible verification efforts is to verify the thick-walled pressure vessel estimation and compare it against the thin-walled equation. This comparison for a representative diameter and wall thickness range can be found in figure 5.13.

This shows that the thick-walled assumption will produce a more conservative estimation of the pressure vessel stress than the thin-walled assumption. Especially for high-pressure applications such as the pressurant tank, it is reasonable to utilise a more conservative estimation method.

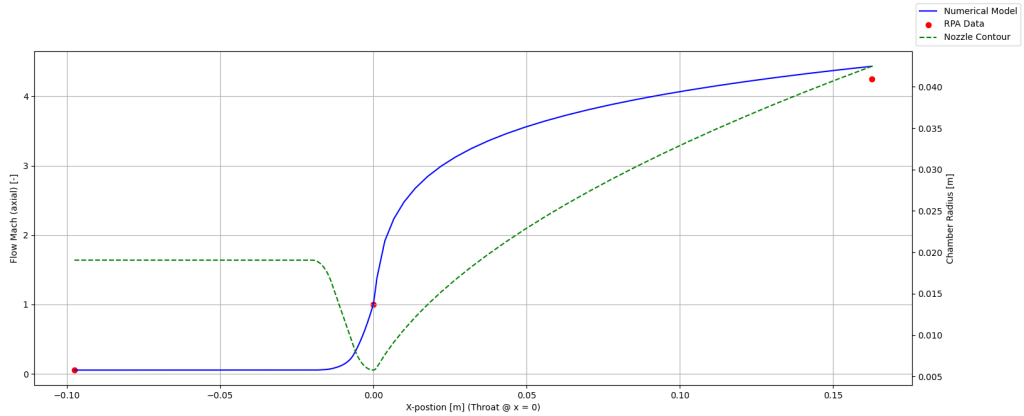

Figure 5.9: Combustion Gas Mach Number along the Nozzle: Numerical Model and RPA

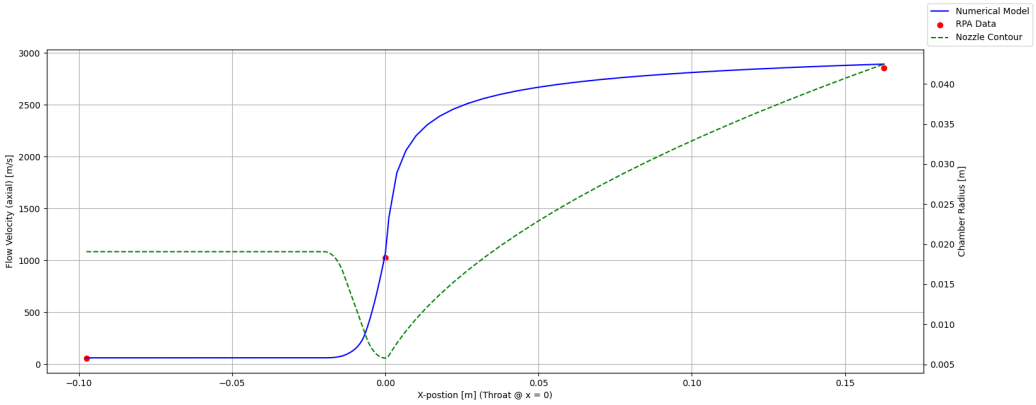

Figure 5.10: Combustion Gas Velocity along the Nozzle: Numerical Model and RPA

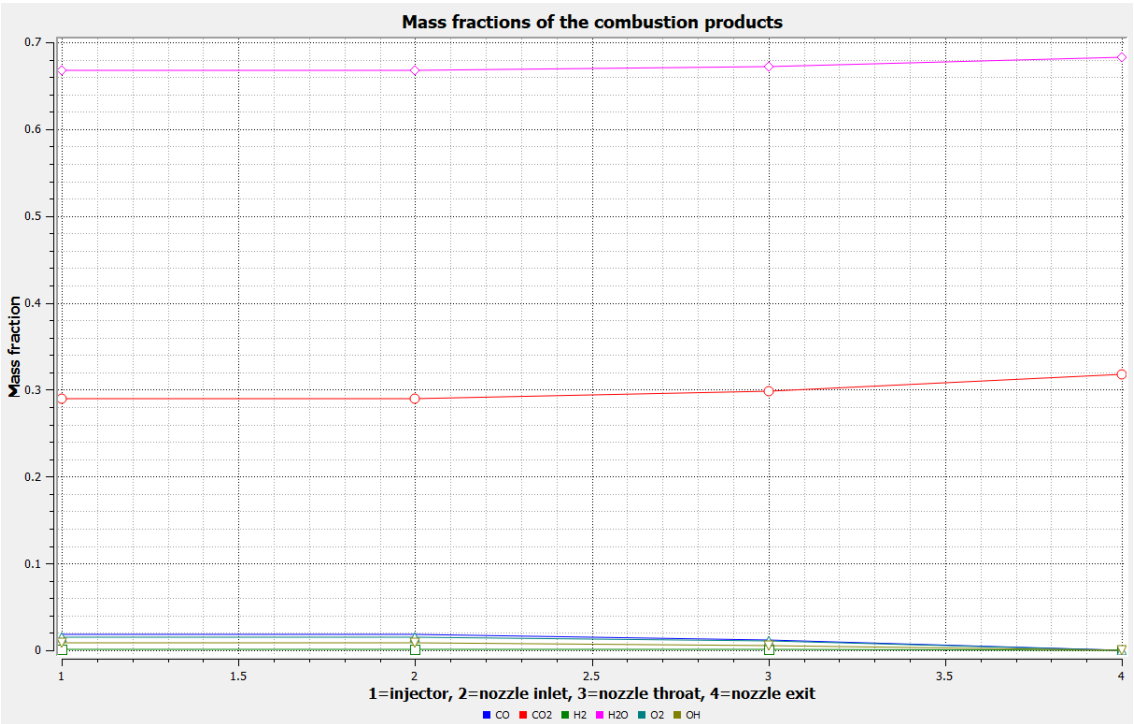

Figure 5.11: Exhaust Composition from RPA Output

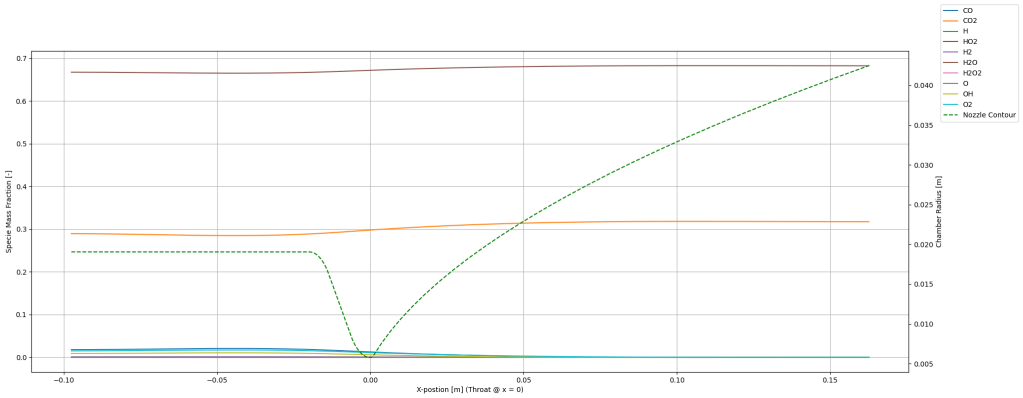

Figure 5.12: Exhaust Composition from Numerical Model

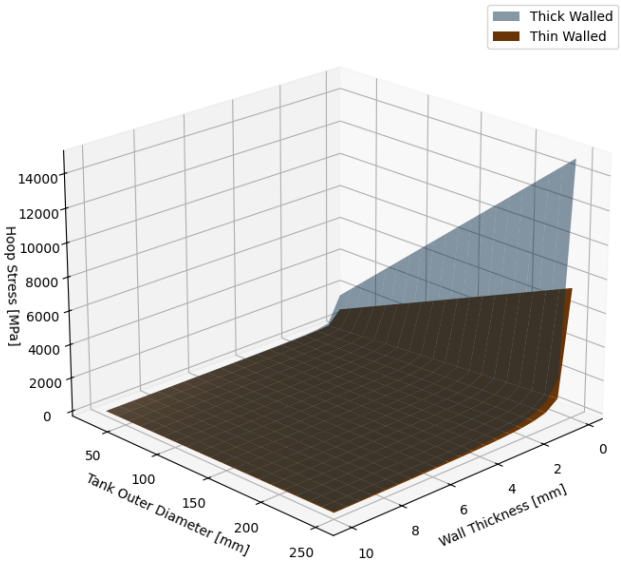

Figure 5.13: Hoop Stress in Cylindrical Pressure Vessel at 60 bar: Thick walled equation equation (4.87) vs thin walled equation equation (4.14a)

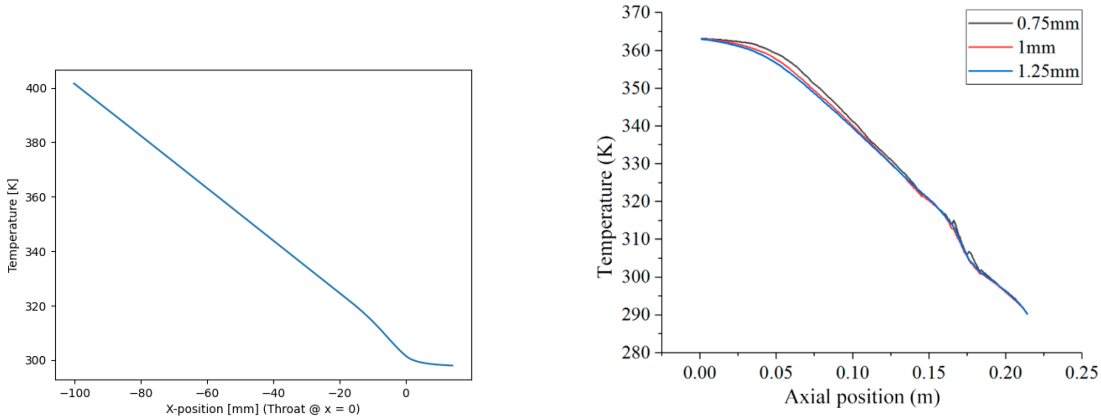

(a) Numerical Model **(b)** Reference System [53]

Figure 5.14: Comparison of HTP temperature in the cooling channels for a 450 [N], 20 [bar] Kerosene-HTP Thruster

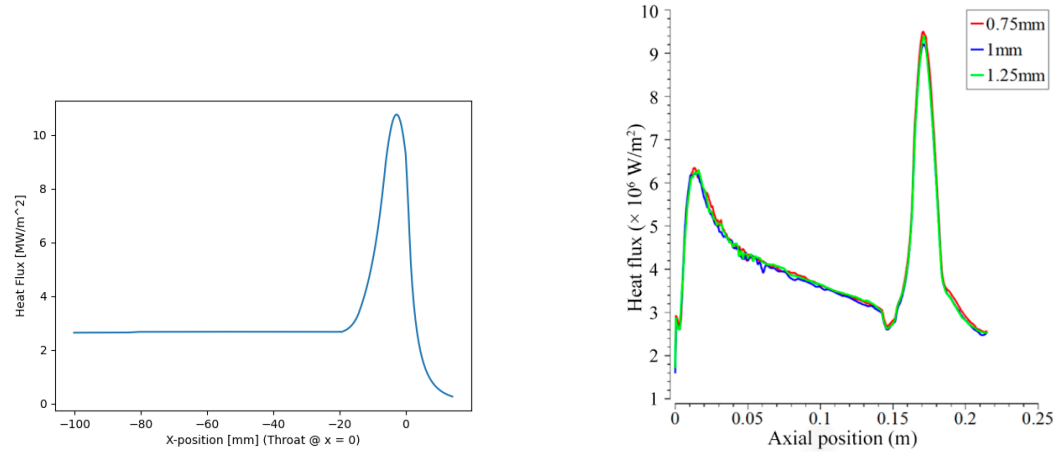

(a) Numerical Model **(b)** Reference System [53]

Figure 5.15: Comparison of chamber heat flux for a 450 [N], 20 [bar] Kerosene-HTP Thruster

5.2.7. Cooling

For the ablative, heat-sink and radiative cooling methods, a similar approach was taken as in the previous subsection for the injector. These methods are based on very few analytical equations and since these were verified using unit testing and other low-level verification during the development of the numerical model.

This however does not hold for the regenerative cooling model. Since the complexity of the regenerative cooling model is higher than the other cooling models, it should be verified against outside sources. In this case, the reference system that will be used is a 450 [N], 20 [bar] Kerosene-HTP staged bipropellant using the HTP to regeneratively cool the combustion chamber [53]. This system crucially features a very similar cooling channel geometry. In figure 5.14, the comparisons of the coolant temperature model between the numerical model and the reference system can be seen.

It can be seen that the model matches the real system rather well. The slopes of the main temperature rises are very similar. Also, the overall temperature increase is very similar. It can be seen that towards the injector the temperature increase in the reference system tails off compared to the numerical model. This is likely because of the ongoing combustion process which might affect the heat flux.

A similar comparison can be made for the heat flux. This comparison can be seen in figure 5.15.

Comparing the two graphs, it can be seen that there is some discrepancy between the numerical model and the reference system near the injector plate. The reference system source reports a higher heat flux

Table 5.9: Injector Performance Comparison: Reference System [54] vs Numerical Model

Parameter	**Reference System**	**Numerical Model**	Deviation
Element Diameter	$1.5494\ [mm]$	$1.5483\ [mm]$	$+0.071\%$
Injection Velocity	$34.40\ \left[\frac{m}{s}\right]$	$34.86\ \left[\frac{m}{s}\right]$	-1.34%
Discharge Coefficient	$0.7753\ [-]$	$0.7783\ [-]$	-0.387%

Table 5.10: Injector Performance Comparison: Reference System [25] vs Numerical Model

Parameter	**Reference System**	**Numerical Model**	Deviation
Element Diameter	$1.367\ [mm]$	$1.311\ [mm]$	$+4.10\%$
Injection Velocity	$22.37\ \left[\frac{m}{s}\right]$	$23.03\ \left[\frac{m}{s}\right]$	-2.95%
Discharge Coefficient	$0.7200\ [-]$	$0.74311\ [-]$	-3.21%

than the numerical model. It should be noted at this point that the numerical model reference case uses Inconel 718 as the chamber material while the literature reference system uses a stainless steel alloy not represented in the numerical model. This means that there is some discrepancy in the thermal properties of the chamber wall which can cause this effect. Next to this, the numerical model assumes a quasi-frozen flow at this stage, where in reality certain mixing effects might cause the non-constant heat flux in the chamber. Most importantly, the spike in heat flux around the nozzle throat matches rather well between the numerical model and the reference system. This is the by far most thermally loaded section of the chamber.

Overall based on this, it can be deduced that while the regenerative cooling model is not capable of predicting the cooling channel temperatures and heat fluxes (and thus other related properties) with pin-point accuracy, the results are more than accurate enough for the trading-off of this cooling method compared to the other implemented methods during the optimisation process.

5.2.8. Injector

Another important sizing module that needs to be verified is the injector sizing code. While the iterative design approach (see section 4.4.8) is validated [44], some verification efforts should still be undertaken using reference thrusters used to verify the nozzle module.

The fuel injector representation is verified using an ethanol injector from an ethanol-liquid-oxygen rocket motor [54]. This injector used the following sizing inputs:

- **Mass Flow (Total):** 1.65 [kg/s]
- **Element Number:** 32 [-]
- **Mass Flow (per element)**: 51.56 [g/s]
- **Pressure Drop:** 7.92 [bar]

Based on these design constraints, the reference systems characteristics as well as the ideal characteristics determined by the numerical model can be found in table 5.9.

This comparison shows a relatively close match between the reference systems and the numerical model. While the injector model is shared between the fuel and HTP injector, it is still useful to verify that the injector model also produces sensible results when using HTP instead of the fuel. For the HTP injector, a 50 N monopropellant thruster [25] is used for verification. The inputs that will be used for this thruster are as follows:

- **Mass Flow:** 45.06 [g/s]
- **Element Number:** 1 [-]
- **Pressure Drop:** 7 [bar]

Based on this, the comparison between this reference system and the numerical model can be found in table 5.10.

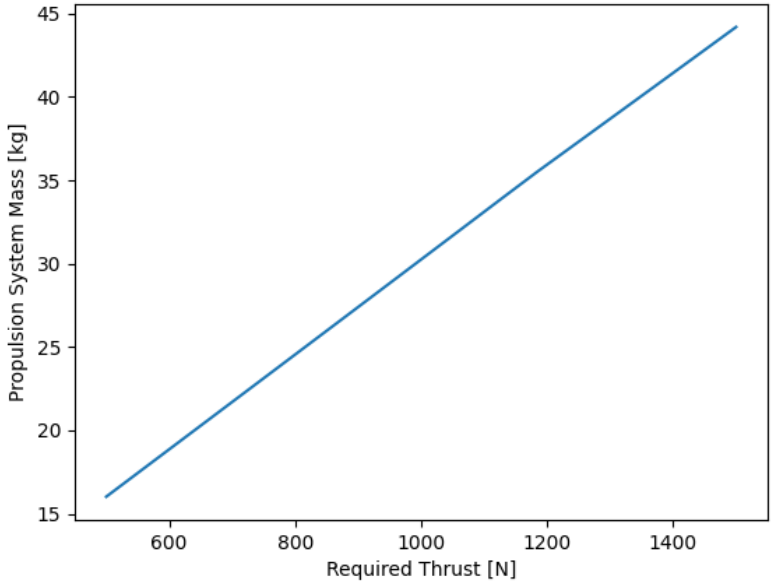

Figure 5.16: Sensitivity Analysis: Thrust vs Total System Mass

In this comparison, the deviation is slightly larger than for the previous ethanol reference case. This is likely due to different HTP concentrations used between the reference case and the numerical model which leads to a difference in density, which itself causes a difference in injector design parameters. Overall, however, the injector design module outputs match reality very well and can thus be used in the optimisation.

5.2.9. Other Verification Efforts

Apart from the more specific verification efforts presented in this previous section, there are also more general verification methods which have been applied to each module. This includes activities such as unit testing, supplying known edge cases to the modules etc. Any discrepancy that was found during these efforts was traced and mitigated.

5.3. Model Verification

To verify the model as a whole, two main steps used are a sensitivity analysis and a comparison with an existing system of similar design. For the latter, this can only be done using one other system due to the low number of comparable propulsion systems with sufficient information available.

5.3.1. Sensitivity Analysis

For the sensitivity, the main focus was put on varying the constrained input parameters and observing the mass output change. Based on this observation, it can be determined whether the modules are connected in a logical way that produces logical outputs based on the input parameter variation. The first parameter variation that was performed is the required thrust, which can be seen in figure 5.16. The thrust was varied between 500 and 1500 [N].

This shows a linear increase of the system mass with increasing thrust. This is to be expected as with constant specific impulse, the thrust is directly linearly related to the mass flow, which itself dictates the amount of propellant required. With a linear increase in propellant, there will also be a linear increase in tank length. Hence the total system mass rises linearly. After this, the burn time was varied, which can be seen in figure 5.17. This parameter was varied between 10 and 100 [s]. This parameter shows the same behaviour as the previous one, and this is also to be expected. In this case, the mass flow is fixed but now the burn time is linearly varied, which leads to the same linear increase in propellant mass and its knock-on effects. Next, the nozzle optimisation altitude was varied, which can be seen in figure 5.18. This parameter

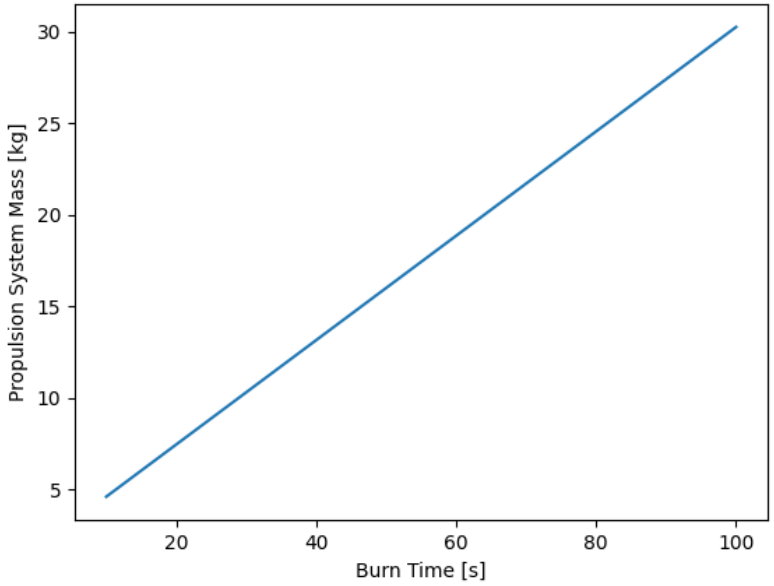

Figure 5.17: Sensitivity Analysis: Burn Time vs Total System Mass

was varied between 0 and 50 [km].

In this figure, it can be seen that at first, the mass decreases with increasing altitude for which the nozzle is optimised. This is because of the increase in specific impulse causing a propellant mass reduction required for the specific burn time. At some point, a minimum is reached. This is also to be expected as at a certain point the mass increase of the nozzle exit diameter increase outweighs the performance benefits. Finally, at the end of the range, it can be seen that the value suddenly plateaus. This is due to the nozzle exit diameter restriction from the available internal rocket diameter becomes the driving constraint at this point. Finally, the HTP concentration is also varied between 50 and 95 [%]. The resulting system mass variation can be seen in figure 5.19

This shows that the total mass decreases with an increase in the HTP concentration. This is to be expected since increased HTP concentration means that the HTP will release more gaseous oxygen per unit mass upon decomposition which makes it a more potent oxidiser. This drives up specific impulses, thereby reducing the propellant mass required.

This analysis can be performed for many more combinations of varied parameters and model outputs, however, reporting them all in this section will exceed the scope of this work. Overall of these tests, including those not presented above, the model does react to the input changes as expected, which leads to the assumption that modules have been integrated correctly into a singular model.

5.3.2. Comparison to Real System

Another method that can be used to increase confidence in the assembled numerical model as a singular unit is to compare it to a reference system. The reference system is the same auto-igniting Kerosene-HTP bipropellant thruster that was used to verify the nozzle module [14]. Its characteristics can be found in table 5.11.

Based on this, the known design parameters of the reference system can be compared to the equivalent outputs from the numerical model. This can be found in table 5.12. Some of these parameters were already compared in previous verification sections.

Considering that it is highly likely that varying design methodologies were used between the two systems, the parameters of both systems match remarkably well. The only exception to this is the chamber length (and to a lesser extent the chamber diameter). This leads to the assumption that the chamber sizing model

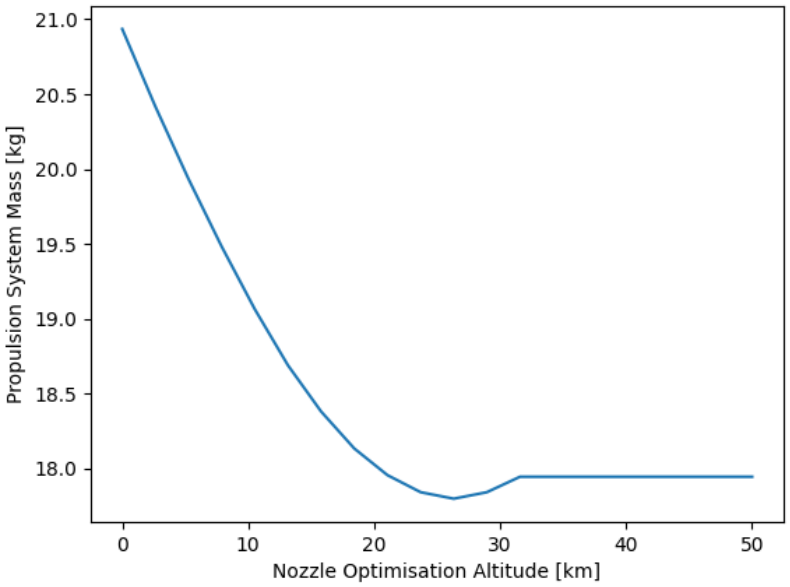

Figure 5.18: Sensitivity Analysis: Nozzle Optimisation Altitude vs Total System Mass

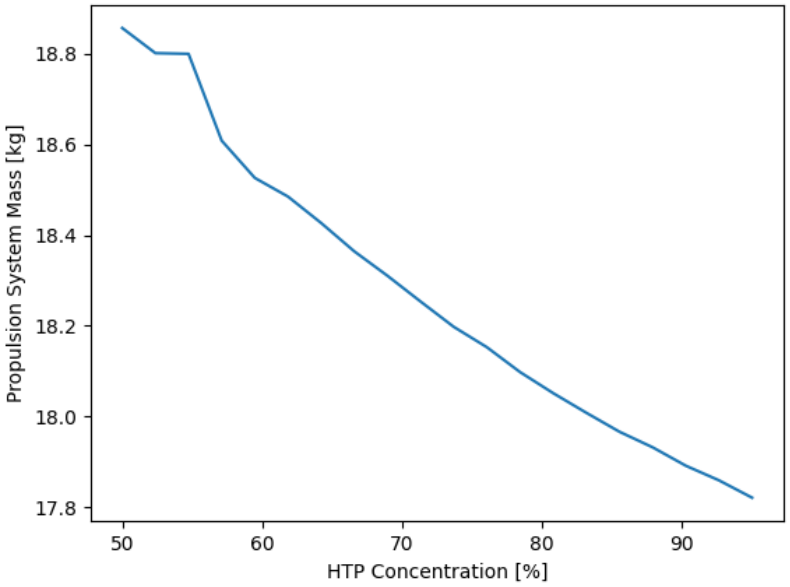

Figure 5.19: Sensitivity Analysis: HTP Concentration vs Total System Mass

Parameter	Value
Thrust	1200 $[N]$
Chamber Pressure	30 $[bar]$
Fuel	Kerosene
HTP Concentration	90 [%]
Nozzle Optimisation Altitude	0 $[km]$

Table 5.11: Comparison Input Parameters based on Reference System [14]

Parameter	Reference System	Numerical Model	Deviation
Characteristic Velocity	1597.8 $[m/s]$	1619.1 $[m/s]$	+1.33%
Characteristic Length	0.95 $[m]$	0.86 $[m]$	−9.47%
Total Mass Flow Rate	417 $[g/s]$	443 $[g/s]$	+6.23%
O/F Ratio	7.2 $[-]$	7.2 $[-]$	±0%
Catalyst Diameter	60 $[mm]$	57.4 $[mm]$	−4.33%
Combustion Chamber Diameter	60 $[mm]$	52 $[mm]$	−13.3%
Combustion Chamber Length	66.25 $[mm]$	96.8 $[mm]$	+46.1%

Table 5.12: Comparison between mutually known characteristics of the reference system [14] and the numerical model output.

used in this work differs from the one used in the reference system. Nonetheless, all outputs still fall within reasonable values, so the numerical can produce reasonable outputs for a given input case.

5.4. Conclusion

This concludes the verification phase of the numerical model. Based on the outcomes of the previous section, it can be assumed that the model is a reasonable representation of an auto-igniting HTP bipropellant engine. Each module was verified individually and the implementation of all modules into one model was also verified.

In order to improve the quality and extent of the verification, more reference cases should be obtained with sufficient known parameters should be found and compared with the model output. While there are several systems comparable to the Barracuda upper-stage propulsion system in literature, many of these do not supply sufficient information in publication to verify various aspects.

More generally, an increase in comparison cases could improve the verification certainty in certain subsystems e.g. the injector module.

Finally, once the proper decomposition module is implemented, this should of course also be verified. However, like the implementation, this is only possible once the HyProp project has performed the first monopropellant thruster tests.

6

Design Optimisation

Part of the objective of this research is to optimise the design of the propulsion system for the Barracuda upper stage. For this, there are two major requirements: A numerical model and a suitable optimisation method. The former was developed as described in chapter 4, and thus this chapter will define the optimisation approach used to optimise the design. Section 6.1 will set out the defined goal of the optimisation approach, section 6.2 defines and elaborates on the chosen optimisation variables and their boundaries, section 6.3 will describe the selection logic of the optimisation method, and finally section 6.4 will present the results of the process.

6.1. Goal

The purpose of design optimisation is to find the design parameter combination within the defined design space that maximises or minimises certain chosen performance parameters. Choosing the design parameter to be optimised will naturally have a large effect on the outcome of the optimisation and thus the optimisation parameter needs to be selected carefully.

For this, three potential performance parameters have been determined:

- Propulsion System Mass
- Cost
- Cost per Dry Payload Mass

The propulsion system mass is one of the first obvious optimisation parameters to be considered. In this application, since the total upper stage mass is fixed to reach a certain minimum altitude, minimising the propulsion system mass will maximise the mass available to payload mass. If the payload mass is fixed, then using this optimisation parameter will instead extend the available apogee/trajectory range. An overview of the impact of mass on the trajectory of the Barracuda sounding rocket can be found in appendix E.

Another possible criterion to optimise for is the cost. This is an attractive option for a profit-oriented company since the more cost-effective solution can often outweigh the direct efficiency of a solution. However, blindly optimising for cost can lead to an inefficient solution that cannot effectively fulfil the defined requirements.

Finally, the last proposed option combines the former two options. Combining these can create a performance parameter which can encapsulate both the mass and cost. However, using this parameter creates the risk of optimising for e.g. a very low payload mass, but a low-cost option which could outscore options with an acceptably higher cost but also better mass performance.

It is important to consider that cost is also a somewhat estimation method. In the current implementation of the model, cost is estimated by raw material cost alone. This however is not necessarily an accurate metric of the actual costs of a given design point. For example, certain material selections might cause increased manufacturing costs which due to the nature of the model cannot be captured and represented.

Table 6.1: Discrete Optimisation Variables

Variable	Values
Pressurant	Helium, Nitrogen, Carbon Dioxide, Argon
Fuel	Ethanol, Methanol, Kerosene, Jet A, Gasoline, Nitromethane
Chamber Material	AISI 304L, AISI 316L, Ti6Al4V, Inconel 600, Inconel 617, Inconel 625, Inconel 290, Inconel 718, Inconel X750, TZM
Fluid Tank Material	EN-AW 1060H12, EN-AW 5253H12, EN-AW 6082T6, AISI 304L, AISI 316L, Ti6Al4V
Pressurant Tank Material	EN-AW 1060H12, EN-AW 5253H12, EN-AW 6082T6, EN-AW 7075T6, AISI 304L, AISI 316L, Ti6Al4V
Nozzle Type	Conical, Bell
Cooling Type	Raditative, Heat-sink, Ablative, Regenerative (Oxidiser), Regenerative (Fuel)
Feed Material	EN-AW 1060H12, EN-AW 5253H12, EN-AW 6082T6, AISI 304L, AISI 316L, Ti6Al4V

In light of this, while cost is a very relevant parameter to the design and optimisation of this propulsion system, it cannot be estimated accurately and consistently within the scope of the numerical model created for this system.

Therefore, the scope of the optimisation algorithm will be set to minimise the mass of the system. Ultimately, this will still ensure a cost reduction to some extent, since an optimisation in mass will always result in less material being used. In the scope of the Barracuda rocket, minimising the mass of the propulsion will provide the largest reliable benefit for the Barracuda upper stage as a whole

6.2. Variables

Fundamentally, an optimisation algorithm aims to minimise or maximise the chosen performance parameter (the propulsion system mass in this case) within a given design space. This design space is defined by the optimisation variables combined with their set ranges.

These variables can be roughly split into two different categories: Discrete and Continuous. Discrete variables are defined by a finite amount of choices that the optimisation algorithm can select for a given variable. Meanwhile, continuous variables are defined by two boundary points between which the optimisation algorithm can select any possible value.

For this design optimisation, the design variables have been based on the variables not constrained by any of the requirements or constraints of the system. The discrete and continuous variables and be found in tables 6.1 and 6.2 respectively.

6.3. Optimisation Method

The choice of the method used to optimise a design model is strongly driven by the characteristics of the design model. Depending on these, some optimisation methods may be more advantageous than others, while other methods may not be applicable altogether. The tree diagram in figure 6.1 provides a process by which the best suite optimisation method can be selected [55].

First, the convexity of the design function needs to be determined. The formal definition of convexity is if, for all pairs of points on the graph, the line segment that connects these two points passes above the curve. In a practical sense for this application, convexity thus refers to the existence of one singular minimum in the design space, as illustrated by figure 6.2. Considering the large number of optimisation variables, and the resulting complex design space, it is highly likely that design space is non-convex. It should be

Table 6.2: Continuous Optimisation Variables

Variable	Boundary			Unit
	Lower	–	***Upper***	
Chamber Pressure	5	–	40	$[bar]$
Nozzle Length Fraction	50	–	95	[%]
Tank Diameter	100	–	180	$[mm]$
Pressurant Pressure	150	–	300	$[bar]$
Fuel Injector Pressure Drop	5	–	15	$[bar]$
Fuel Injector Element Number	5	–	12	$[-]$
Fuel Injector Length	1	–	10	$[mm]$
HTP Injector Pressure Drop	5	–	15	$[bar]$
HTP Injector Element Number	5	–	8	$[-]$
HTP Injector Length	1	–	10	$[mm]$
Nozzle Exit Diameter Use	50	–	95	[%]
HTP Concentration	50	–	80	[%]

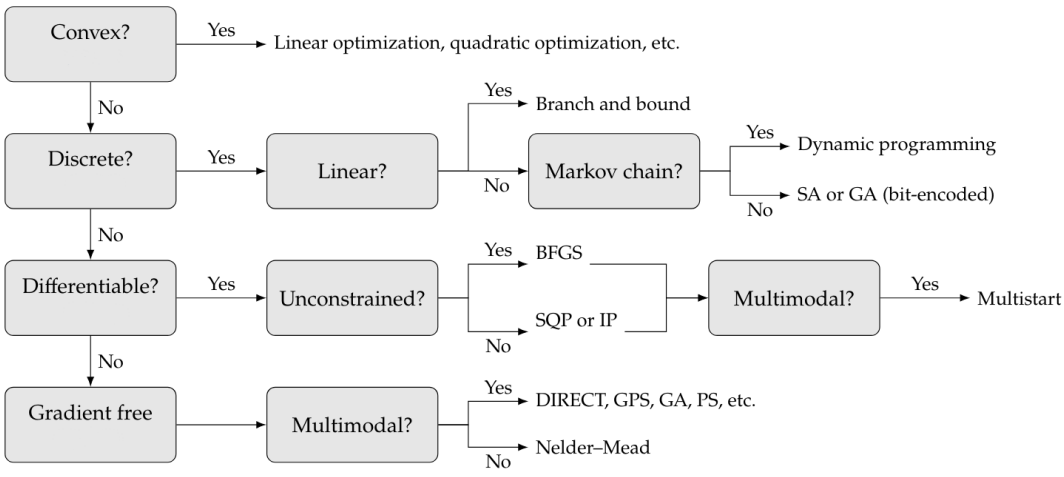

Figure 6.1: Optimisation Method Selection Tree [55]

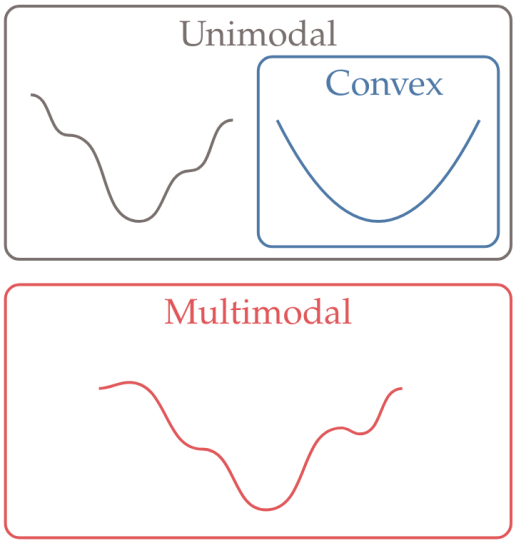

Figure 6.2: Convexity vs Non-convexity [55]

made clear that this is an assumption since determining the design space convexity would involve mapping out large parts of the design space, which itself would make selecting a different optimisation method obsolete.

Following the path on the tree diagram in figure 6.1, the next step is to determine whether the model is continuous or discrete. This is defined through the type of optimisation variables used. In this case, as introduced in section 6.2, there are both discrete and continuous variables. However, while the continuous variables can be discretised, the discrete design options (such as e.g. material selection) cannot be interpolated. Thus the problem should be treated as a discrete problem.

From this, the next decision point is to determine the linearity of the model. This can be determined by analysing the impact of certain variables on the model. Figure 6.3 shows that for example, the influence of the selected initial pressurant pressure is non-linear. This also occurs with other variables such as the chamber pressure, the nozzle length fraction etc. Therefore, it can be concluded that the model is to be treated as non-linear for the optimisation method selection.

Finally, the model does not fulfil the criteria for a Markov Chain since it is a fully deterministic model and thus, the selected optimisation method will be a genetic algorithm.

A genetic algorithm (GA) is a search heuristic inspired by the principles of natural selection and genetics, used to find approximate solutions to optimisation and search problems. GAs work by mimicking the process of evolution, where a population of potential solutions evolves over time. Each individual is represented by a chromosome, which encodes a possible solution to the problem. The algorithm begins with a randomly generated population and iteratively applies genetic operators such as selection, crossover (recombination), and mutation to evolve the population towards better solutions. Figure 6.4 shows the iteration sequence of a GA.

During each iteration or generation, individuals are evaluated based on a fitness function, which measures how well they solve the problem at hand. The fittest individuals are more likely to be selected for reproduction, allowing them to pass their genes to the next generation. Crossover combines the genetic information of parent individuals to produce offspring with potentially better traits, while mutation introduces random changes to individual chromosomes, ensuring genetic diversity within the population. Over successive generations, the population converges towards an optimal or near-optimal solution. GAs are particularly useful for complex problems where traditional methods may be inefficient or infeasible, therefore it is well-suited for this application.

Based on the reasoning in section 6.1, the fitness function for this genetic algorithm is defined as the total mass of the propulsion system. The genetic algorithm will attempt to minimise the mass as much as

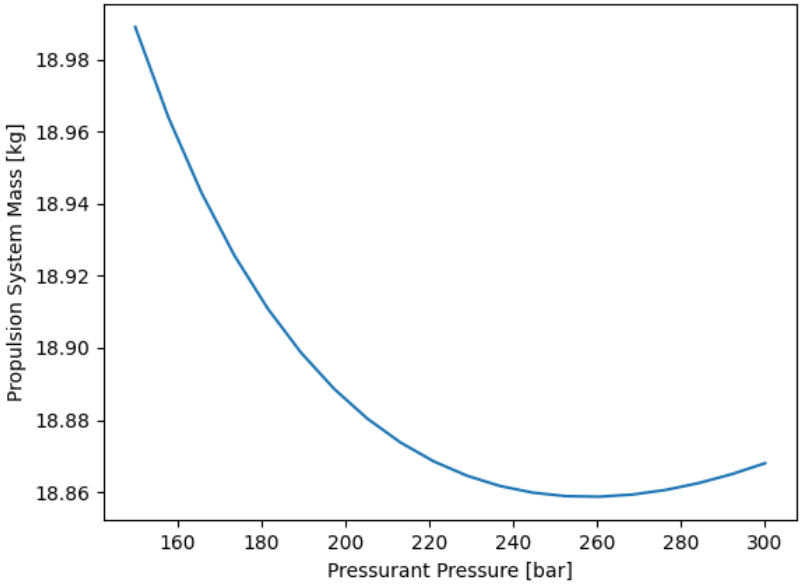

Figure 6.3: Exepmplary Impact of Initial Pressurant Pressure on Total System Mass

Table 6.3: Genetic Algorithm Parameter used for the Optimisation

Parameter	Value
Maximum Number of Generations	300
Population Per Generation	20
Mutation Probability	0.1
Elite Ratio	0.01
Crossover Probability	0.5
Parents Portion	0.3

possible. To implement this in the model, a pre-existing Python implementation for genetic algorithms is used [56]. This model allows for the mixed implementation of both discrete and continuous variables and allows for the adjustment of various algorithm parameters such as:

- Maximum Number of Generations
- Population Per Generation
- Mutation Probability
- Elite Ratio
- Crossover Probability
- Parents Portion

The major advantage of using the preexisting genetic algorithm implementation is that the implementation is already well validated, and thus very few additional verification efforts need to be undertaken in order to ensure the algorithm performs a reasonable optimisation. The major disadvantage is that certain break conditions e.g. an insufficient injector design (see section 4.4.8) are more difficult to implement. In this model, this has been done by imposing mass penalties, which will ensure that any design that does not meet certain criteria gets removed during the iteration of the genetic algorithm.

For the optimisation performed on the numerical model for this propulsion system, the parameters used can be found in table 6.3.

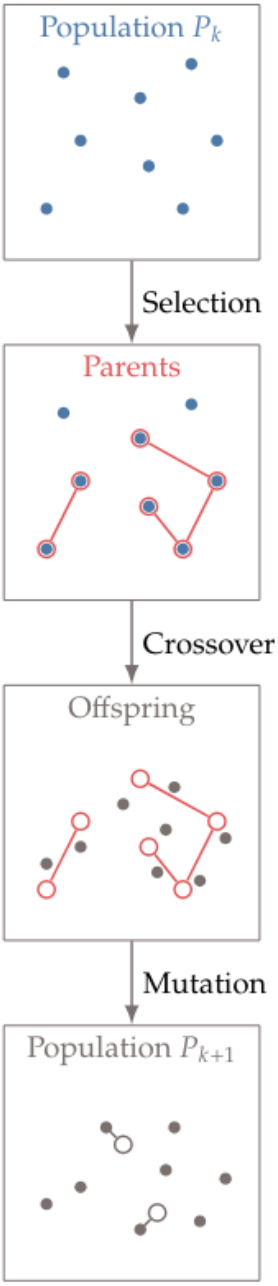

Figure 6.4: Genetic Algorithm Iteration Sequence [55]

Table 6.4: Optimised Design Model Input Parameters

Parameter	Value
Pressurant	He
Fuel	Gasoline
Chamber Material	Inconel 690
Fluid Tank Material	Titanium Ti6Al4V
Pressurant Tank Material	Titanium Ti6Al4V
Nozzle Type	Bell
Cooling Type	Regenerative (Oxidiser)
Feed Material	Aluminium EN-AW 6082T6
Chamber Pressure	12.97 $[bar]$
Nozzle Length Fraction	54.0%
Tank Diameter	139.9 $[mm]$
Initial Pressurant Pressure	261.5 $[bar]$
Fuel Injector Pressure Drop	6.12 $[bar]$
Fuel Injector Elements	9
Fuel Injector Length	2.23 $[mm]$
HTP Injector Pressure Drop	5.69 $[bar]$
Fuel Injector Elements	1
Fuel Injector Length	6.07 $[mm]$
Nozzle Exit Diameter Use	50.3%
HTP Concentration	78.3%

6.4. Results

This section contains the results of the optimisation algorithm. This specifically means the optimised model inputs that were determined by the genetic algorithm. These can be found in table 6.4. The resulting propulsion system characteristics can be found in appendix D.

The convergence plot of the optimisation algorithm can be found in figure 6.5.

6.5. Conclusion

With the presentation of the optimised design results, the optimisation phase can be concluded. The next phase will consider the outcomes of the optimisation and determine their sensibility and whether they comply with requirements from chapter 3.

For future work, some additional attention could be paid to the optimisation algorithm parameters. At this point, the optimisation algorithm uses mostly the standard parameters apart from some alterations to the population size and generation number. In the future, variations could be performed on the optimisation algorithm parameters and observe the impact created by this.

Ultimately, the design derived from this optimisation phase however will be used in the further phases of this thesis project.

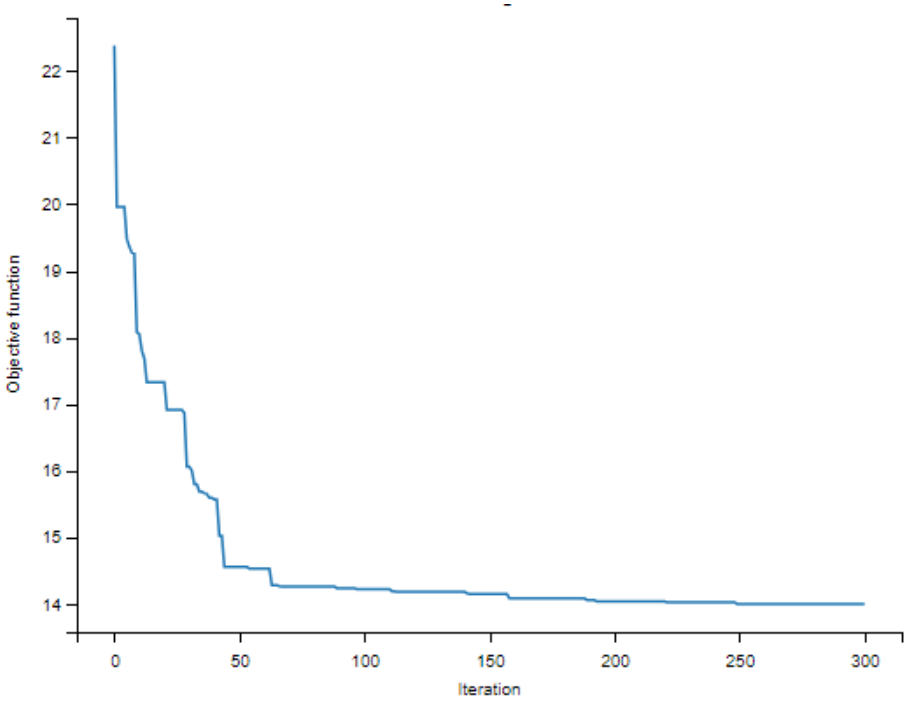

Figure 6.5: Convergence Plot of the Genetic Algorithm

7

Result Validation

With the propulsion system design optimised, the outcomes of the optimisation process now need to be validated. Firstly, the overall sensibility of the design choices made by the optimisation algorithm (thus the chosen inputs to the numerical model) needs to be validated by considering if these design decisions are implementable in the real world and determining future recommendations based on this. Afterwards, and after potential adjustments to the design choices based on the discussion of the results, the design will be validated against the requirements defined in chapter 3. Finally, recommendations for future validation activities will be made.

7.1. Result Discussion

The outcomes of the optimisation algorithm can be found in section 6.4. While the design model was verified, the optimised input parameters for the model should be validated to be feasible in the real world to be implemented into a propulsion system. For this, each optimised parameter will be discussed for its feasibility.

7.1.1. Pressurant Type

The possible pressurant types to be selected were Nitrogen, Helium, Argon, and Carbon Dioxide. The optimisation algorithm determined that Helium would make the most mass-efficient option out of all possible pressurant gasses. When considering real-world systems, helium is commonly used due to its lightness [29], [57] so the algorithm selecting this pressurant is consistent.

The main challenge that comes with helium as a pressurant gas is the creation of a leak-tight system [58]. Due to the small size of a helium atom, creating a fully leak-tight system requires high accuracy in production, since the atoms can use the smallest crevices to vent to the outside. Additionally, Helium gas is a rare resource and because of this, it is more expensive than e.g. Nitrogen. However, this effect is somewhat offset by the low amount of substance required to set a certain pressure at a certain volume.

Therefore, it is recommended that for initial verification testing, Nitrogen is substituted to develop the system, and Helium is only used for flight-validation testing and subsequent flight applications. This can reduce the time required per verification test, and more importantly, reduce costs during the final development phases of the propulsion system.

7.1.2. Fuel

The possible fuel options were Ethanol, Methanol, JetA, Kerosene, Gasoline, and Nitromethane. Out of these, Gasoline was selected. Gasoline is one of the most easily obtainable fuels out of the possible selection list and it is also the second cheapest option after Kerosene per unit mass. Hence this choice supports repeated testing and also does not drive the operational costs of the system excessively high.

As a long-chain hydrocarbon, gasoline is prone to coking [59]. This can lead to e.g. clogging in the injector orifices, which can affect the injector performance which itself will throw off the mixture ratio and therefore

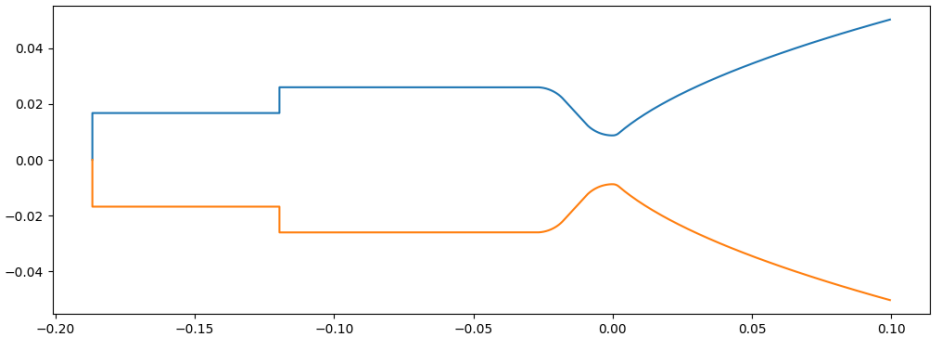

Figure 7.1: Contour of the Decomposition Chamber, Combustion Chamber, and Nozzle of the Resulting Thruster

the performance of the entire system. This can be counteracted to a certain extent by using gasoline (or even pure octane) at higher purity levels.

7.1.3. Chamber Material

For the chamber material, there is an array of different material options that the algorithm can select from. Some options include stainless steels or refractory metal alloys such as TZM or Inconel. Ultimately, the optimisation algorithm selected Inconel 690.

The Inconel alloys are characterised by their high thermal resistance as well as resistance to corrosion in oxygen-rich environments. It is therefore very well suited to be used as a material for the combustion chamber of a rocket engine. However, it may be beneficial to consider the use of Inconel 718 instead of Inconel 690. Inconel 718 has very similar properties to Inconel 690, but Inconel 718 is more readily available for additive manufacturing processes. Given both the regenerative cooling and bell nozzle design choices, utilising additive manufacturing could greatly benefit the manufacturing process of the combustion chamber.

7.1.4. Fluid and Pressurant Tank Material

For both the fluid and pressurant tanks, the optimisation algorithm selected the use of the Titanium alloy Ti6Al4V. This Titanium alloy is commonly used in aerospace applications for pressure vessels, especially for pressurant tanks [60]. Titanium Ti6Al4V has a high strength-to-weight ratio and as such is often used for thin-walled tanks.

It should be noted that the thin-walled nature of the Titanium tank would likely make it fall outside the manufacturing capability of T-Minus Engineering. Whether this is deemed acceptable largely depends on the cost of manufacturing the tank externally and whether its benefits outweigh the benefits of manufacturing an e.g. thicker-walled aluminium tank in-house. This cannot be determined at this point, however, thus for now the Titanium tanks are kept.

7.1.5. Nozzle Type

The nozzle type selected was the bell nozzle (or parabolic nozzle). As the material selection of the chamber was previously changed to enable regenerative cooling, the nozzle shape imposes next to no challenges on the manufacturing process. Therefore, the benefits of the parabolic nozzle can be taken advantage of without many of the manufacturing drawbacks.

The chamber-nozzle contour can be seen in figure 7.1.

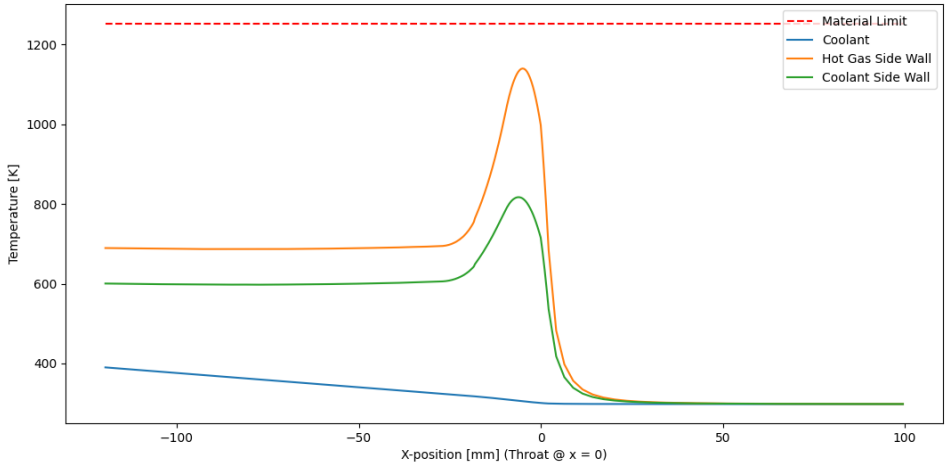

Figure 7.2: Temperature of the chamber-side wall, the coolant-side wall, and the HTP in the cooling channel in relation to the maximum allowable temperature of Inconel 718

7.1.6. Cooling Method

The selected cooling method is regenerative cooling using the HTP. While this is relatively uncommon among liquid rocket engines, it does make sense in this application. Considering appendix A.2, it can be seen that out of all available cooling fluids, HTP does have the most advantageous properties. One concern that does need to be addressed is to ensure that the HTP will not be thermally catalysed into decomposition based on the heating in the cooling channels. Otherwise, this could lead to unpredictable behaviour which in the worst case could lead to a back-travel of the decomposition into the HTP tank, which could cause a catastrophic failure.

As can be seen in figure 7.2, while the temperatures of the wall remain within material limits, the HTP temperature never exceeds 400 [K]. It is known that the activation energy for the decomposition of HTP without the presence of a catalyst is around 75 [kJ/mol] [61]. Meanwhile, HTP has a specific heat of about 50 [J/mol/K]. This means that an increase of around 100 [K] equates to an energy increase of 5 [kJ/mol]. This leaves more than sufficient margin, even if certain amounts of catalysing substances were to be present.

It should be noted that based on the wall temperature, the coolant might only be introduced into the nozzle from a certain diameter range onwards, such that the latter stages of the nozzle divergent remain uncooled. This can reduce the overall pressure drop over cooling channels, which itself reduces tank mass.

7.1.7. Feed Line Material

For the feed lines, Aluminium EN-AW 6082T6 was selected. This material selected material makes a good choice for the feed lines since it combines excellent manufacturability with decent mechanical properties, all while being lightweight. This aluminium alloy is also compatible with HTP (for limited exposure times like in this system), thus it is very suitable to use on all lines in the propulsion system.

7.1.8. Chamber Pressure

The optimal chamber pressure was determined to be 12.97 [bar]. This value will be rounded to 13 [bar] as this will not make any large differences in the design of the propulsion system. This chamber pressure is closer to the low end of the allowed chamber pressure range. This is to be expected as the defined operating altitude of 60 [km] makes this engine a quasi-vacuum thruster. For vacuum-optimised thrusters, there is not nearly as much gain from higher chamber pressures as for sea-level thrusters and thus the algorithm tends towards lower pressure since this reduces tank and feed system mass.

7.1.9. Nozzle Design

The nozzle has an exit diameter use fraction of 50.3%. This means that the nozzle exit diameter is 50.3% of the maximally allowable exit diameter, which is constrained by the rocket's internal diameter. Furthermore, the nozzle length fraction has been reduced to 54%. Both of these measures will reduce the length of the nozzle.

This is to be expected as minimising both of these values reduces the nozzle mass. This then shows that the effects of the reduced area expansion ratio and higher final parabola angle still do not outweigh the gains from a shorter and thus lighter nozzle. Additionally, this leads to a more compact design, which can be more easily integrated and reduces the tendency of the divergent section of the nozzle to vibrate at low frequencies.

7.1.10. Tank Diameter

If only the cylindrical section of the tank is considered, then the optimisation algorithm would attempt to increase the diameter tank to the maximum possible limit of 180 [mm], since a reduction in diameter by a factor x will lead to a length reduction of factor x^2. However, due to the effect of end caps in the design, the optimisation algorithm finds some middle ground between those boundary points. Therefore, it makes sense that it determines to most optimal tank diameter neither close to the low end nor to the high end of the permissible diameter range. The diameter will also be rounded to 140 [mm].

7.1.11. Fuel Injector Design

The ideal fuel injector was determined to use 9 elements, at a pressure drop of 6.12 [bar], with an orifice length of 2.23 [mm] each. The pressure drop will be rounded to 6 [bar], similar to the combustion chamber pressure. The injector length will be rounded to 2 [mm], since this will improve the manufacturability of the system, by using standard stock material sizes. The number of orifices also is reasonable, producing a mass flow of 19.8 [g/s] per orifice, which is in the same order of magnitude as the verification cases. The resulting orifice diameter of 0.4 [mm] is also within reasonable values compared to some of the verification cases.

7.1.12. HTP Injector Design

The ideal HTP injector was determined to use 1 element, with a pressure drop of 5.69 [bar], and an orifice length of 6.07 [mm]. Similar to the fuel injector, the pressure drop is rounded to 6 [bar], and the injector orifice length is rounded to 6 [mm]. Using single-orifice injectors is also commonly seen on HTP monopropellant thrusters [11], [25]. Therefore, this is a reasonable injector arrangement that is reasonable for injecting HTP onto a catalyst bed.

7.2. Requirement Validation

The output of the optimisation algorithm is the optimised inputs to the numerical model. After validating these inputs, it is important to ensure that the propulsion system based on these optimised inputs produces a propulsion system design which complies with the requirements. This will be done for each of the requirements from section 3.1. It should be noted that not all high-level requirements of the propulsion system apply to this modelling and optimisation work and therefore, not all requirements can be validated at this stage.

- **PROP-REQ-1:** The propulsion system has been designed with the 600 [N] thrust requirement. This requirement can be validated by using equation (4.2a), filling in the mass flow and specific impulse determined from the model output. Once this is done, it can be found that the propulsion system does indeed provide 600 [N] of thrust.
- **PROP-REQ-2:** The compliance with this requirement can be determined using equations (4.2b), (4.3a) and (4.3b) to determine the fuel and oxidiser mass flows, and then compared this to the fuel and oxidiser mass determined from the model output. When running this verification step, it can be found that the propulsion system can operate for 60 [s] exactly. However, some small additional amount of propellant should be added such that the requirement can also be fulfilled under non-ideal cases, e.g. when fluid gets trapped in fittings or other parts of the feed lines.
- **PROP-REQ-3:** This requirement is fulfilled due to the propulsion system being able to open and close

the fuel and oxidiser main valves. Since both of these valves are designed as actively controlled solenoid valves, the propulsion system can be extinguished at any moment, thus it fulfils this requirement.

- **PROP-REQ-4:** The propulsion system is designed without an ignition system being required. This is due to the catalytic decomposition of the HTP before combustion combined with the careful fuel selection allowing for auto-ignition of the propellant combination. In the tests as part of the HyProp project, it has been demonstrated that the same catalyst bed can be used multiple times, thus after extinguishing the engine it can also be re-ignited easily multiple times after each other. Naturally, the start-up of a liquid rocket motor does cause wear, so, during validation testing of this system, tests with repeated re-lighting should be run to determine any possible effects of repeated re-lighting on the propulsion system.
- **PROP-REQ-5:** This requirement is fulfilled based on the work performed in chapter 6. Especially figure 6.5 shows that the total system mass was minimised and has decently converged. The numerical model is designed in such a way that it allows for the implementation of more refined models for each module without needing to reconstruct the entire model. Therefore, it may be beneficial in the future to re-run the optimisation with improved models for the various subsystems
- **PROP-REQ-6:** A major point in which the requirement is upheld is using the technology of the HTP decomposition from the HyProp project. This includes utilising HTP as an oxidiser in the first place and using the same type of catalyst as the HyProp project. Apart from this, there are only very few and more niche technologies in T-Minus Engineering that can be utilised for a liquid propulsion system, e.g. limiting the pressurant pressure to 300 [bar] because of the limitations of the existing gas compressor. However, if these exist then they were utilised or taken into consideration, therefore this requirement can be considered validated at this point.
- **PROP-REQ-7:** This requirement can ultimately only be validated once the final system is produced. However, many manufacturing considerations were taken into account for this design in nearly every subsystem. While it may not be possible to produce each component within T-Minus Engineering, the bulk of the system can be constructed and manufactured in this way.
- **PROP-REQ-8:** This requirement will only be fully validated once the system has been constructed and integrated with the remainder of the Barracuda rocket system. However, the propulsion system as designed in this research has been designed with all constraints from Barracuda taken into account e.g. for the tank diameter constraints or the nozzle exit diameter restrictions.
- **PROP-REQ-9:** Finally, this requirement can also only be validated once the upper stage has been constructed and more importantly once the remaining subsystems like electronics and structures have been designed. Until then this requirement cannot be validated by this work alone.

Next to validating compliance with the requirements set out at the start of this work, the compliance with the imposed constraints in table 3.2 should also be validated.

- **PROP-CON-1:** The largest diameter component of the propulsion system design derived from the optimisation algorithm is the fuel or oxidiser tank at 140 [mm]. Therefore, the constraint is validated.
- **PROP-CON-2:** Validating this constraint of the propulsion system falls outside the scope of this research. Especially when considering the complex vibrational loads introduced by the first stage's solid rocket motor, this type of analysis simply exceeds the scope of this research and therefore should be performed at a later stage.
- **PROP-CON-3:** Similarly to the previous constraint, this constraint will require additional modelling and testing after further design iterations.
- **PROP-CON-4:** The ground support infrastructure considerations were mostly left untreated in this work, therefore this requirement cannot be fully validated at this point. However, it should be noted that a large number of design decisions were precisely made with this requirement in mind. Some additional mobile ground support equipment will likely be required (e.g. for propellant loading), but none of these systems should require permanent infrastructure. This requirement will be validated once the ground support infrastructure has been designed.
- **PROP-CON-5:** Ground testing will ultimately reveal the manpower required to operate this system. However, considering the limited complexity (compared to other liquid propulsion systems) of the

system, it is feasible that this constraint can be achieved. However, this can only be validated after testing of the ground system

7.3. Suggested Future Validation Activities

While the results of the design optimisation have been validated to the extent possible within the scope of this work, there are more possible validation efforts that exceed the scope of this project.

Due to the lack of existing or accessible validation data, the construction of a first prototype thruster could provide valuable data on the accuracy of the chosen modelling methods. While this system should be constructed based on the outcome of this work, it should be constructed in a modular fashion such that it can be adapted easily based on findings during testing. Differences between this ground testing system and the flight system for the upper stage would include using cheaper materials such as stainless steel, utilising heat-sink cooling, and consequently limiting the burn times. A set-up like this can then also be used to validate the designs of various subsystems such as injector, chamber, or nozzle. Furthermore, various components such as the nozzle can be produced in variations to evaluate the effects of e.g. different chamber pressures. The data gathered from these systems can then ultimately be used to improve the numerical model.

Once such a system has been constructed it can also be used to test and validate various operational concepts of this propulsion system. One of the reasons for choosing HTP as the oxidiser for this system was its ability to be decomposed and auto-ignited with the chosen fuel. This negates the need for a dedicated ignition system and in theory allows for unlimited relights of the engine. However, this relight capability needs to be validated in the real world.

Some further analysis should also be performed about the in-house manufacturability of the system. During the advance of the design from the current subsystem-level detailed design to the subsystem- and component-level critical design, an analysis should be made for each component about its manufacturing requirements. Based on this, decisions can be made on how components are produced (internally or externally) and based on this the design can be adjusted. This analysis is not fully possible at this stage, but it will ensure that the propulsion system remains within the scope of T-Minus Engineering.

Additionally, at this stage, the design of the remaining upper stage of the Barracuda Rocket must also be advanced. This is needed to explore which constraints various other subsystems of the upper stage would impose on the propulsion system, and also to determine in which manner the propulsion system interfaces with other subsystems of the upper stage. For this, a more specified application case for the upper stage should be determined, and based on this a subsystem architecture should be defined similar to the approach for this propulsion system.

7.4. Conclusion

Due to the lack of validation data, the validation efforts needed to focus on the results of the optimisation process. In this case, the result validation was performed primarily using "Engineering Sense" and previous experience. While this is a valuable step as part of the validation process, it cannot replace validation against real test data. This however can only be obtained, once more testing in the HyProp project has been performed.

One remarkable design choice is the use of HTP for the regenerative cooling of the combustion chamber. This is a very uncommon solution but it promises the best performance over the fuels as a cooling fluid due to its superior thermal properties. One concern with this solution is the premature thermal decomposition of the HTP, but the analysis in section 7.1.6 has shown that the HTP will not prematurely decompose in the current design.

However, from the validation activities that were performed, the results are logical and are practically applicable in the real world, apart from some minor changes to the model output. The ultimate goal of the thesis project was to find an optimal design point in the given design space rather than determine a propulsion system design that can be entered into production after this project. In this light, the results are certainly usable in further iterations of system design, however, the options for adjusting the design parameters should always left open if the necessity arises.

8

Conclusion

The goal of this research project was defined in chapter 1 as follows:

> *"Design, model, and mass-optimise a propulsion system for the steerable upper stage for the T-Minus Barracuda using hydrogen peroxide that falls within the operational and technological envelope of T-Minus Engineering"*

This goal thus defined three main points that needed to be addressed as part of this work: The conceptual system-level and to some extent subsystem-level design, the creation of a numerical model capable of representing the previously established design, and the optimisation of the design to find an optimised point in the available design space. From each of these major steps, conclusions will be drawn which can then ultimately also refer back to the research objectives and questions. These can then be used to put the outcome of the research into the right context and to determine future recommended activities.

One of the unique challenges of this project was to design a propulsion system within the constraints imposed by T-Minus Engineering. This not only includes the requirements set out for the propulsion system but also the constraints that the small-scale, agile nature of T-Minus Engineering imposes. Next to determining some additional constraints in section 3.2 on to the design, one of the major conclusions from the initial literature review for the research [6] was to utilise existing technologies. Due to its close relation to this project, the HyProp project was especially considered in chapter 2. The major conclusion of this phase was that HTP should be utilised as the oxidiser for the Barracuda upper-stage propulsion system, because of the existing supply lines, and the operational advantages and experience. Next to this, the further HyProp project stages can be utilised as a test bed and validation data source for this design of the Barracuda upper-stage propulsion system. Finally, due to unforeseen delays in the project, a surrogate model will be required in the numerical model to represent the HTP decomposition process until suitable test data is obtained.

With these insights, the next phase aimed at defining the propulsion system's preliminary design, which initially established the final requirements and constraints for the subsystem. Based on this a system-level concept was chosen. The system will utilise the catalytic decomposition of HTP combined with the auto-igniting properties of a carefully selected fuel, with the auto-ignition temperature being a primary selection criterion. The preliminary architecture was defined, and fuel candidates were chosen based on various criteria related to the operations, handling, and modelling of the propulsion system. The preliminary design of each subsystem was detailed to the extent required to be able to model and integrate each into a numerical model.

A numerical model was developed based on the preliminary design to cover all aspects of designing and sizing the various subsystems of the propulsion system. This object-oriented model allows for optimisation using 19 parameters, which can vary within defined ranges, and generates numerous output parameters for verification, validation, and component sizing. Although the model has some inherent limitations, such as only considering steady-state operation, relying on a fixed decomposition temperature, assuming 1D flow in the chamber, and using a simplified regenerative cooling model, these do not obstruct the original

goal of the optimisation process. Future data from the HyProp project will help address these limitations, particularly in updating the decomposition model. The current model serves as a robust foundation for the initial design phase, and its outputs will undergo further analysis and refinement before transitioning into a critical design stage, ultimately leading to manufacturing and testing.

After the numerical model was constructed, it was verified. Based on the verification outcomes, the model reasonably represents an auto-igniting HTP bipropellant engine, with each module verified individually and collectively. To enhance verification quality, more reference cases with sufficient parameters should be obtained for comparison. While comparable systems exist in literature, they often lack detailed information needed for thorough verification. Increasing comparison cases could improve verification certainty, especially for subsystems like the injector module. Additionally, the proper decomposition module should be verified after the HyProp project's initial monopropellant thruster tests.

Once the numerical model was verified, the optimisation method was selected based on the method selection tree in figure 6.1. Based on various criteria, a genetic algorithm was determined as the ideal optimisation method for the numerical model. For this, optimisation variables were assigned a set of possible values or ranges. Finally, the optimisation algorithm parameters were set and an optimised design was created. With this phase completed, the third major aspect of the research question was covered.

Finally, the outcomes of the optimisation process were validated. Due to the lack of real-world validation data, the validation efforts focused on the results of the optimisation process, relying on "Engineering Sense" and previous experience rather than real test data, which will only be available after further testing in the HyProp project. A notable design choice is using HTP for the regenerative cooling of the combustion chamber, an uncommon solution that offers superior performance due to HTP's thermal properties. Although there were concerns about premature thermal decomposition, analysis showed that HTP would not decompose prematurely in the current design. The validation activities indicated that the results are logical and applicable, despite minor model output adjustments. The project's ultimate goal was to find an optimal design point rather than a production-ready propulsion system, and the results are valuable for future design iterations, with design parameters remaining adjustable as needed.

8.1. Research Questions

To conclude this project, the research questions defined in table 1.1 will be revisited. For each question, conclusions will be drawn based on the work performed in this thesis project, and if needed future work to further answer these questions will be suggested.

8.1.1. RES-Q-1

How can hydrogen-peroxide be used as a basis for the propulsion system of the Barracuda upper stage?

This set of questions is primarily aimed at determining the feasibility of using HTP for the propulsion system and determining which technologies are the most advantageous to be used in combination with this oxidiser.

RES-Q-1A: Can it be used in a bi-propellant system?
HTP is a commonplace oxidiser in many space propulsion systems. It is the second most potent oxidiser after liquid oxygen [10]. This work has found multiple examples of HTP bi-propellant propulsion systems [12]–[14], [27] and the validated outcomes of the design and optimisation process also confirm this. As determined in section 3.4.1, HTP brings many advantages in terms of handleability and operations (e.g. non-cryogenic, liquid at 1 [atm]) but also possesses some unique characteristics that if harnessed can significantly simplify the design of the propulsion system, such as the catalytic decomposition capability. Therefore, the HTP can be viably used in a bi-propellant system such as the one for the Barracuda Upper Stage.

RES-Q-1B: Is a bi-propellant system advantageous over a mono-propellant system?
To some extent this question was already addressed during the literature review for this work [6]. The propulsion system designed in this work should provide a specific impulse over 300 [s]. Compared to the 150-180 [s] produced by HTP monopropellant systems, this means an up to two-fold performance increase between the HTP bi-propellant and mono-propellant systems. Thus, implementing a propulsion system as

a bi-propellant system rather than a mono-propellant has significant performance advantages, and if the catalytic decomposition auto-igniting property is utilised, this improvement comes at a low increase in complexity.

RES-Q-1C: Which technologies can be used to achieve decomposition?
The work especially in chapters 2 and 3 has shown that T-Minus Engineering already has developed suitable in-house manufacturable technology. Primarily, the technology for the production of Manganese-Oxide Coated Nickel Foam catalyst beds has been shown to produce catalyst beds capable of decomposing the HTP, and with further development and characterisation of these catalyst beds ongoing, it is clear that this technology is of great relevance to this work and thus should be utilised as much as possible, with the biggest advantage being their in-house manufacturing process and therefore there ability to be rapidly developed. There may be other catalyst types that could be used in this application, but these would require further research.

Towards Overarching Question
Utilising HTP and its decomposition properties can be used to significantly simplify the propulsion design within the design space given by the requirements and constraints. Since its decomposition products are heated enough to auto-ignite with many fuels, among which the chosen fuel, Gasoline, the need for an ignition system is completely negated. Through its theoretically unlimited amounts of relights, this then allows for pulsed operation, which itself also negates the need for a throttling system. This simplifies the system even further and allows for more design freedom with regard to the feed system and injector design.

Additionally, the outcomes of the numerical model have shown that the HTP can be used to regeneratively cool the combustion chamber due to its superior thermal properties over the any of potential fuels. It was shown that this can be done safely without risking premature decomposition of the HTP in the cooling channels and without the HTP changing phase. This pre-heating of the HTP also has the potential to increase the overall efficiency of the decomposition process in the catalyst bed, but further research and testing are required in this direction to quantify the effect of this.

Ultimately, the use of HTP greatly simplifies the propulsion system which majorly aids in integrating this propulsion system into the upper stage of a sounding rocket, especially within the operational constraints of T-Minus Engineering. The two aforementioned advantages combined with its handling characteristics are the key drivers of why this oxidiser is likely the ideal choice for this application.

8.1.2. RES-Q-2

How can multiple parameter design optimisation methods be used to maximise the performance of the Barracuda upper-stage propulsion system?

This set of questions is aimed at determining how the system can be modelled, how it can optimised, and what goal it should be optimised for.

RES-Q-2A: How can such a propulsion system be numerically modelled?
The numerical model for this application was developed using a subsystem-by-subsystem modular approach. This means that for each subsystem, a module was developed that allowed for the representation of this subsystem. This approach was chosen because some systems require more discretised models (e.g. chamber transport, see section 4.4.6) while others could be modelled using just a few analytical equations (e.g tank module, see sections 4.4.10 and 4.4.11). Next to this, it became also clear that using and combining existing models can greatly reduce the development time of the model. In this case, the combustion module was largely based on the NASA CEA thermo-chemical equilibrium code [31], [32]. This saves time not only in model development but also during verification and validation.

Another major conclusion considering the modelling of the propulsion system is the consideration of the model run time. With the chosen optimisation method, the algorithm iterates through more than 5000 instances of the numerical model. This means that even small run-time changes in the numerical model itself can have large impacts on the runtime of the implemented optimisation algorithm. Therefore, a major recommendation is that for future refinements of the numerical model, the run time should always remain a primary consideration.

Finally, while it has been determined that this modelling approach adequately represents the propulsion system for the purpose of design optimisation, further refinements can be made in order to improve the overall accuracy of the model. This will be elaborated on in chapter 9.

RES-Q-2B: How can such a propulsion system be numerically optimised?
Based on the construction of the numerical model and the goals of the optimisation, the optimisation that best suited the given problem was a genetic algorithm. This method was selected from a large array of other methods based on the decision tree in figure 6.1. This method was successfully implemented with the numerical model and did produce results that can be implemented in the real world, pending more detailed subsystem-level analysis, verification and validation. However, based on the method selection it becomes clear that the selection of the method (thus the "how"-aspect of the optimisation) is more directly dependent on the design of the numerical model itself rather than the propulsion system design. Naturally to a lesser, the latter influences the former, but the direct dependency lies with the architecture of the numerical model.

RES-Q-2C: Which parameters should it be optimised for?
Initially, the goal was to factor both cost and mass into the fitness function for the optimisation method. However, during the construction of the numerical model, it quickly proved challenging to implement representative cost estimates for such a physically small system into a numerical model. Due to the small physical size of the system, the cost of the system is mainly driven by man-hours and machine-hours in production and testing rather than raw material costs. Even when using the most expensive materials in the selection (TZM or Inconel X750) the cost of e.g. the combustion chamber would not exceed the 400-500 [$] range. Compared to the man-hours required at common rates, this cost is a small fraction of the total cost. Next to this, some of the design choices that can be made as part of the optimisation process can imply largely different manufacturing requirements, and by extension, costs. For example, a radiatively cooled conical nozzle has largely different manufacturing requirements when compared to a regeneratively cooled bell nozzle.

Overall, it can be concluded that for an optimisation process that includes higher-level design decisions such as the one described above, mass is the ideal and most accurately quantifiable optimisation parameter. If cost is desired to be implemented into the fitness function for the optimisation process, then the suggested approach is to first optimise the system like in this work based on mass, and then constrain many of the higher level design decisions and perform a further optimisation in a more restricted design space.

Towards overarching question
The biggest insight of this work with regards to the design optimisation was that while the design optimisation process cannot produce a ready-to-manufacture design, it can allow to narrow down the available design space considerably. While additional analysis and lower-level design adjustments will be required, this approach allowed the progression of the design from a high-level conceptual design to a subsystem-level detailed design.

Finally, the work has also shown that given the small-scale nature of the propulsion system and the relation between mass and performance of the Barracuda sounding rocket found in appendix E, optimising for lowest mass brings the best performance benefit for the upper stage as whole. Next to this, out of the other possible optimisation parameters, mass has been determined to be the most accurately quantifiable metric for the optimisation of such a system.

8.1.3. RES-Q-3

How can the Barracuda upper-stage propulsion system be integrated and interfaced with the existing Barracuda system?

This research question was aimed at considering the aspect of integrating the propulsion system with the remainder of the Barracuda rocket and which implications this has on the propulsion system design itself.

RES-Q-3A: Which constraints does the existing Barracuda system impose?
The constraints affecting the propulsion system design are primarily related to geometric and physical integration, which dictate how various components fit and function within the Barracuda rocket. The most driving of these has been determined by the available internal diameter, especially for the propellant tanks.

Additionally, operational constraints imposed by the launcher infrastructure and the limited availability of personnel play significant roles. These operational limitations include the capabilities of the launch infrastructure, as well as the number of personnel available to support the operations. As a result, the overall efficiency and effectiveness of the system are influenced by both the physical design parameters and the practical operational environment. Next to this, the Barracuda rocket also imposes constraints on the system based on its flight performance and trajectory. The exact effect of this should be analysed further in future work.

RES-Q-3B: Can the propulsion system provide the necessary performance?
As can be seen in figure 6.5, the total mass of the propulsion system including propellants has converged to approx. 15 [kg] in the optimisation process. Based on the graphs in appendix E, specifically figures E.5 and E.6 show that for a total payload mass of 40 [kg], the Barracuda rocket is still capable of carrying the upper stage either to an apogee of 120 [km] using a high launch-angle or to an apogee velocity around Mach 3 for shallow launch angles. The two primary envisioned applications for this upper stage are hovering flight at altitude [6], [8] and sustained hypersonic testing [6], [62]. Using pulsed operations (either fully pulsing the propulsion system, or alternating between bi-propellant and mono-propellant mode), this upper stage could hover at a given altitude range for at least 60 [s] and possibly up to 90 [s] and more. Meanwhile, this system is capable of providing nearly 1100 [m/s] of delta-V, which means that it can accelerate a payload to hypersonic speeds, depending on the trajectory. Overall, the current design of the system and its performance allow for all of the previously suggested uses for the upper stage [6]. In the future, more detailed analysis should be made towards the possible upper-stage trajectories and how they can be achieved most effectively, and then based on this a performance envelope should be generated.

RES-Q-3C: Can the propulsion system leave sufficient payload mass margin?
The upper stage design provides a substantial margin in payload mass, with the current configuration leaving an additional 25 kg available. This extra capacity can be utilised for other subsystems, such as the electronics or structural subsystems. Even while accommodating these subsystems, there should still be a sufficient margin to support the payload mass. Furthermore, the payload mass can potentially exceed 40 kg if the trajectory requirements are adjusted sufficiently, offering greater flexibility in payload accommodation. However, the total upper stage mass should not exceed 60 [kg] since with the current design thrust, the upper stage is not able to hover a mass larger than 60 [kg].

Towards overarching question
This work has shown that a propulsion system designed to the requirements and constraints from sections 3.1 and 3.2 can be physically integrated into the Barracuda rocket upper stage. In order to determine how well the system can interface with the remainder of the upper stage, the design of the remainder of the upper stage will have to be progressed further. Next to this, further analysis of how the dynamics of the rocket's motion affect the behaviour of the propulsion system (e.g. propellant sloshing) should be performed.

8.1.4. RES-Q-4

How can the Barracuda upper-stage propulsion system be constructed and operated by T-Minus Engineering?

Finally, this last question was primarily aimed at ensuring that the propulsion system design remains within the capabilities of T-Minus Engineering and if not, in which manner T-Minus Engineering should expand its capabilities.

RES-Q-4A: What are the technical limitations of T-Minus Engineering?
The main limitation encountered was the lack of experience with liquid bipropellant systems, which extended to the testing systems and processes necessary for their effective implementation. However, efforts are underway to address these challenges through the HyProp project, aimed at enhancing expertise and capabilities with HTP, its catalysts, and liquid feed systems in general. Additionally, while there are production limitations, the possibility of partial external manufacture offers a viable solution to mitigate these constraints and support the overall development process.

RES-Q-4B: What are the operational limitations of T-Minus Engineering?
The most pressing limitation is the low number of personnel, with the propulsion system alone requiring three individuals according to operational requirements. Additionally, all infrastructure related to launch

operations must be fully mobile, as no permanent hardware installations are permissible. This necessity for mobility adds a layer of complexity to the operations. Furthermore, the launch location's environmental aspects, e.g. low temperatures for potential launches in the Arctic Circle, must be taken into account. Thus efforts should be undertaken to reduce the number of required personnel needed to operate the propulsion system to as low as possible.

RES-Q-4C: How does this technology require T-Minus Engineering to expand its capabilities?
Expanding knowledge and experience in liquid propulsion systems and their related components, such as feed systems and propellant handling, is essential, especially considering the little previous experience with this type of system within T-Minus Engineering. Alongside this, it is important to consider upgrading manufacturing capabilities based on the final chosen design. This could involve the implementation of advanced techniques like additive manufacturing or the enhancement of existing CNC capabilities to ensure precision and efficiency in production.

Towards Overarching Question
This work has shown that T-Minus Engineering does possess the baseline capabilities to design, construct and operate a propulsion system like the one designed in this work. However, in order to determine which exact capabilities need to be expanded, the design of the propulsion system needs to be advanced to the critical subsystem-level design.

9 Recommendations

This final chapter contains the recommendations of this thesis report. They are based on the conclusion drawn in chapter 8 as well as various recommendations drawn from the conclusion of each chapter.

9.1. Design Improvements

The design of the upper-stage propulsion system still has some elements which require further attention after this work. To advance the design to an operational state, further detailed analysis will need to be made for most subsystems. To name a few examples, the combined flow through the combustion chamber and nozzle should be analysed in greater detail. The current 1D model is sufficient for sizing and trading off the cooling methods, but for the detailed sizing, a more realistic higher dimensional model that accounts for flow property variations in all directions in the chamber should be implemented. Another example is the implementation of fluid sloshing analysis in the tanks and their effect on the dynamics of the rocket's first-stage flight. For most of the subsystems of the propulsion system, some additional design analysis should be performed and all of the design should ultimately be advanced to a component-level critical design, such that the first ground-testing prototype system can be manufactured and tested. Next to this, the other subsystems of the upper stage of the rocket should be designed such that their relationship with the propulsion system can be quantified more thoroughly. It is ultimately also recommended to adjust any of the current design input parameters (i.e. the model input parameters from the optimisation in table 6.4) if further analysis shows that this is beneficial.

9.2. Model Improvements

Apart from the design, some recommendations for the numerical model as well as the optimisation process can be made. The following recommendation can be made to improve the numerical model itself:

- As previously mentioned, a large improvement can be made in the chamber-nozzle transport module. The implementation of a multi-dimensional flow model could allow for a more precise analysis of the combustion process, mixing of the injected propellants, thermal loads on the chamber walls etc.
- Similarly, the cooling module can be improved by using a more modular approach. Currently, the cooling module only represents one of the cooling mechanisms described in section 4.4.7 at a time. Especially when considering heat-sink and radiation cooling, all of the cooling mechanisms are present in some form or another in most designs. This means that e.g. when designing a heat-sink cooling system, there will always be some form of radiation cooling in reality which the model neglects. This could be improved by developing and implementing a more sophisticated thermal model, that can represent multiple heat-transfer mechanisms simultaneously.
- Derived from the previous recommendation, the cooling module can also be improved by accounting for uneven heat transfer throughout the material. Previously this model weakness was mitigated by using more conservative maximum temperatures for each material but accounting for more localised heating and accounting for transient heat transfer effects in general would allow for a more accurate

thermal model.

- Currently, in the numerical model's material database, the maximum allowable temperature of a material is set to the point where the material begins to lose mechanical strength due to heating. In reality, of course, the strength follows a decreasing curve from that point. This means that higher material temperatures might still be mechanically possible depending on the design and the cooling method. Therefore, strength-temperature curves should be added for the materials in appendix A.1.
- There are two supplemental cooling methods that could be implemented into the numerical model. Firstly, a thermal barrier coating (TBC) model could be added. They can reduce the heat flux transmitted into the wall. For a similar effect, a film cooling model could also be added to the cooling module. This would also allow for a reduction in heat transfer to the chamber walls. In section 3.6.1, the latter method was mentioned as a supplemental cooling method to aid the primary cooling method.
- For the regenerative cooling module specifically, varying cooling channel geometries should be considered. These might offer better performance than the currently used simple geometry seen in figure 4.12.
- As described in section 4.4.1, an HTP decomposition model should be created based on the test data from HyProp catalyst bed characterisation tests once these have been performed.
- For future optimisation runs, the model can be accelerated by re-using previous results. As an example, instead of running the CEA algorithm each time, an array of pre-determined results could be interpolated. Especially if the model is run in quick succession, this can significantly accelerate the run time of the model.

Next to this, there are also a few more recommendations for future additional or improved design optimisations:

- Further research should be performed concerning the genetic algorithm parameters. Ideally, an analysis would be performed that quantifies the impact of each parameter on the optimisation process when implemented with this specific numerical model. This also could help to accelerate the run time of the optimisation process in the future.
- At a later design stage, another optimisation run should be performed using a fitness function that involves some form of cost estimation. For this however, the design space should be a lot more constrained such that the cost can be quantified more accurately for just a few select design options rather than the entire model.

9.3. Future Activities

Finally, based on the work of the project, the following future activities for the development of the upper stage are suggested:

- The design of the remaining upper stage for the Barracuda rocket should be advanced to a more detailed level. Not only would this advance the entire upper-stage design but it would also support the next development stages of the propulsion systems. When designing the individual components of the propulsion system, some input parameters based on the other subsystems might be required.
- As part of the previous recommendation, the structural systems which mount the propulsion system to the remaining upper stage should be designed. This was not possible as part of this work since it largely also depends on the design of the remaining upper stage. During this phase, the structural loading of the upper stage based on the rocket's flight dynamics should be determined.
- An in-depth analysis of the operational constraints should be performed to improve this set of constraints which will ultimately drive how the preparations and operational procedure of the propulsion system will be designed.
- Depending on a change in mission profile, some of the constrained parameters in table 4.2 such as thrust or burn time should be adjusted. In this case, the entire optimisation process needs to be repeated but in principle, the numerical model and optimisation algorithm allow for this.
- If possible, it might be worthwhile to investigate various other catalyst bed designs. For this, the catalyst test bed system of the HyProp project could be used. Depending on material costs,

performance, mass etc., a different catalyst might offer a better solution than the current selection. This however can only be determined with more characterisation tests.

- Any form of results from the various tests described in chapter 2 as part of the HyProp project will be useful for the validation of the numerical model. Next to this, the later stages of the project can and should be used as a test bed for this propulsion system. Finally, the project can also be used to gain experience in the design, construction and operation of liquid mono- and bi-propellant rocket engines.
- A ground-testing version of the propulsion system should be constructed. This system should be constructed using easily replaceable components, which allow for more design iteration during testing as well as reducing the impact of potential test anomalies. This system can also be used to validate operational concepts, and the ground testing system can be upgraded subsystem-by-subsystem to the flight system for the upper stage, which can then be validated.
- With this ground testing setup, various operational concepts for the propulsion system should be tested. This includes but is not limited to:
  - Throttling
  - Re-lighting
  - Switching between mono- and bi-propellant mode
  - Cooling Concepts
- Finally, it is recommended that at least the ground testing system is in-house manufactured to the largest extent possible such that components can be quickly iterated during testing and dependency on external factors during this phase is reduced.

These recommendations are aimed at guiding the overall development of the upper stage further beyond its current state. While the propulsion system is certainly one of the more key systems on the upper stage, only the advance of the remaining will allow the propulsion system design to advance into a state that can be produced and tested, and hence advancing this design should have a high priority.

References

[1] A. Stamminger, J. Ettl, G. Blochberger, *et al.*, "Mapheus-the maiden flight of a new vehicle for microgravity experiments," *IAC Proceedings 2009*, 2009.

[2] G. Seibert and B. T. Battrick, *The history of sounding rockets and their contribution to European space research*. ESA Publications division Noordwijk, 2006.

[3] J. S. Lingard, A. Saunders, J. C. Underwood, S. Rogers, J. Merrifield, and L. Ferracina, "Supersonic parachute testing using a maxus sounding rocket piggy-back payload," in *24th AIAA Aerodynamic Decelerator Systems Technology Conference*, 2017, p. 3724.

[4] K. Goto, K. Matsuoka, K. Matsuyama, *et al.*, "Flight demonstration of detonation engine system using sounding rocket s-520-31: Performance of rotating detonation engine," in *AIAA Scitech 2022 Forum*, 2022, p. 0232.

[5] O. Persson and M. Hörschgen, "Rexus 2-the first eurolaunch project," 2005.

[6] W. Jodehl, "Upper stage propulsion system for the t-minus barracuda - literature study," 2023.

[7] M. J. Palmer, "Experimental evaluation of hydrogen peroxide catalysts for monopropellant attitude control thrusters," Ph.D. dissertation, University of Southampton, 2014.

[8] K. Naumann, C. Kirchberger, O. Drescher, *et al.*, "Design of a hovering sounding rocket stage for measurements in the high atmosphere," 2020.

[9] D. Hargarten, J. Ettl, and K. Naumann, "Trajectory and control systems design for a hovering mesopause probe," 2018.

[10] W. Kopacz, A. Okninski, A. Kasztankiewicz, P. Nowakowski, G. Rarata, and P. Maksimowski, "Hydrogen peroxide – a promising oxidizer for rocket propulsion and its application in solid rocket propellants," *FirePhysChem*, vol. 2, no. 1, pp. 56–66, 2022, Progress in Solid Rocket Propulsion - Part A, ISSN: 2667-1344. DOI: https://doi.org/10.1016/j.fpc.2022.03.009. [Online]. Available: https://www.sciencedirect.com/science/article/pii/S2667134422000141.

[11] S. Cassese, G. Gallo, S. Mungiguerra, A. Cecere, and R. Savino, "Preliminary design and study of 5n htp monopropellant thruster for small satellites," *Acta Astronautica*, vol. 202, pp. 94–103, 2023.

[12] M. Santi, M. Fagherazzi, F. Barato, and D. Pavarin, "Design and testing of a hydrogen peroxide bipropellant thruster," in *AIAA Propulsion and Energy 2020 Forum*, 2020, p. 3827.

[13] P. Surmacz, K. Sobczak, B. Bartkowiak, *et al.*, "Development status of 500 n-class htp/tmpda bi-propellant rocket engine," in *Proceedings of the 69th International Astronautical Congress, Bremen, Germany*, 2018, pp. 1–5.

[14] S. Jo, S. An, J. Kim, H. Yoon, and S. Kwon, "Performance characteristics of hydrogen peroxide/kerosene staged-bipropellant engine with axial fuel injector," *Journal of Propulsion and Power*, vol. 27, no. 3, pp. 684–691, 2011.

[15] S. Zakel, E. Brandes, and V. Schröder, "Reliable safety characteristics of flammable gases and liquids–the database chemsafe," *Journal of Loss Prevention in the Process Industries*, vol. 62, p. 103 914, 2019.

[16] C. Taylor, *Rocketcea*, 2015. [Online]. Available: https://rocketcea.readthedocs.io/en/latest/.

[17] S. Jung, S. Choi, S. Heo, and S. Kwon, "Scaling of catalyst bed for hydrogen peroxide monopropellant thrusters using catalytic decomposition modeling," *Acta Astronautica*, vol. 187, pp. 167–180, 2021.

[18] B. Zandbergen, *Thermal Rocket Propulsion*, Version 2.08. Aug. 2020.

[19] M. Dobrovolsky, *Liquid fuel rocket enginesdesign fundamentals*, 1969.

[20] P. R. Gradl, S. E. Greene, C. Protz, *et al.*, "Additive manufacturing of liquid rocket engine combustion devices: A summary of process developments and hot-fire testing results," in *2018 Joint propulsion conference*, 2018, p. 4625.

[21] C. L. Resch, "Ablation models of thermal protection materials," *Johns Hopkins APL Technical Digest*, vol. 13, pp. 426–426, 1992.

[22] S. Shine and S. S. Nidhi, "Review on film cooling of liquid rocket engines," *Propulsion and Power Research*, vol. 7, no. 1, pp. 1–18, 2018.

[23] T. J. Fritz, W. Huebsch, and J. Wilhelm, "Analysis of 3d printed titanium rocket nozzle," in *58th AIAA/ASCE/AHS/ASC Structures, Structural Dynamics, and Materials Conference*, 2017, p. 0510.

[24] D. K. Huzel and D. H. Huang, *Modern engineering for design of liquid-propellant rocket engines*. AiAA, 1992, vol. 147.

[25] N. Othman, S. Krishnan, W. K. W. Ali, and M. N. M. Jaafar, "Design and testing of a 50n hydrogen peroxide monopropellant rocket thruster," *Jurnal Mekanikal*, 2011.

[26] A. H. Lefebvre and V. G. McDonell, *Atomization and sprays*. CRC press, 2017.

[27] H. Quintens, B. Boust, M. Bellenoue, R. Beauchet, and Y. Batonneau, "Experimental comparison of hydrogen peroxide catalysts for a hydrogen peroxide/n-decane bipropellant combustor," *Journal of Propulsion and Power*, vol. 38, no. 5, pp. 690–700, 2022.

[28] *Bipropellant tanks for satellites and spacecraft*. [Online]. Available: `https://www.space-propulsion.com/spacecraft-propulsion/bipropellant-tanks/index.html`.

[29] G. P. Sutton and O. Biblarz, *Rocket propulsion elements*. John Wiley & Sons, 2011.

[30] P. Linstrom and W. Mallard, "The nist chemistry webbook: A chemical data resource on the internet," en, no. 46, 2001.

[31] S. Gordon and B. J. McBride, *Computer program for calculation of complex chemical equilibrium compositions and applications. Part 1: Analysis*. NASA Lewis Research Center, 1994, vol. 1.

[32] S. Gordon and B. J. McBride, *Computer program for calculation of complex chemical equilibrium compositions and applications. Part 2: Users Manual and Program Description*. NASA Lewis Research Center, 1996, vol. 2.

[33] D. G. Goodwin, H. K. Moffat, I. Schoegl, R. L. Speth, and B. W. Weber, *Cantera: An object-oriented software toolkit for chemical kinetics, thermodynamics, and transport processes*, `https://www.cantera.org`, Version 3.0.0, 2023. DOI: `10.5281/zenodo.8137090`.

[34] G. P. Smith, D. M. Golden, M. Frenklach, *et al.* [Online]. Available: `%5Curl%7Bhttp://www.me.berkeley.edu/gri_mech/%7D`.

[35] P. Nair, A. Suryan, and H. Kim, "Computational study on flow through truncated conical plug nozzle with base bleed," *Propulsion and Power Research*, vol. 8, Mar. 2019. DOI: `10.1016/j.jppr.2019.02.001`.

[36] B. Dietrich, W. Schabel, M. Kind, and H. Martin, "Pressure drop measurements of ceramic sponges—determining the hydraulic diameter," *Chemical Engineering Science*, vol. 64, no. 16, pp. 3633–3640, 2009.

[37] S. S. Gill, *The Stress Analysis of Pressure Vessels and Pressure Vessel Components: International Series of Monographs in Mechanical Engineering*. Elsevier, 2016, vol. 3.

[38] A. Calvi, "Spacecraft loads analysis," *ESA/ESTEC, Noordwijk, The Netherlands November*, vol. 21, p. 126, 2011.

[39] G. Rao, "Recent developments in rocket nozzle configurations," *ARS journal*, vol. 31, no. 11, pp. 1488–1494, 1961.

[40] D. Bartz, "Turbulent boundary-layer heat transfer from rapidly accelerating flow of rocket combustion gases and of heated air," in *Advances in Heat Transfer*, vol. 2, Elsevier, 1965, pp. 1–108.

[41] H. Pina and J. Fernandes, "Applications in transient heat conduction," *Basic Principles and Applications*, pp. 41–58, 1984.

[42] C. U. Kirchberger, "Investigation on heat transfer in small hydrocarbon rocket combustion chambers," Ph.D. dissertation, Technische Universität München, 2014.

[43] L. Denies, "Regenerative cooling analysis of oxygen/methane rocket engines," M.S. thesis, Delft University of Technology, 2015.

[44] International Symposium on Liquid Rocket Propulsion (2nd : 1995 : Châtillon-sur-Chalaronne, France), *Liquid rocket thrust chambers* (Progress in Astronautics & Aeronautics), en, Vigor Yang, M. Habiballah, M. Popp, and J. Hulka, Eds. Reston, VA: American Institute of Aeronautics & Astronautics, Oct. 2004.

[45] Y. Mishra, "Droplet size, concentration, and temperature mapping in sprays using slipi-based techniques," Ph.D. dissertation, Jan. 2018.

[46] J. M. Powers, *Mechanics of Fluids*. Cambridge University Press, 2023.

[47] C. F. Colebrook and C. M. White, "Experiments with fluid friction in roughened pipes," *Proceedings of the Royal Society of London. Series A-Mathematical and Physical Sciences*, vol. 161, no. 906, pp. 367–381, 1937.

[48] M. Rowe, "Measurements and computations of flow in pipe bends," *Journal of Fluid Mechanics*, vol. 43, no. 4, pp. 771–783, 1970.

[49] Babcock and W. Company, *Steam: its generation and use*. Kessinger Publishing, 2005.

[50] G. E. Maddux, L. A. Vorst, F. J. Giessler, and T. Moritz, "Stress analysis manual," *Dayton: Technology Incorporated*, 1969.

[51] A. Ponomarenko. [Online]. Available: `https://www.rocket-propulsion.com/index.htm`.

[52] P. Virtanen, R. Gommers, T. E. Oliphant, *et al.*, "SciPy 1.0: Fundamental Algorithms for Scientific Computing in Python," *Nature Methods*, vol. 17, pp. 261–272, 2020. DOI: `10.1038/s41592-019-0686-2`.

[53] C. Zhou, N. Yu, S. Wang, *et al.*, "The influence of thrust chamber structure parameters on regenerative cooling effect with hydrogen peroxide as coolant in liquid rocket engines," *Aerospace*, vol. 10, no. 1, p. 65, 2023.

[54] W. Bashore, T. Lippman, M. Moberg, S. Reiter, W. Stillman, and D. Myre, "Design considerations for a student designed liquid bipropellant rocket motor," in *47th AIAA/ASME/SAE/ASEE Joint Propulsion Conference & Exhibit*, 2011, p. 5937.

[55] J. R. Martins and A. Ning, *Engineering design optimization*. Cambridge University Press, 2021.

[56] "Geneticalgorithm - an easy implementation of genetic-algorithm (ga) to solve continuous and combinatorial optimization problems with real, integer, and mixed variables in python." (), [Online]. Available: `https://github.com/rmsolgi/geneticalgorithm` (visited on 06/07/2024).

[57] S. Guo, M. Xiao, F. Xie, *et al.*, "Optimization of helium consumption for feedback pressurization in liquid oxygen tanks," *International Journal of Heat and Mass Transfer*, vol. 230, p. 125 739, 2024.

[58] A. Teissier and C. Bass, "Liquid helium storage for ariane 5 main stage oxygen tank pressurization," in *31st Joint Propulsion Conference and Exhibit*, 1995, p. 2956.

[59] T. Badawy, M. A. Attar, P. Hutchins, H. Xu, J. K. Venus, and R. Cracknell, "Investigation of injector coking effects on spray characteristic and engine performance in gasoline direct injection engines," *Applied energy*, vol. 220, pp. 375–394, 2018.

[60] J. Benton, I. Ballinger, D. Jaekle, and M. Olson, "Design and manufacture of a propellant tank assembly," in *43rd AIAA/ASME/SAE/ASEE Joint Propulsion Conference & Exhibit*, 2007, p. 5559.

[61] A. Bansal, "Determining the activation energy of the decomposition of aqueous hydrogen peroxide in the presence of catalase by manipulating the temperature of the decomposition reaction and measuring the time taken for 40.0 ml of oxygen gas to be evolved," Feb. 2018. DOI: `10.13140/RG.2.2.20165.60646`.

[62] H. Weihs, "Sounding rockets for entry research: Shefex flight test program," in *Proceedings of the 21st ESA Symposium on Rocket and Balloon Programmes*, ESA Communications, 2013, pp. 143–152.

[63] *Hydrogen peroxide material compatibility chart*, `https://www.industrialspec.com/images/files/hydrogen-peroxide-materialcompatibility-chart-from-ism.pdf`, [Accessed 01-07-2024], 2020.

[64] H. Olthof and L. Pepermans, "Low-cost hypersonic flight testing using the t-minus rocket motors," 2022.

A

Material Property Database

This appendix contains the representation of all materials used in the model as well as their sources.

A.1. Metals

Table A.1: EN-AW 1060-H12

Property	Value	Unit
Density	2700	$\left[\frac{kg}{m^3}\right]$
Young's Modulus	68	$[GPa]$
Yield Strength	61	$[MPa]$
Ultimate Strength	85	$[MPa]$
Thermal Conductivity	230	$\left[\frac{W}{m \cdot K}\right]$
Specific Heat Capacity	900	$\left[\frac{J}{kg \cdot K}\right]$
Max. Temp	443	$[°C]$
Cost per kg	3.0	$\left[\frac{US\$}{kg}\right]$

Table A.2: EN-AW 5253-H12

Property	Value	Unit
Density	2700	$\left[\frac{kg}{m^3}\right]$
Young's Modulus	68	$[GPa]$
Yield Strength	200	$[MPa]$
Ultimate Strength	270	$[MPa]$
Thermal Conductivity	130	$\left[\frac{W}{m \cdot K}\right]$
Specific Heat Capacity	900	$\left[\frac{J}{kg \cdot K}\right]$
Max. Temp	463	$[°C]$
Cost per kg	3.0	$\left[\frac{US\$}{kg}\right]$

Table A.3: EN-AW 6082-T6

Property	Value	Unit
Density	2700	$\left[\frac{kg}{m^3}\right]$
Young's Modulus	69	$[GPa]$
Yield Strength	250	$[MPa]$
Ultimate Strength	290	$[MPa]$
Thermal Conductivity	160	$\left[\frac{W}{m \cdot K}\right]$
Specific Heat Capacity	900	$\left[\frac{J}{kg \cdot K}\right]$
Max. Temp	443	$[°C]$
Cost per kg	3.0	$\left[\frac{US\$}{kg}\right]$

Table A.4: EN-AW 7075-T6

Property	Value	Unit
Density	3000	$\left[\frac{kg}{m^3}\right]$
Young's Modulus	70	$[GPa]$
Yield Strength	480	$[MPa]$
Ultimate Strength	560	$[MPa]$
Thermal Conductivity	130	$\left[\frac{W}{m \cdot K}\right]$
Specific Heat Capacity	870	$\left[\frac{J}{kg \cdot K}\right]$
Max. Temp	473	$[°C]$
Cost per kg	5.0	$\left[\frac{US\$}{kg}\right]$

Table A.5: Inconel 600

Property	Value	Unit
Density	8470	$\left[\frac{kg}{m^3}\right]$
Young's Modulus	80	$[GPa]$
Yield Strength	310	$[MPa]$
Ultimate Strength	655	$[MPa]$
Thermal Conductivity	14	$\left[\frac{W}{m \cdot K}\right]$
Specific Heat Capacity	444	$\left[\frac{J}{kg \cdot K}\right]$
Max. Temp	1073	$[°C]$
Cost per kg	45.0	$\left[\frac{US\$}{kg}\right]$

Table A.6: Inconel 617

Property	Value	Unit
Density	8360	$\left[\frac{kg}{m^3}\right]$
Young's Modulus	81	$[GPa]$
Yield Strength	383	$[MPa]$
Ultimate Strength	758	$[MPa]$
Thermal Conductivity	13	$\left[\frac{W}{m \cdot K}\right]$
Specific Heat Capacity	419	$\left[\frac{J}{kg \cdot K}\right]$
Max. Temp	1123	$[°C]$
Cost per kg	52.0	$\left[\frac{US\$}{kg}\right]$

Table A.7: Inconel 625

Property	Value	Unit
Density	8440	$\left[\frac{kg}{m^3}\right]$
Young's Modulus	207	$[GPa]$
Yield Strength	460	$[MPa]$
Ultimate Strength	880	$[MPa]$
Thermal Conductivity	9	$\left[\frac{W}{m \cdot K}\right]$
Specific Heat Capacity	410	$\left[\frac{J}{kg \cdot K}\right]$
Max. Temp	1073	$[°C]$
Cost per kg	52.0	$\left[\frac{US\$}{kg}\right]$

Table A.8: Inconel 690

Property	Value	Unit
Density	8190	$\left[\frac{kg}{m^3}\right]$
Young's Modulus	211	$[GPa]$
Yield Strength	461	$[MPa]$
Ultimate Strength	758	$[MPa]$
Thermal Conductivity	13	$\left[\frac{W}{m \cdot K}\right]$
Specific Heat Capacity	450	$\left[\frac{J}{kg \cdot K}\right]$
Max. Temp	973	$[°C]$
Cost per kg	52.0	$\left[\frac{US\$}{kg}\right]$

Table A.9: Inconel 718

Property	Value	Unit
Density	8190	$\left[\frac{kg}{m^3}\right]$
Young's Modulus	211	$[GPa]$
Yield Strength	1100	$[MPa]$
Ultimate Strength	1375	$[MPa]$
Thermal Conductivity	11	$\left[\frac{W}{m \cdot K}\right]$
Specific Heat Capacity	435	$\left[\frac{J}{kg \cdot K}\right]$
Max. Temp	1253	$[°C]$
Cost per kg	54.0	$\left[\frac{US\$}{kg}\right]$

Table A.10: Inconel X750

Property	Value	Unit
Density	8280	$\left[\frac{kg}{m^3}\right]$
Young's Modulus	211	$[GPa]$
Yield Strength	850	$[MPa]$
Ultimate Strength	1250	$[MPa]$
Thermal Conductivity	12	$\left[\frac{W}{m \cdot K}\right]$
Specific Heat Capacity	431	$\left[\frac{J}{kg \cdot K}\right]$
Max. Temp	1253	$[°C]$
Cost per kg	101.0	$\left[\frac{US\$}{kg}\right]$

Table A.11: AISI 304L

Property	Value	Unit
Density	8000	$\left[\frac{kg}{m^3}\right]$
Young's Modulus	193	$[GPa]$
Yield Strength	215	$[MPa]$
Ultimate Strength	505	$[MPa]$
Thermal Conductivity	16	$\left[\frac{W}{m \cdot K}\right]$
Specific Heat Capacity	500	$\left[\frac{J}{kg \cdot K}\right]$
Max. Temp	773	$[°C]$
Cost per kg	3.7	$\left[\frac{US\$}{kg}\right]$

Table A.12: AISI 316L

Property	Value	Unit
Density	8000	$\left[\frac{kg}{m^3}\right]$
Young's Modulus	193	$[GPa]$
Yield Strength	205	$[MPa]$
Ultimate Strength	515	$[MPa]$
Thermal Conductivity	14	$\left[\frac{W}{m \cdot K}\right]$
Specific Heat Capacity	500	$\left[\frac{J}{kg \cdot K}\right]$
Max. Temp	773	$[°C]$
Cost per kg	5.8	$\left[\frac{US\$}{kg}\right]$

Table A.13: TZM

Property	Value	Unit
Density	10160	$\left[\frac{kg}{m^3}\right]$
Young's Modulus	325	$[GPa]$
Yield Strength	400	$[MPa]$
Ultimate Strength	500	$[MPa]$
Thermal Conductivity	118	$\left[\frac{W}{m \cdot K}\right]$
Specific Heat Capacity	250	$\left[\frac{J}{kg \cdot K}\right]$
Max. Temp	1673	$[°C]$
Cost per kg	100	$\left[\frac{US\$}{kg}\right]$

Table A.14: Ti-6Al-4V

Property	Value	Unit
Density	4400	$\left[\frac{kg}{m^3}\right]$
Young's Modulus	110	$[GPa]$
Yield Strength	910	$[MPa]$
Ultimate Strength	1000	$[MPa]$
Thermal Conductivity	6	$\left[\frac{W}{m \cdot K}\right]$
Specific Heat Capacity	560	$\left[\frac{J}{kg \cdot K}\right]$
Max. Temp	603	$[°C]$
Cost per kg	21	$\left[\frac{US\$}{kg}\right]$

A.2. Fluids

Table A.15: Ethanol

Property	Value	Unit
Density	785	$\left[\frac{kg}{m^3}\right]$
Specific Heat Capacity	2460	$\left[\frac{J}{kg \cdot K}\right]$
Thermal Conductivity	0.17	$\left[\frac{W}{m \cdot K}\right]$
AIT	636	$[K]$
Dynamic Viscosity	1.075	$[mPa \cdot s]$
Surface Tension	0.022	$\left[\frac{N}{m}\right]$
Cost per kg	5.1	$\left[\frac{US\$}{kg}\right]$
CAS Number	64-17-5	$[-]$

Table A.16: Gasoline

Property	Value	Unit
Density	725	$\left[\frac{kg}{m^3}\right]$
Specific Heat Capacity	1800	$\left[\frac{J}{kg \cdot K}\right]$
Thermal Conductivity	0.15	$\left[\frac{W}{m \cdot K}\right]$
AIT	553	$[K]$
Dynamic Viscosity	0.51	$[mPa \cdot s]$
Surface Tension	0.021	$\left[\frac{N}{m}\right]$
Cost per kg	2.9	$\left[\frac{US\$}{kg}\right]$
CAS Number	540-84-1	$[-]$

Table A.17: H2O2

Property	Value	Unit
Density	1450	$\left[\frac{kg}{m^3}\right]$
Specific Heat Capacity	2619	$\left[\frac{J}{kg \cdot K}\right]$
Thermal Conductivity	0.586	$\left[\frac{W}{m \cdot K}\right]$
AIT	0	$[K]$
Dynamic Viscosity	5.5784	$[mPa \cdot s]$
Surface Tension	0.0804	$\left[\frac{N}{m}\right]$
Cost per kg	0.0	$\left[\frac{US\$}{kg}\right]$
CAS Number	7722-84-1	$[-]$

Table A.18: JetA

Property	Value	Unit
Density	775	$\left[\frac{kg}{m^3}\right]$
Specific Heat Capacity	1800	$\left[\frac{J}{kg \cdot K}\right]$
Thermal Conductivity	0.1268	$\left[\frac{W}{m \cdot K}\right]$
AIT	483	$[K]$
Dynamic Viscosity	1.3562	$[mPa \cdot s]$
Surface Tension	0.023	$\left[\frac{N}{m}\right]$
Cost per kg	1.6	$\left[\frac{US\$}{kg}\right]$
CAS Number	91-20-3	$[-]$

Table A.19: Kerosene

Property	Value	Unit
Density	820	$\left[\frac{kg}{m^3}\right]$
Specific Heat Capacity	2010	$\left[\frac{J}{kg \cdot K}\right]$
Thermal Conductivity	0.145	$\left[\frac{W}{m \cdot K}\right]$
AIT	493	$[K]$
Dynamic Viscosity	1.64	$[mPa \cdot s]$
Surface Tension	0.028	$\left[\frac{N}{m}\right]$
Cost per kg	3.0	$\left[\frac{US\$}{kg}\right]$
CAS Number	91-20-3	$[-]$

Table A.20: Methanol

Property	Value	Unit
Density	785	$\left[\frac{kg}{m^3}\right]$
Specific Heat Capacity	2530	$\left[\frac{J}{kg \cdot K}\right]$
Thermal Conductivity	0.196	$\left[\frac{W}{m \cdot K}\right]$
AIT	737	$[K]$
Dynamic Viscosity	0.543	$[mPa \cdot s]$
Surface Tension	0.022	$\left[\frac{N}{m}\right]$
Cost per kg	14.5	$\left[\frac{US\$}{kg}\right]$
CAS Number	67-56-1	$[-]$

A.3. Pressurants

Table A.21: Nitrogen

Property	Value	Unit
Molecular Mass	28.0134	$\left[\frac{g}{mol}\right]$
Specific Heat Ratio	1.4	$[-]$
Gas Constant	296.798	$\left[\frac{J}{mol \cdot K}\right]$
Cost per kg	5.97	$\left[\frac{US\$}{kg}\right]$

Table A.22: Helium

Property	Value	Unit
Molecular Mass	8.0052	$\left[\frac{g}{mol}\right]$
Specific Heat Ratio	1.667	$[-]$
Gas Constant	1038.6144	$\left[\frac{J}{mol \cdot K}\right]$
Cost per kg	504.7	$\left[\frac{US\$}{kg}\right]$

Table A.23: Carbon Dioxide

Property	Value	Unit
Molecular Mass	44.0095	$\left[\frac{g}{mol}\right]$
Specific Heat Ratio	1.28	$[-]$
Gas Constant	188.921	$\left[\frac{J}{mol \cdot K}\right]$
Cost per kg	8.0	$\left[\frac{US\$}{kg}\right]$

Table A.24: Argon

Property	Value	Unit
Molecular Mass	39.948	$\left[\frac{g}{mol}\right]$
Specific Heat Ratio	1.667	$[-]$
Gas Constant	208.1286	$\left[\frac{J}{mol \cdot K}\right]$
Cost per kg	11.27	$\left[\frac{US\$}{kg}\right]$

B

Feed System Symbology

This appendix contains an overview of the feed system symbology used in figure 3.12.

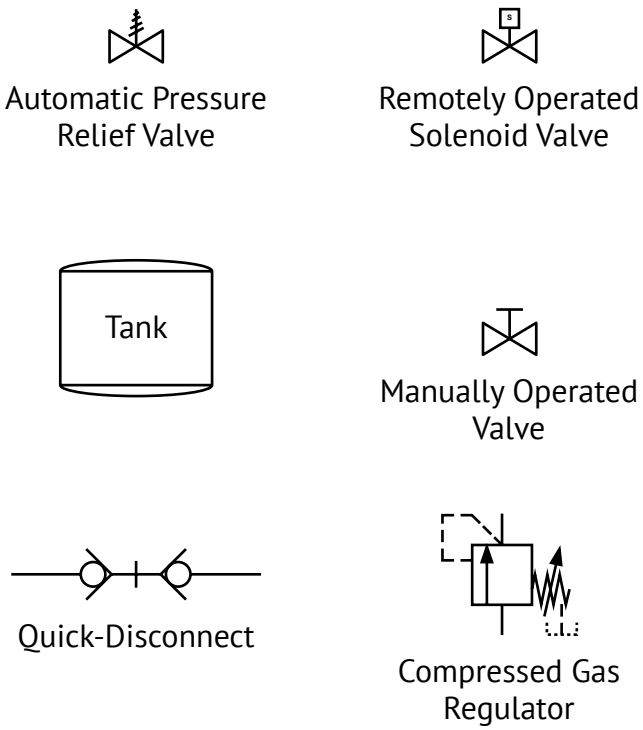

Figure B.1: Feed System Symbols from Diagram in figure 3.12

C

HTP Material Compatibility

This appendix contains a HTP material compatibility chart adapted from [63].

Table C.1: Hydrogen Peroxide Material Compatibility

Material	Compatibility			
	10% H_2O_2	30% H_2O_2	50% H_2O_2	100% H_2O_2
Legend: • **A:** Suitable. • **B:** Good, minor effect, slight corrosion or discoloration. • **F:** Fair, moderate effect, not recommended for continuous use. Softening, loss of strength, and/or swelling may occur. • **X:** Do Not Use - severe effect, not recommended for ANY use • **NA:** Information Not Available • **1:** Satisfactory to 120° F (48° C) • **2:** Satisfactory for O-rings, diaphragms or gaskets				
304 stainless steel	B[1]	B[1]	B[1]	B[1]
316 stainless steel	B	B	A[1]	A[1]
416 stainless steel	B	B	F	X
440C stainless steel	B	B	A	X
ABS plastic	A	A	A	A
Acetal (Delrin®)	X	X	X	X
Acrylic (PMMA)	B	F	NA	X
Alloy 20 (Carpenter 20)	F	B	B	X
Aluminum	A	A	A	A
Brass	X	X	X	X
Bronze	B	B	B	B
Buna N (Nitrile)	X	X	X	X

Continued on next page

Hydrogen Peroxide Material Compatibility – continued from previous page

Material	Compatibility			
	10% H_2O_2	30% H_2O_2	50% H_2O_2	100% H_2O_2

Legend:

- **A:** Suitable.
- **B:** Good, minor effect, slight corrosion or discoloration.
- **F:** Fair, moderate effect, not recommended for continuous use. Softening, loss of strength, and/or swelling may occur.
- **X:** Do Not Use - severe effect, not recommended for ANY use
- **NA:** Information Not Available

- **1:** Satisfactory to 120° F (48° C)
- **2:** Satisfactory for O-rings, diaphragms or gaskets

Carbon graphite	F	F	F	F
Carbon steel	X	X	X	X
Cast iron	F	X	X	X
Ceramic Al2O3	A	A	A	A
Ceramic magnet	A	A	A	A
Copper	X	X	X	X
CPVC	A	A	A	A
EPDM	A	B	B	X
Epoxy (epoxide polymers)	F	B	B	X
FKM (fluoroelastomers, Viton®)	A	A	A	A
Hastelloy-C®	A	A	A	A
HDPE	A	A	A	X
Hypalon®	X	X	X	X
Hytrel® (polyester elastomer)	X	X	X	X
LDPE	A	F[1]	F[1]	F[1]
Natural rubber	B	F	F	F
Neoprene	X	X	X	X
NORYL®	A[1]	A[1]	A	A
Nylon (polyamides)	F	X	X	X
PCTFE (Kel-F® and Neoflon®)	A[1]	A[1]	A [1]	X
PFA (perfluoroalkoxy alkanes)	A	A	A	A
Polycarbonate	A[1]	A[1]	A[1]	A
Polypropylene	A	B	B	B
PP-363 (plasticized vinyl)2	A	A	A	X
PPS (Ryton®)	A	A	F	F

Continued on next page

Hydrogen Peroxide Material Compatibility – continued from previous page

Material	Compatibility			
	10% H_2O_2	30% H_2O_2	50% H_2O_2	100% H_2O_2
Legend: • **A:** Suitable. • **B:** Good, minor effect, slight corrosion or discoloration. • **F:** Fair, moderate effect, not recommended for continuous use. Softening, loss of strength, and/or swelling may occur. • **X:** Do Not Use - severe effect, not recommended for ANY use • **NA:** Information Not Available • **1:** Satisfactory to 120° F (48° C) • **2:** Satisfactory for O-rings, diaphragms or gaskets				
PTFE (Garlock Glyon® 3500)2	A	A	A	X
PTFE (Teflon®), virgin2	A	A	A	A
PVC	A	A	A	A
PVDF (Hylar®)	A[1]	A[1]	X	X
PVDF (Kynar®)	A	A	A	A
PVDF (Solef®)	A[1]	A[1]	X	X
Silicone	A	B	B	B
SPR (styrene butadiene rubber)	X	X	X	X
Thiokol™ (polysulfide polymers)	X	X	X	X
Titanium3	A	B	B	B
TPE (thermoplastic elastomers)	X	X	X	X
TPU (thermoplastic polyurethanes)	X	X	X	X
Tygon®	B	B	B	B
Tungsten carbide	X	X	X	X
Viton®	A[2]	A	A	A

D

Optimised Design Model Output

```
----------------------Combustion--------------------
Specific Impulse:         308.3 [s]
C*:                       1573.2 [m/s]
O/F Ratio:                8.5 [-]
Specific Heat Ratio:      1.13 [-]
Chamber Temperature:      2595.6 [K]
Chamber Density:          1.221 [kg/m3]
Critical Throat Diameter: 17.49 [mm]


----------------------Chamber-----------------------
Length:                   96.9 [mm]
Diameter:                 52.1 [mm]
Characteristic Length:    0.86 [m]
Velocity:                 71.3 [m/s]
Mach:                     0.07 [-]
Contraction Ratio:        8.86 [-]
Sonic (TRP):              1059.7 [m/s]
Sonic (CEA):              1059.7 [m/s]


----------------------Catalyst----------------------
Length:                   77.6 [mm]
Diameter:                 38.8 [mm]
Pressure Drop:            2.219 [bar]


----------------------Fuel Injector-----------------
Atomsiation:              Good
Element Number:           9.0 [-]
Element Diameter:         0.4 [mm]


----------------------HTP Injector------------------
Atomsiation:              Good
Element Number:           1.0 [-]
Element Diameter:         2.7 [mm]
```

```
----------------------Nozzle-------------------------
Area Expansion:           33.3 [-]
Throat Diameter:          17.51 [mm]
Exit Diameter:            100.99 [mm]

Nozzle Contour

Initial Parabola Angle:   40.5 [deg]
Final Parabola Angle:     15.48 [deg]
Quadratic Parameter (x^2): 0.0297841936392105 [1/mm]
Linear Parameter (x):     0.6018342879750087 [-]
Constant Parameter (1):   -6.297021522267132 [mm]


----------------------Tanks--------------------------
Propellant Mass:          11.908 [kg]
Propellant Mass Flow:     0.198 [kg/s]
Fuel Mass:                1.254 [kg]
Fuel Mass Flow:           0.021 [kg/s]
Oxidizer Mass:            10.655 [kg]
Oxidizer Mass Flow:       0.178 [kg/s]
Pressurant Mass:          0.076 [kg]

Fuel Tank
Tank Type:                Extended Sphere
Tank Pressure:            19.11 [bar]
Tank Diameter:            139.9 [mm]
Tank Length:              171.2 [mm]
Tank Wall Thickness:      0.33 [mm]
Tank Mass:                0.11 [kg]

Oxidizer Tank
Tank Type:                Extended Sphere
Tank Pressure:            21.07 [bar]
Tank Diameter:            139.9 [mm]
Tank Length:              577.6 [mm]
Tank Wall Thickness:      0.37 [mm]
Tank Mass:                0.41 [kg]

Pressurant Tank
Tank Type:                Spherical
Tank Pressure:            261.45 [bar]
Tank Diameter:            126.3 [mm]
Tank Length:              126.3 [mm]
Tank Wall Thickness:      4.0 [mm]
Tank Mass:                0.828 [kg]
```

E

Performance of the T-Minus Barracuda

This appendix provides a more detailed overview of the performance of the Barracuda under various payload masses and launch angles [64].

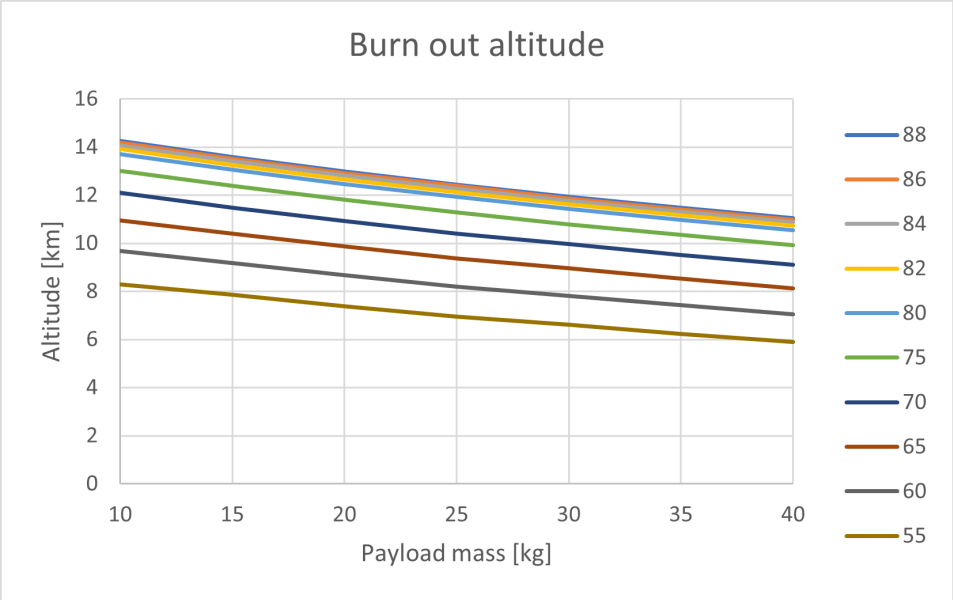

Figure E.1: Burn out altitude

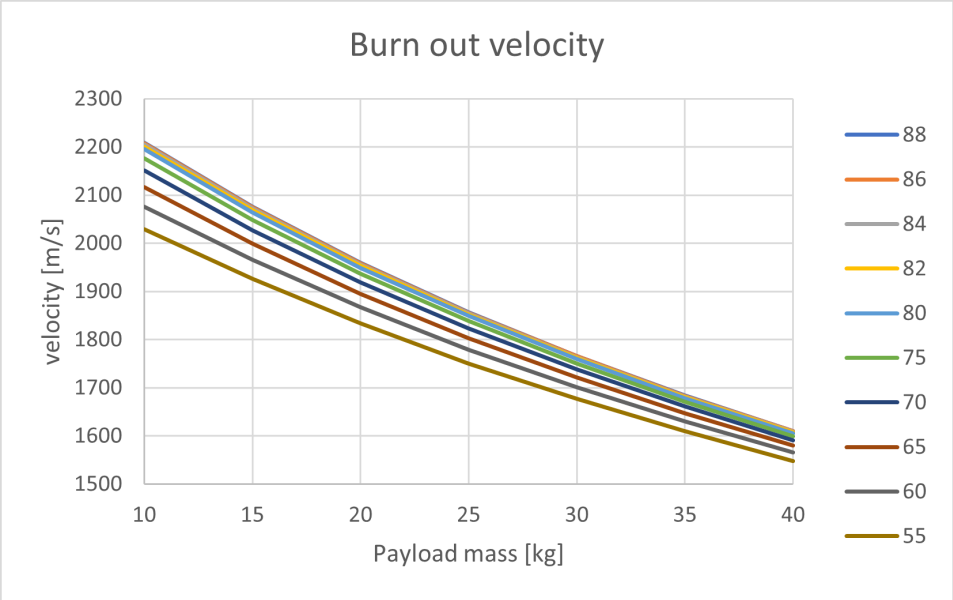

Figure E.2: Burn out velocity

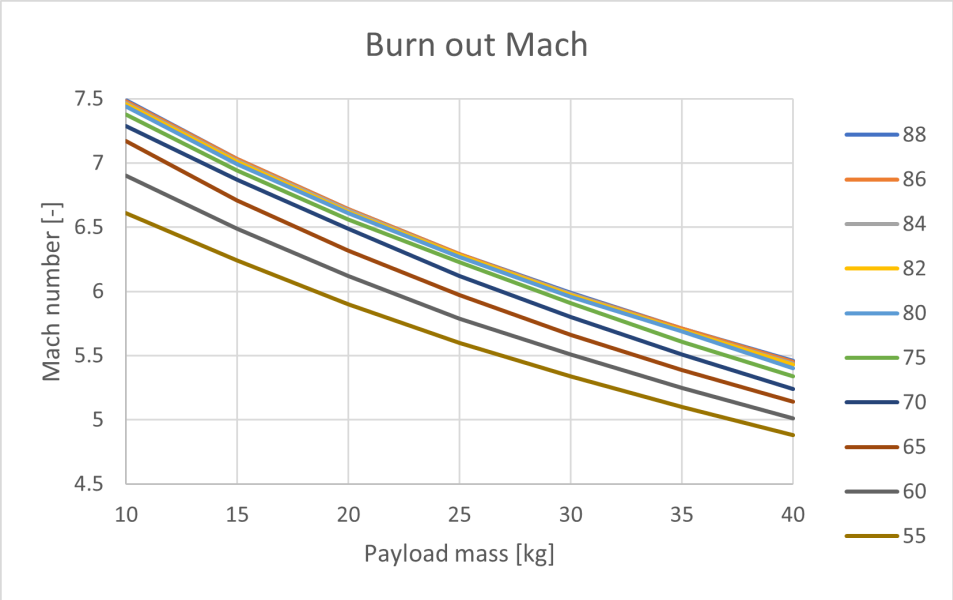

Figure E.3: Burn out Mach

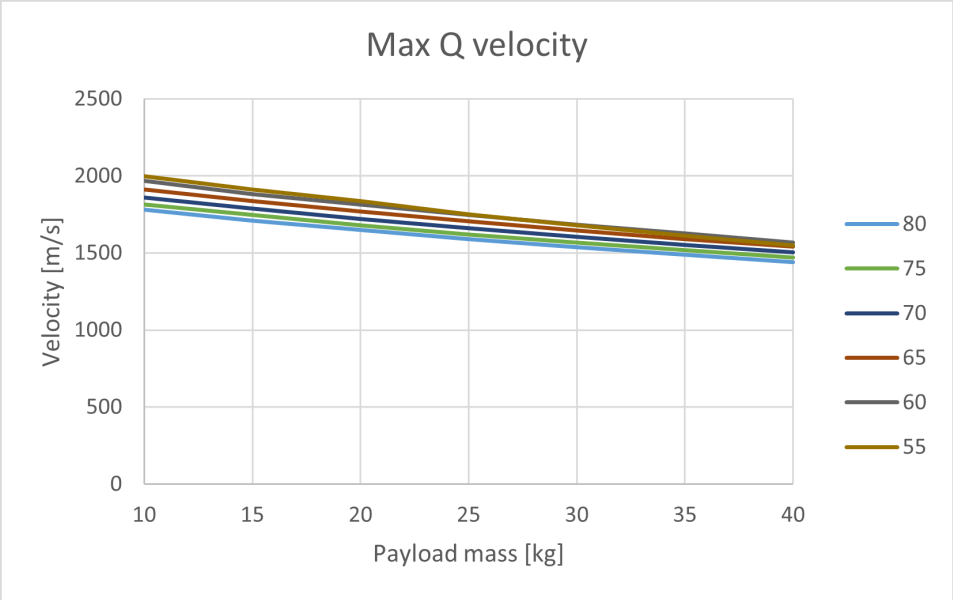

Figure E.4: Burn out max q velocity

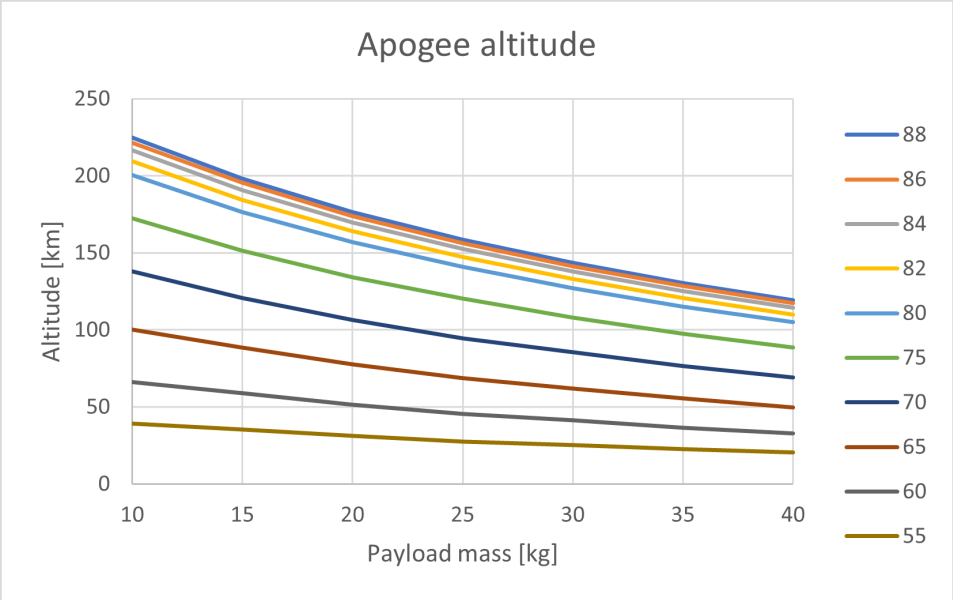

Figure E.5: Apogee altitude

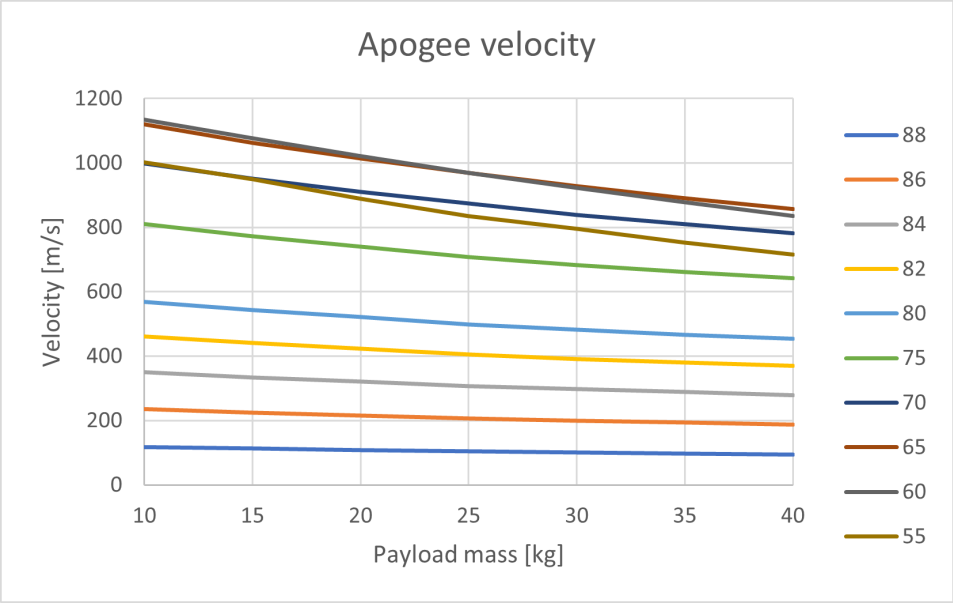

Figure E.6: Apogee velocity

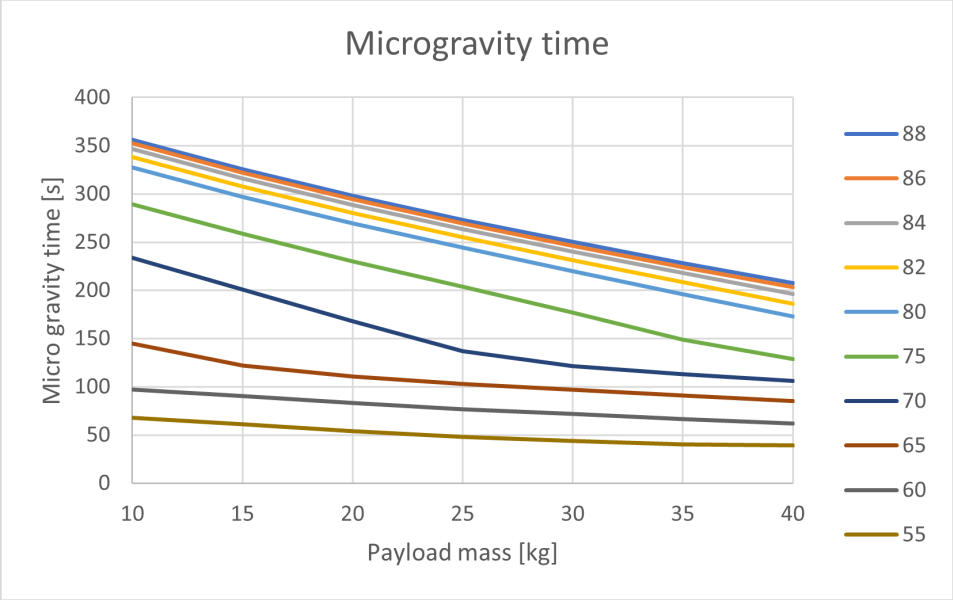

Figure E.7: Microgravity time